ORP-58617
Revision 0

# Computer Simulation Study of the Behavior of Noble Metals in the WTP HLW Melter, VSL-05R5740-2, Rev. 0

Prepared for the U.S. Department of Energy
Assistant Secretary for Environmental Management


**P.O. Box 450**
**Richland, Washington 99352**

**Approved for Public Release;**
**Further Dissemination Unlimited**

ORP-58617
Revision 0

# Computer Simulation Study of the Behavior of Noble Metals in the WTP HLW Melter, VSL-05R5740-2, Rev. 0

C. C. Chapman
EnergySolutions

W. Lutze
EnergySolutions

Date Published
August 2005

Prepared for the U.S. Department of Energy
Assistant Secretary for Environmental Management


**P.O. Box 450**
**Richland, Washington 99352**

***APPROVED***
***By Ashley R Jenkins at 8:49 am, Mar 10, 2015***

Release Approval | Date

**Approved for Public Release;**
**Further Dissemination Unlimited**

**TRADEMARK DISCLAIMER**

Reference herein to any specific commercial product, process, or service by tradename, trademark, manufacturer, or otherwise, does not necessarily constitute or imply its endorsement, recommendation, or favoring by the United States Government or any agency thereof or its contractors or subcontractors.

This report has been reproduced from the best available copy.

Printed in the United States of America

VSL-05R5740-2

# Final Report

# Computer Simulation Study of the Behavior of Noble Metals in the WTP HLW Melter

*Compiled by*

**Christopher C. Chapman[1] and Werner Lutze[2]**

**[1]Duratek, Inc., Columbia, MD**
**[2]Vitreous State Laboratory**
**The Catholic University of America**

*for*

**Duratek, Inc.**

*and*

**Bechtel National, Inc.**

**August 8, 2005**

***Rev. 0***

## Preamble

This report is based on work conducted by Glass Service, Inc. under sub-contract to the Vitreous State Laboratory (VSL) of The Catholic University of America (CUA). Two reports prepared by Dr. Schill of Glass Service, Inc. are appended. Dr. Schill and staff from VSL, Duratek, and WTP R&T participated in a review of the results presented in the first report, out of which additional cases for modeling were identified. The second report presents the results from the additional cases.

## Synopsis

The noble metals ruthenium (Ru), rhodium (Rh), and palladium (Pd) are present to various extents in defense and commercial high-level nuclear waste streams. Usually, their concentrations are higher in commercial waste. Ru, Rh, and Pd are sparingly soluble in silicate glass melts and they therefore form separate metal, oxide, or other phases. These phases are generally denser than the glass melt and tend to sediment to the bottom of the melter, where they form a "sludge" layer. Since the sludge layer has a higher electrical conductivity than the molten glass, accumulation of sludge can ultimately lead to electrical disruption of the operation of the melter. In addition, the sludge reduces the melt volume, which also changes the operational characteristics of the melter. The noble metals sludge is a highly viscous mixture of melt and noble metal phases. The concentration of noble metals in the sludge may be 10 to 100 times higher than that in the drained glass.

The reference design of the Waste Treatment Plant (WTP) High-Level Waste (HLW) melter includes a large accumulation volume (approximately 2,400 liters) for sludge inside the melt cavity [1]. Essentially, the lifetime of the melter is reached when the cavity fills with sludge.

The phenomenon of noble metal retention has been studied widely and is well documented in the literature. However, large uncertainties arise when using literature data to estimate melter lifetimes in general and that of the WTP HLW melter in particular. Uncertainty is further enhanced because the WTP HLW melter will use bubblers to increase the glass production rate. Bubbling can affect noble metal particle agglomeration, particle morphology, particle settling rates, particle entrainment into the poured glass stream, and enhance transport of noble metals to the off-gas. Furthermore, recycling the fraction of noble metals captured in the off-gas to the melter will increase the steady-state concentration of noble metals in the melter feed.

To address the risks related to noble metals impacts on HLW vitrification, VSL has performed analysis, testing, and modeling work in support of the WTP HLW vitrification program. That work is being performed under a WTP Test Specification [2] and associated Test Plans [3-5]. The overall strategy that has been developed to address this issue, which has been reported elsewhere [6], employs a combination of noble metals testing at laboratory scale (gradient furnace testing) and testing in small- (DM10) and

pilot-scale (DM1200) melters, assisted by computer modeling that is being performed through a sub-contract with Glass Service, Inc., Czech Republic. These results will be used to reduce uncertainties in WTP HLW melter lifetime estimates.

VSL has conducted a series of noble metals tests in the DuraMelter DM1200, the results of which have been documented in three technical reports [7 - 9]. The data from tests in which simulated AZ-101 waste feed was spiked with Ru, Rh, and Pd [7] or Ru only [8] were provided to Glass Service, Inc. for them to model the behavior of noble metals in the DM1200 melter; the results from that work have been presented elsewhere [10]. The test data and the modeling results for the DM1200 melter serve to calibrate the Glass Services model, which can then be used to investigate various test cases for the full-scale WTP HLW melter. The results of this latter step form the subject of the present report.

The goal of the present work was to use the calibrated Glass Services computer code to mathematically model the transport and settling of noble metals in the WTP HLW melter. As described above, the modeling was performed in two steps. In the first step, an initial set of cases was modeled. Based on the results of the initial set of cases, an additional set of cases was identified for modeling. Each of these sets are discussed below.

Initial Set of Modeling Cases

The modeling cases that were used in the initial set are listed in Table S1 and the results are presented in the first Glass Service report. In the text of this report, the cases are referred to as shown in Column 1 of Table S1. Each case describes the particular set of melter operating conditions or malfunctioning conditions for which the accumulation of noble metals was calculated using several physical assumptions. A set of melter operations data and other design features were provided to the modeler (Dr. Schill).

In every modeling case, noble metals (Ru, Rh, and Pd) were represented by Ru alone. Ru was assumed to be present in the melt solely as $RuO_2$ crystals (needles), with a size distribution based on data from the DM1200 melter and laboratory work reported previously. However, for modeling purposes, the particles were converted from rods to cubes of the same mass. These particles were assumed not to grow or form larger particles (clusters) or to otherwise evolve into particles with different morphology.

Four key assumptions were used to perform the modeling:

1. The volume fraction of noble metals in the sludge is 0.06.
2. The existence of an entrapment layer (represented by a "settling parameter"), in which $RuO_2$ particles are irreversibly captured upon entering. This is explained in reference [10].
3. A geometric factor can be used to represent needle-shaped particles.
4. The electrical conductivity of the $RuO_2$ sludge can be estimated.

For practical reasons, the computational time for the modeling calculations had to be short compared with periods of time (presumably several years) of actual melter operation, after which effects from noble metals could become significant. Thus, additional assumptions had to be made to allow estimation of longer-term noble metals settling. The approach used to numerically accelerate the accumulation of noble metals involved:

- Increasing the concentration of noble metals by a factor of 20, from 0.09 wt% to 1.8 wt%; and
- Increasing the so-called entrapment zone by nearly a factor of 10, from 0.1 mm to 1.0 mm.

These assumptions together contracted the computation time by a factor of approximately 52. Using these higher values, accumulations of noble metals could be mapped within 20 to 50 hours of computational time. It was observed that the maximum temperature within the melter cavity suddenly increased after only about 30 days of real melter operations. In actual operation, however, these hot spots would likely go unnoticed. Although this computational observation is interesting and localized hot spots are likely representative of reality, they are not indicative of melter failure.

To account for accumulations of noble metals sludge, each of the cells on the floor of the melter accumulates noble metals according to the settling criteria. When a computational cell is filled with $RuO_2$ sludge (i.e., the volume fraction has reached 6%), the computational cell is converted from a glass cell to a sludge cell, whereupon no further flow in or through this cell is allowed. However, the cell still participates in joule heating and heat transfer. The experimental noble metals particle size distribution [10] is simplified into an average diameter with a range into which each particle size falls. The settling velocity is determined for the average particle size and density. Since the flow across the bottom is predominately horizontal, the noble metals flow horizontally past the underlying computational cells and the code determines which, if any, particles are captured. These particles are removed from the concentration in the bulk glass and stored in the computational cell in which they settled. Experimental data from the noble metals test in the DM1200 were used to calibrate the computational model for settling [10]. To match the experimental results, an additional height, called the entrapment distance, was added to the calculated settling height in order to better model the results from the DM1200 tests [10]. In the DM1200 noble metals modeling study [10], this distance was determined to be 0 mm to match modeling results to the experimental data for palladium. However, this distance had to be increased to 1 mm for the model results to be in agreement with the DM1200 $RuO_2$ settling data (moderate bubbling of 40 L per minute with a specific throughput of 500 $kg/m^2/d$). The distance had to be increased to nearly 5 mm in order to yield satisfactory agreement with DM1200 ruthenium settling data in a test where a reduced melter feed (sugar added) produced larger ruthenium metal nodules; the test results for that melter run resulted in about 80% retention. From this modeling

effort it is evident that additional parameters are needed to fully describe the nature of the noble metals settling process.

It should be noted that, at this point, the entrapment height is simply an empirical modeling parameter that had to be introduced in order to bring the model results into agreement with the DM1200 test results [10] and its true physical significance is not entirely clear. Consequently, it is difficult to select a meaningful value in the absence of experimental noble metals settling data for a given set of melter operating conditions. Phenomenologically, however, this parameter represents the effect of a presumed "sticky boundary" that results in additional particle settling beyond that due to the normal stokes settling velocity.

Rectangular computational cells of varying size were used to simulate the WTP HLW melter. The locations of the bubbler nozzles were adjusted to fall within a computational cell. Thus, the location in the computational model is slightly different from that in the actual plant melter design. However, the greatest variance between the design position and the modeling position was less than 0.8 inches; the average distance deviation was about 0.4 inches, which is well within the anticipated location error of a bubbling nozzle.

The rate of noble metals accumulation was calculated for two different values of noble metals concentration (0.09 and 1.8 wt%) and entrapment heights (0.1 and 1.0 mm). This is shown in Figure 30 of the first report. After reaching a steady state, the rate of accumulation is approximately linear. The calculated accumulation rates for the two cases, 1.8 wt% and 1 mm versus 0.09 wt% and 0.1mm, differed by a factor of 52. This factor represents the approximate increase in the computed rate compared to the actual melter accumulation rate.

Using the calculated mass accumulation for a ruthenium concentration of 0.09 wt% and an entrapment height of 0.1 mm, the rate of accumulation was found to be 0.0367 kg/hr. At this accumulation rate the melter cavity fills to the discharge throat (13.2 inches), which is assumed to be the criterion for melter failure, after 596 days or 1.63 years of operation.

The accumulation of noble metals on the bottom of the melter was not uniform. In particular, piles of noble metals accumulated near the bubbler nozzles. However, these calculated accumulations, with extremely high height-to-base ratios, are not realistic because there was no allowance in the calculations for such piles to slump, fall over, or otherwise respond in a realistic fashion. Thus, a modeling criterion that accounted for this behavior would need to be incorporated but was beyond the scope of the present work. Nonetheless, the modeling result that noble metals accumulation occurs around the bubblers does not seem to be unrealistic. The result that noble metals are deposited on the slanted walls of the cavity is also important because such deposits could support preferential flow of electrical current between electrodes earlier than would otherwise be expected.

Finally, after 250 hours of idling, the model predicted that essentially all of the noble metals in the melter would settle out on the bottom.

Additional Set of Modeling Cases

The additional cases that were modeled are summarized in Table S2 and discussed below.

**Case A1: Electrical response to prescribed accumulated noble metals sludge**

For this case, the shape and depth of the noble metals sludge was prescribed. The form of the noble metals sludge layer is shown in Figure S1. The distance between the closest accumulated noble metals sludge and the bottom of the electrodes varied in three of the runs and was negative (layer overlapped the electrodes by about 1 inch in the northeast and northwest corner) in the fourth run.

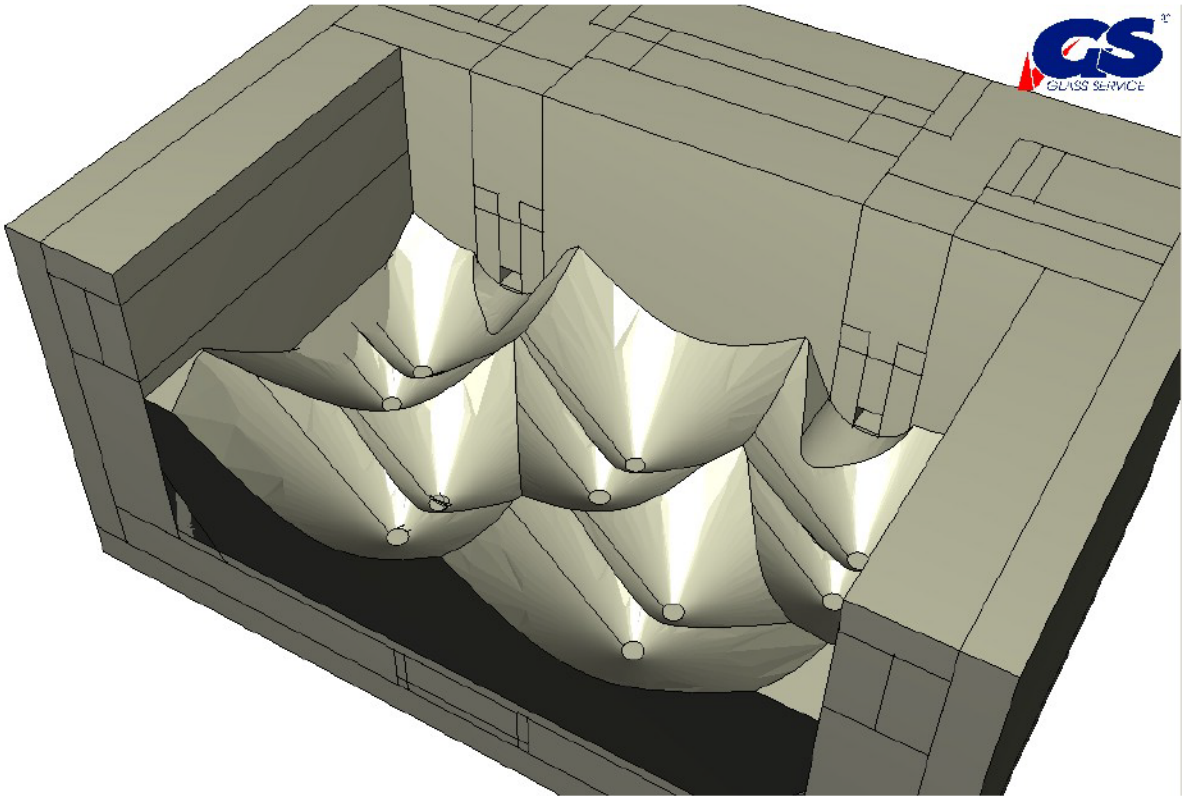

**Figure S1. Model approximation of the NM sludge.**

The calculated melter electrical operating parameters for these four cases and for a melter with and without noble metals sludge are presented in Table S3. The calculated results indicate little sensitivity to the physical proximity of the noble metals sludge to the power of electrodes. As the sludge moved closer, to the electrodes (distance decreased from 3 to 2 to 1 inch), the voltage remained the same, while the electrode current increased by 10%. When the sludge overlapped the electrodes, the current increased by 260%. In the model, the power was controlled such that the control thermocouples remained at the 1150°C set point. In reality, however, if the power supply is unable to deliver the necessary current, the bulk glass temperature would decrease. The modeling results in Table S3 also indicate that the margin between operability and failure of the melter is fairly narrow once noble metal sludge is only a few inches away from the electrodes.

Due to variations in the high-level waste compositions in different tanks at Hanford there are variations in the glass properties. The variations for the different melt conductivities are comparable and in some cases higher than the increase in melter conductivity resulting from noble metals sludge, except for case A1-d (Table S2). Bulk glass temperature variations over the course of a melter's life could also introduce changes in the melter's conductivity that are comparable to those due to noble metals sludge (prior to contact with the electrodes). These findings suggest that it may be difficult to unambiguously attribute changes in operational parameters to accumulation of noble metals sludge and any pre-indications of impending contact of the noble metals sludge with the electrodes and consequent melter failure may be very subtle relative to normal operating variations.

**Cases A2, A3, and A4: Influence of higher bubbling rate on glass temperatures and flow**

The influence of bubbling on the glass flow field is significant and depends on the bubbling rate. The convention of the WTP Project has been to define the bubbling rate at standard conditions. GS uses the nominal standard volumetric flow rate directly in their modeling. The travel time of the bubbling air in the bubbler pipe leading to the nozzle is long enough to significantly increase the gas temperature. To account for heating the bubbling gas, calculations were completed to determine the temperature increase [11]. The exit temperature of the bubbling gas was estimated to be about 630°C. Thus, the actual volumetric flow rate for bubbling the melt was a factor of 2.8 above the standard volumetric values. Since the prior model cases used the standard volumetric bubbling rate without adjustment to the actual volumetric flow rate, cases A2, A3, and A4 were commissioned to determine the influence of the bubbling rate on the temperature field and the flow field. A comparison is provided in Table S4.

Modeling results of flow and temperatures at significantly higher bubbling rates are as expected. Maximum melt flows occur near the ascending bubbles. These values are shown as negative numbers due to selection of the coordinate system. Higher bubbling rates produces higher vertical velocities. The increase in the minimum or negative

vertical velocity is generally proportional to the increased bubbling rate. Higher bubbling rates increase the maximum positive or descending flow rate. Tripling the bubbling rate produced an increase in the down flow by about 20 to 30%.

The influence of the bubbling rate on the average glass temperature inside the melting cavity was modest. No change was observed for the average glass temperature when the set point was at 1150°C. The more noticeable change occurred for the idling case. For the idling case at a set point temperature of 1050°C and a low flow rate of 0.3 SCFM, the average temperature was about 20°C below the set point. At the higher bubbling rate of 3.5 SCFM, the average glass temperature was only 6°C below the set point. Since most of the lowest temperatures are nearest the bottom, higher bubbling rates during idling would keep floor temperatures significantly higher.

The GS report on the additional cases provides detailed figures that portray glass flow, joule heating, electric current density, iso-potential lines, and variations in electrical conductivity within the melting cavity for the additional cases.

## Quality Assurance

This work was conducted under a quality assurance program based NQA-1 (1989) and NQA-2a (1990) Part 2.7 that is in place at the VSL. This program is supplemented by a Quality Assurance Project Plan for RPP-WTP work [12] that is conducted at VSL. Test and procedure requirements by which the testing activities are planned and controlled are also defined in this plan. Glass Services prepared project-specific QA plan (QAPP) for this work that was reviewed and approved by VSL prior to initiating this work. Glass Services implemented VSL software control procedures for this work and provided copies of all required documentation to VSL for approval.

This work did not generate data to support waste form qualification activities; nor did it generate data to support environmental regulatory data to support permitting activities. Therefore, this work was not subject to DOE/RW-0333P or the WTP QAPjP [13] for environmental regulatory data.

## References

[1] C.C. Chapman, "Reducing Noble Metals Precipitation and Extending Melter Life," Internal Report, CH2MHill Hanford Group, Inc., Richland Washington, February 2001.

[2] C. A. Musick, "HLW Noble Metal Testing," WTP Test Specification, 24590-HLW-TSP-RT-02-010, Rev 0, 21 May 2002.

[3] W. Lutze, W. Gong, and I. L. Pegg, "Noble Metals Testing to Support RPP-WTP HLW Vitrification: Gradient Furnace, Crucible, and Melter Testing," Test Plan, VSL-02T7400-1, Rev. 0, September 23, 2002.

[4] W. Lutze, W. Gong, P. Schill, C. C. Chapman, and I. L. Pegg, "Modeling the Behavior of Noble Metals During HLW Vitrification," Test Plan, VSL-03T3740-1, Rev. 1, August 6, 2003.

[5] W. Lutze, W. Gong, and I. L. Pegg, "Noble Metals Testing in a Modified DuraMelter 10 to Support Computer Modeling," Test Plan, VSL-03T3740-2, Rev. A, September 17, 2003.

[6] W. Lutze, W. Gong, I. L. Pegg, "Proposed Noble Metals Testing to Support RPP-WTP HLW Vitrification," VSL-02R7400-1, Rev. 0, April 15, 2002.

[7] W. Lutze, W. Gong and I. L. Pegg, "Noble Metals Testing on the DM1200 Pilot Melter System with AZ-101 HLW Simulants," VSL-03R3740-2, Rev. 0, December 17, 2003.

[8] K. S. Matlack, W. Gong, T. Bardakci, N. D'Angelo, W. Lutze, P. M. Bizot, R. A. Callow, M. Brandys, W. K. Kot, and I. L. Pegg, "Integrated DM1200 Melter Testing of Redox Effects Using HLW AZ-101 and C-106/AY-102 Simulants," VSL-04R4800-1, Rev. 0, May 6, 2004.

[9] K. S. Matlack, W. Gong, T. Bardakci, N. D'Angelo, W. Lutze, R. A. Callow, M. Brandys, Wing K. Kot, and I. L. Pegg, "Integrated DM1200 Melter Testing of Bubbler Configuration Using HLW AZ-101 Simulants," VSL-04R4800-4, Rev. 0, October 5, 2004.

[10] W. Lutze, "Modeling the Behavior of Noble Metals During HLW Vitrification in the DM1200 Melter," VSL-05R5740-1, Rev. 0, May 5, 2005.

[11] R.K. Mohr, C.C. Chapman, and I.L. Pegg "High-Level Waste Melter Alternate Bubbler Configuration Testing," VSL-04R4800-3, Rev. 0, June 18, 2004.

[12] "Quality Assurance Project Plan for RPP-WTP Support Activities Conducted by VSL," Vitreous State Laboratory, QAPP Rev. 6, November 12, 2003.

[13] D. B. Blumenkranz, "Quality Assurance Project Plan for Testing Programs Generating Environmental Regulatory Data," PL-24590-QA00001, Rev. 0, Bechtel National Inc., Richland, WA, June 7, 2001.

**Table S1. Identification of Modeling Tasks and Initial Set of Modeling Cases.**

| Modeling case and reference | Modeling task | Runs |
|---|---|---|
| GS quote 106-040056, July 12, 2004), position **B1** | Modify grid structure, adapt model to design changes. Change model to allow for thick layer modeling with pile up of noble metals between bubblers. | 1 |
| **Case 1** [GS quote 106-040056, July 12, 2004), position **B2**] | Let NM accumulate in piles (find out whether this can happen at all). Let layer grow to bottom of discharge port. Use VSL $RuO_2$ particle data (needles) as supplied and VF(max) = 0.06; Total noble metals concentration is 0.09 wt% (as $RuO_2$) in the glass. Use nominal bubbling rate. | 1 |
| **Case 2 A** [GS quote 106-040056, July 12, 2004, position **B3**] | Continue Case 1 until effect of NM accumulation on operation parameters (electrical field or other) becomes evident. | 1 |
| **Case 2 B** [GS quote 106-040056, July 12, 2004), position **B4**] | As Case 1 but determine effect of higher electrical conductivity of sludge on operation parameters. (Is a factor of 2 enough?) | 3 |
| **Case 2 C** [GS quote 106-040056, July 12, 2004), position **B5**] | As Case 1 but one bubbler fails (Turn off top left bubbler of Figure 3 with two bubblers). What is the effect on NM settling? | 1 |
| **Case 2 D** [GS quote 106-040056, July 12, 2004), position **B6**] | As Case 1 but two bubblers fail. (Turn off top left bubbler of Figure 3 with two bubblers AND bottom left in the row of three bubblers.) What is the effect on NM settling? | 1 |
| **Case 2 E** [GS quote 106-040056, July 12, 2004), position **B7**] | As Case 1 but no feeding. Melter is idle. Run until 90% of NM settle, No feeding. | 1 |

**Table S2. Additional Set of Modeling Cases.**

| Case ID (GS ID) | Summary Description of Case |
|---|---|
| Case A1 (B2 NM filled) | Case A1 includes 5 sub-cases calculating the total electrode current, voltage, flow and temperature fields for five assumed noble metals sludge depths. The first condition (A1-0) was no noble metals sludge. Case A1-0 was used for subsequent comparisons. In cases A1-a to A1-d the form and depth of collected noble metals sludge was prescribed. The form of the accumulated sludge was defined as a cuboid of selected depth with sludge excluded in the space vertically above each bubbler nozzles in the form of a frustum of a cone. The bottom surface of the frustum of each cone was a circle 3 inches in diameter at the nozzle outlet. The sides were at a 45° angle from the vertical. For the conditions with noble metals sludge, this general form was used with increasing sludge depths that approached the side electrodes. In case A1-d the settled sludge layer overlapped the electrodes in the northeast and northwest corners by about 1 inch. |
| Case A2 (B1 HBR) | Case A2 assessed the influence and contrasted the temperature and flow fields for a noble-metals-free cavity but using a higher bubbling rate than in previous calculations. A bubbling rate of 100 liters per minute per nozzle (3.5 SCFM), 10 nozzles, 170 bubbles per minute with a "hemispherical" bubble diameter of 130 mm (6.3 inches) was prescribed. |
| Case A3 (B6 HBR) | Case A3 assessed the influence and contrasted the temperature and flow fields for the earlier case, B6, using a higher bubbling rate. In this case, it was assumed that two of the five bubbler assemblies were not operational. A bubbling rate of 100 liters per minute per nozzle (3.5 SCFM), 6 nozzles, 170 bubbles per minute with a "hemispherical" bubble diameter of 130 mm (6.3 inches) was prescribed. |
| Case A4 (B7 HBR) | Case 4A determined the bulk glass temperature and flow fields during idling using a higher bubbling rate and higher set point temperature. The glass set point temperature was increased from 1050ºC (used in the earlier case B7) to 1075ºC and the bubbling rate was increased to 100 liters per minute per nozzle (3.5 SCFM), 10 nozzles, 170 bubbles per minute with a "hemispherical" bubble diameter of 130 mm (6.3 inches). |

**Table S3. List of Calculated Electrical Quantities for Cases A1-0 to A1-d.**

| Case | Minimum distance: sludge to electrode | Maximum sludge height | Electrode voltage | Electrode current | Total power |
|---|---|---|---|---|---|
| | (mm) | (mm) | [V] | [A] | [kW] |
| A1-0 | - | 0 | 156 | 3,439 | 536 |
| A1-a | 76 | 708 | 134 | 4,316 | 578 |
| A1-b | 50 | 734 | 134 | 4,464 | 597 |
| A1-c | 25 | 759 | 134 | 4,730 | 635 |
| A1-d | -29 | 813 | 144 | **12,258*** | **1,770*** |

* Value exceeds the plant design capacity

**Table S4. Influence of Higher Bubbling Rate on Glass Temperatures and Flow Rate for Several Assumed Melter Operating Conditions.**

| **Characteristic of modeling** | **Case** | **Number of nozzles** | **Nozzle flow rate, SCFM** | **Glass flow; min. rate, mm / s** | **Glass flow; max. rate, mm / s** | **Flow rate at center of center bubbler at bottom of electrode elevation** | **Control temperature, °C** | **Ave. glass temperature, °C** | **ACFM / $m^2$** | **SCFM / $m^2$** |
|---|---|---|---|---|---|---|---|---|---|---|
| Nominal, no sludge | A1 | 10 | 1.15 | -83 | 57 | -82 | 1150 | 1146 | 3.09 | 0.7 |
| Nominal, high bubbling rate | A2 | 10 | 3.50 | -264 | 75 | -183 | 1150 | 1142 | 9.41 | 2.2 |
| Two bubblers off | 2 D | 6 | 1.15 | -79 | 59 | -78 | 1150 | 1139 | 1.85 | 0.4 |
| Two bubblers off, high bubbling rate | A3 | 6 | 3.50 | -244 | 72 | -163 | 1150 | 1139 | 5.65 | 1.3 |
| Idling, temp. 1050°C, modest bubbling | B7 | 10 | 0.30 | -6.3 | 11 | -3.5 | 1050 | 1030 | 0.81 | 0.2 |
| Idling, temp. 1075°C, high bubbling | A4 | 10 | 3.50 | -221 | 44 | -152 | 1075 | 1069 | 9.41 | 2.2 |

Glass Service Inc.
Rokytnice 60
755 01 Vsetin
Czech Republic

# SIMULATION STUDY OF THE WTP MELTER

## Report

*Prepared by*

Petr Schill

Glass Service, Inc.
Rokytnice 60, Vsetin 75501
Czech Republic

*for*

Vitreous State Laboratory
The Catholic University of America
Washington, D.C.20064

November 30, 2004

## CONTENTS

# INTRODUCTION

The goal of this project was to mathematically model the dynamics of transport and settling of noble metals (NM) (here $RuO_2$) in temperature- and electrical-fields in the WTP Duratek melter which is based on Duratek's HLW melter described in the Report "HLW Melter Thermal-Hydraulic Model" prepared by GS for Duratek in November 2001 [4]. The WTP melter differs from the melter modeled in 2001 by modest shift of the discharge throat upward by 3.6 inches and replacement of the bottom electrode found in the model in 2001 by refractory. The bubbler design was also mollified from the prior five single nozzles to five bubbler assemblies with two nozzles each.

One basic case and two modified cases with simulated bubbler failures, and one idling case were modeled. The creation of a NM sludge layer of non-constant thickness using the "thick approximation" (see below) has been studied. Modeling of the noble metals sludge settled on the bottom provided an estimation of the effect of NM accumulation on melter operation.

Modeling is based on physical-chemical processes describing particle formation, transport, and settling in a given melter configuration and with a given set of operating conditions. For this purpose, particle transport and settling models have been integrated into the GS-GFM computer code. In the first step, the code calculates thermal, electrical, chemical, and flow processes in the glass melt. Noble metal particles are treated as chemically and physically inert. They are assumed to enter the melt from the cold cap bottom; thus, any changes in size or composition are neglected. Inertness means here that the noble metals do not undergo chemical reactions in the melt. Since their size is not allowed to change, Ostwald ripening and formation of larger clusters in the melt is neglected. Input data includes NM injection rate, particle size distribution, feed input rate, water content in the feed, and glass production rate.

Noble metals settling leads to retention and accumulation of particles at the bottom of the melter. To support the modeling work, experimental values characterizing the particle properties (density, size distribution) and thermo-physical properties of the melt, such as density, viscosity, thermal and electrical conductivity, are used to calculate particle retention rates. The volume fraction (VF) of particles in the bottom sludge layer is treated as an experimental constant (0.06 vol%). In the calculation it is assumed that the NM layer becomes thick enough to have an effect on the characteristics of the melt pool (mainly the electrical conductivity near the bottom). This approach is called the 'thick layer approximation'. This permits estimation of early accumulation rates and includes the effect of the layer growth on flow and other glass characteristics that may affect the melter behavior.

Unfortunately, four important physical quantities cannot be estimated precisely without experimental measurement: the volume fraction (VF) of NM in sludge, the entrapment parameter for settling, the geometrical factor for needle-shaped particles, and the electrical conductivity of the sludge (depending on glass composition, temperature, and VF). The

actual settling of noble metals in the real melter as well as the mathematical simulation can take time spans measured in years. To circumvent the long time demand on the computer modeling, a new approximation method was used to address the deficiency of physical properties and lack of computational time. This method is based on simulation of additional cases with higher initial NM concentration, various entrapments, and the use of several kinds of extrapolations.

## MODEL DESCRIPTION - THEORY

Mathematical modeling is based on a numerical solution of field equations (temperature, velocity, electric potential and power, particle concentration, etc.) on a system of three-dimensional discrete grids by the control-volume method enabling proper balance of the relevant parameters. The model involves routines coupling the steady-state temperature and flow fields with transient concentration fields. This approach is a good approximation because the particle concentration in the majority of the melt is low enough not to affect the glass properties significantly. In the sludge layer, the particle concentration is high compared with that in the melt. The particle concentration in the growing sludge layer is simulated by the thick layer approximation. In this approximation the maximum particle concentration $VF_{NM}$ in the sludge must be known. The cold cap behavior and effects (water evaporation, conversion-to-glass-, flow-, and temperature-fields) are calculated by a procedure used for batch melting in a commercial glass furnace. The thermo-physical properties of the feed (heat of reaction, thermal conductivity, viscosity, etc.) must be known for this calculation. Calculation of the electrical field requires iteratively calculating the distribution of electrical potentials and the Joulean heat generated in the melt and in other materials. The temperature functions of electrical conductivity of the glass melt, feed, sludge and other materials (refractory, insulation, electrodes, etc.) are used. The electrical power generation is then calculated directly within the subroutine.

The Glass Furnace Model (GFM), a code developed in Glass Service, Inc, was used for mathematical modeling of the flow, temperature and electrical quantities in HLW melter. The GFM consist of two main parts: the glass space (glass model, GM) and the combustion space (combustion model, CM). The GM was used for glass space and the CM was used for plenum space simulation. The GM and CM are bounded by a special program COUPLE which periodically transfers heat fluxes and temperatures between the GM and CM.

The noble metals settling was calculated by connecting other programs, PACO and SETUP, to the GM and CM programs. All the programs are grouped and started from main GFM window.

## GLASS FURNACE MODEL (GFM)

The GFM is a complex code used for mathematical simulation of the whole glass melting furnace. The heat transfer (resulting in temperatures) and momentum transfer (resulting in velocities) inside glass, the batch melting, water evaporation, energy generated by electrodes immersed in glass, radiation in gas, flow of gas, and temperature-concentration functions of thermodynamic properties, are in principle considered in the glass furnace model. The calculation procedure covers glass, batch, walls and plenum space and it involves a special coupling mechanism among all the furnace sections. The GFM consists of two main parts: Glass Model (GM) – used for melter and Combustion Model (CM) – used for plenum space. Each part is divided into five program groups: Preprocessors, Solvers, Coupling, Utilities, and Postprocessors. The most valuable preprocessor - called GS-CAD - enables the transfer of the real furnace geometry into model format including automatic grid generation and user specification of the boundary conditions in a fast and friendly manner. The postprocessor group involves important programs for 2D and 3D graphical display, tracking of particles, etc. The GM part contains procedures for coupling GM-CM and GM-PC

(PC means particle concentration solver). All the programs are designed for running under Windows operating system (NT, 95, 98, 2000, or XP). Most of the programs are graphical tools, which allow use of familiar elements of the Windows user interface, such as pull-down menus, toolbars, dialog boxes and other features of Windows NT. All the programs can be started from the main Glass Furnace Model Window.

## BASIC PRINCIPLES OF THE GLASS MODEL (GM)

The model approximates the partial differential equations by the numerical finite difference method on a system of staggered grids. Several general assumptions are used in the glass-melt: (a) Principle of incompressible Newtonian fluid. The buoyancy is driven by temperature variations of density (Boussinesq approximation). (b) Viscous heat dissipation effects are negligible. (c) Molten glass is optically thick (Rosseland approximation). (d) Batch to glass conversion is a continuous process governed by melting kinetics. This model involves three-dimensional steady-state calculation of temperature, velocity, and electrical quantity distributions and of the batch melting process.

Most of the governing equations are based on one simple transport equation, only, as was pointed out by Patankar [1]. The temperatures and velocities (having discrete form of three-dimensional fields) are governed by laws of conservation and can be expressed mathematically using partial differential equations.

The model equations follow:

**Heat transfer:**

$$\nabla \cdot \left( a_{ef} \nabla T \right) - \vec{V} \cdot \nabla T = -Q \qquad \textbf{(1)}$$

**Momentum:**

$$\nabla \cdot \left( \nu \nabla \vec{V} \right) - \left( \vec{V} \cdot \nabla \right) \vec{V} - \nabla P = g\beta \left( T - T_R \right) \qquad \textbf{(2)}$$

**Continuity:**

$$\nabla \cdot \left( \vec{V} \right) = 0 \qquad \textbf{(3)}$$

**Electric potential $\Phi$:**

$$div\left( \sigma grad \Phi \right) = 0 \qquad (4)$$

The designation of all the symbols is familiar. Here, T is temperature, V is velocity, $\mathrm{P}$ is the fictive pressure $\mathrm{P} = \mathrm{P}_{tr} / \rho_R - gz$ ($\mathrm{P}_{tr}$ is the true pressure). The frequency-mean volumetric heat source-term Q is calculated by a formula

$$Q_v = \frac{1}{tp} \int_0^{tp} \sum \sigma \left( x_i, T \right) \left( \frac{\partial \Phi}{\partial x_i} \right)^2 \qquad (5)$$

where $t_p$ is time period of A. C. current and $\Phi \equiv \Phi(x_i)$ is electric potential that is given by solving of (Eq. 4).

To generate a set of algebraic equations (i.e., finite-difference eqs.) a modified differencing technique of Patankar [1] is used involving partial integration of the model

equations (1-3) over control volumes (CV). A stabilized scheme (for large grid Peclet numbers and large Reynolds ones) based on exponential particular solutions is used.

The SCGS (Symmetric Coupled Gauss-Seidel) algorithm is used for solving temperature and momentum and continuity difference equations.

The resulting finite-difference equation valid for one CV (having center node P) using dummy velocity component V is written (x-direction as an example) in correction form for unknown corrections $\delta V\rho$ and $\delta P\rho$ follows:

$$A\rho\delta V\rho - \delta P\rho / \delta x\rho = \sum{}' A_I V_I - \left(P_{p+1} - P_p\right)/\delta x_p - A_P V_P \equiv \mathrm{Re}\, s\left(V_P\right) \qquad \textbf{(6)}$$

The summation $\sum{}'$ is taken over surrounding nodes of the central node $\mathrm{P}$. Some modifications have to be made for velocity component with buoyancy term and for boundary CVs. The coefficients $A_I$ are of the form

$$A_I = G\left(\mathrm{Re}_i\right).\nu_i /\left(\delta x_I.\delta x_i\right);\ G(y) = \exp\left\{y/\left(e^y - 1\right)\right\} \qquad \textbf{(7)}$$

The capital indices "$I, \mathrm{P}$" represent the central nodes of CVs, while the "$i, \rho$" represent "wall nodes" of CVs. Staggered node-positions for different velocity components must be considered.

A set of 6 eqs. of type (6) together with one continuity eq. (in similar correction form) are collected to one block for each CV. An analytical solution of this linear set of 7 algebraic eqs. yields the corrections $\delta U$, $\delta V$, $\delta W$ to the velocity components on the faces of CV and the correction $\delta P$ to the pressure $P$ in the center of each CV. The principle of the iterative procedure consists of sweeping through the entire domain while solving the small sets of eqs. in each block. The energy eq. (1) is solved in a similar manner and it may be added to the set of block eqs. The under-relaxation factors are used to support the convergence.

Calculation of the furnace proceeds through glass melt and all walls while all the thermophysical properties (density $\rho$(T), kinematic viscosity $\nu$(T) thermal effective diffusivity aeff(T), electrical conductivity $\sigma$(T), etc.) are recalculated by user specified temperature functions.

## BASIC PRINCIPLES OF THE COMBUSTION MODEL(CM)

An original code GS-Combustor was developed to simulate the physical phenomena in combustion space of a glass melting furnace. Here, only the parts which are needed for plenum space simulation are described:

### *Flow Field Calculation*

SCGS algorithm is employed to solve momentum and continuity equations:

$$div(\rho\vec{u}u) = div\left[\left(\mu + \frac{\mu_t}{\sigma_v}\right)\vec{\nabla}u\right] - \frac{\partial p}{\partial x}, \qquad div(\rho\vec{u}) = 0 \qquad (8,9)$$

where $\mu$ denotes viscosity of gas, $\mu_t$ is turbulent viscosity and $\sigma_v$ is turbulent Schmidt number for velocities.

### *Turbulence*

The standard $k-\varepsilon$ model is used. The steady $k-\varepsilon$ model is governed by two transport equations for the turbulence kinetic energy k and for the viscous dissipation of turbulence energy ε. We have the following system of equations:

$$\mu_t = c_D \cdot \rho \cdot \frac{k^2}{\varepsilon},$$

**(10)**

$$div\left(\rho \vec{u} k\right) = div\left(\frac{\mu_t}{\sigma_k} \cdot \vec{\nabla} k\right) + \rho(P - \varepsilon),$$

**(11)**

$$div\left(\rho \vec{u} \varepsilon\right) = div\left(\frac{\mu_t}{\sigma_\varepsilon} \cdot \vec{\nabla} \varepsilon\right) + \rho\left(c_1 P - c_2 \varepsilon\right) \cdot \frac{\varepsilon}{k},$$

**(12)**

**where P is the production of the turbulence kinetic energy given by**

$$\rho P = \mu_t \cdot \left(\frac{\delta u^i}{\delta x^j} + \frac{\delta u^j}{\delta x^i}\right) \cdot \frac{\delta u^i}{\delta x^i} + \frac{2}{3} k \cdot \left(\vec{u}.\vec{\nabla}\rho\right) \quad \textbf{(13)}$$

**and $c_1$, $c_2$ are constants. Values of constants follow from various experiments as**

$$c_D = 0.09, \quad c_1 = 1.44, \quad c_2 = 1.92, \quad \sigma_k = 1.0, \quad \sigma_e = 1.3. \quad \textbf{(14)}$$

**The Wall function approach is used to approximate the transition layer near solid walls.**

### *Radiation*

Gray, non-scattering gas is considered. By Kirchnoff's law, the absorption coefficient is equal to emission coefficient for gray gases. The radiation transport equation is then

$$\frac{dI}{ds} = \vec{s}.\nabla I_{\vec{s}} = \alpha(\sigma T^4 - I_{\vec{s}}),$$

(15)

where $I_{\vec{s}}$ denotes radiative intensity coming from direction $\vec{s}$, $\alpha$ is absorption coefficient and $\sigma = 5.6693.10^{-8} W/(m^2 K^4)$.

The equation is subject to boundary conditions

$$I_{\vec{s}} = \varepsilon_W \sigma T^4 + \frac{\varepsilon_W}{\pi} \int_{\vec{n}\cdot\vec{s}'<0} I_{\vec{s}'} \left|\vec{n} \cdot \vec{s}'\right| d\Omega',$$

(16)

where $\varepsilon_W$ is wall emissivity and $\vec{n}$ denotes wall surface normal.

We can see that solution of the radiation transport equation involves solving radiative intensities for each direction $\vec{s}$. The discrete ordinates method introduces discretization of the

directions, i.e., solves the radiative transport equations for $n$ discrete directions $\vec{s}_1$, $\vec{s}_2$, …, $\vec{s}_n$. The integrals over direction are replaced by numerical quadratures, that is

$$\int_{4\pi} f(\vec{s})d\Omega \cong \sum_{i=1}^{n} w_i f(\vec{s}_i),$$

(17)

where $w_i$ are the quadrature weight associated with discrete directions $\vec{s}_i$. The radiative transport equation is then replaced by a set of $n$ equations,

$$\vec{s}_i.\nabla I_{\vec{s}_i} = \alpha(\sigma T^4 - I_{\vec{s}_i}),$$

(18)

subject to boundary conditions

$$I_{\vec{s}_i} = \varepsilon_W \sigma T^4 + \frac{\varepsilon_W}{\pi} \sum_{\vec{n}\cdot\vec{s}_j<0} I_{\vec{s}_j} \left|\vec{n}\cdot\vec{s}_j\right| w_j, \qquad \vec{n}\cdot\vec{s}_i < 0$$

(19)

GS Combustor offers three sets of discrete ordinates (i.e., discrete directions with quadrature weights): S4, S6 and S8 approximations (24, 48 and 80 discrete ordinates, respectively). S4 approximation is usually sufficient but the user can employ more discrete ordinates when needed, e.g., in case of complex geometries.

The total radiative intensity is the weighted average of intensities coming from all directions:

$$I = \frac{\sum_{i=1}^{n} I_{s_i} w_i}{4\pi}$$

(20)

The resulting intensity is then used as a heat source in the energy equation:

$$Q_{rad} = 4\alpha(\pi I - \sigma T^4)$$

(21)

***Temperature***

Instead of directly solving the temperature equation, an enthalpy equation is solved because we have to take into account the fact that the specific heat depends on the local gas composition and temperature. The temperature is then calculated using the relationship between enthalpy and temperature:

$$h = \int_{T_0}^{T} c_p dT$$

(22)

The energy equation contains source terms that represents heat incoming and outgoing due to radiation ($Q_{rad}$) and heat released by combustion ($Q_{chem}$ is equal zero in this application):

$$div(\rho\vec{u}h) = div\left[(\lambda + \mu + \frac{\mu_t}{\sigma_h})\vec{\nabla}h\right] + Q_{rad} + Q_{chem}$$

(23)

## PRINCIPLES OF THE GM-CM COUPLING

The whole glass furnace model is able to work properly by using special coupling procedures, which connect the glass space (flow, temperature, electric boost and batch melting) to combustion (plenum) space. This coupling is based on energy and mass transfer located on coupling plane which is represented by glass level (as being seen from both sides).

Radiation in combustion space: The heat flux on glass level is given by the difference between emitted radiation and absorbed portion of the incident radiation R:

$$q_C = \varepsilon \cdot \left(\sigma T^4 - R\right).$$

(24)

Rosseland approximation of heat transfer in glass space : The heat flux through glass level is given by conduction with effective thermal conductivity:

$$q_G = \lambda_{ef} \frac{dT}{dz}$$

(25)

Heat balance on glass level: Compare the heat fluxes from both the sides

$$\varepsilon \cdot \left(\sigma T^4 - R\right) = . \lambda_{ef} \frac{dT}{dz}$$

(26)

Methods of solution - the sequence of variable transfer on the coupling plane is important in following steps:

a) temperature and batch gases from glass space into combustion space

b) several iterations in combustion model

c) heat flux from combustion space into glass space

d) several iterations in glass space and go back to item a)

The relaxation of the transferred variables on both sides is recommended.

# PARTICLE CONCENTRATION AND SETTLING CALCULATION BY SEMI-TRANSIENT APPROACH

### *Basic conception*

Coupling of the two models, the dynamic calculation of particle concentration and the steady state calculation of flow-, temperature- and electric fields, is called the "semi-transient model." The concentration of particles in the melt depends on glass composition and is affected by flow, temperature and Joule heat production and distribution in the melter. The GS-GFM code couples the particle concentration field with temperature and flow distribution in the melter. The particle concentration field is obtained by a dynamic calculation of particle behavior (transport and settling) in the fixed temperature- and velocity-field [2], [3]. Noble metal particles are treated as inert, meaning that no nucleation, growth, or dissolution processes are considered here.

### *Dynamic calculation of particle concentration*

To represent the size distribution in each volume element of the melt, particles are divided into size classes (n). Each class $i$ is described by its mean size $a_i$ and by the width of the class ( $w_i$ ) such that the class $i$ represents particles of sizes between $a_i - w_i/2$ and $a_i + w_i/2$. The particle size distribution in a volume element is represented by number density values ( $N_{Vi}$ ) where $N_{Vi}$ is the number of particles per volume of the i-th class. The volume concentration of particles in a volume element is calculated as:

$$C_{cr} = \sum_{i=1}^{n} N_{v_i} a_i^3 \quad (27)$$

For each size class, the code stores the number density of particles. The settling of particles according to Stokes´ law and the particle transport by melt convection are used to calculate the particle size distribution in the melt by solving the following transport equation (without the diffusion term) for each $N_{Vi}$ :

$$\frac{\partial}{\partial t}(N_{V_i}) + \frac{\partial}{\partial x}(uN_{V_i}) + \frac{\partial}{\partial y}(vN_{V_i}) + \frac{\partial}{\partial z}((w + w_s)N_{V_i}) = 0 \quad (28)$$

where $w_s$ is the Stokes velocity of particles in glass; u, v, and w, are the components of the velocity vector of the glass melt at the location in question. The Stokes velocity is given by:

$$w_s = \frac{f_G.g.(\rho_p - \rho_{gl}).a_i^2}{\eta} \quad (29)$$

where $f_G$ is a particle geometry factor (e.g., $f_G$ = 0.202 for cubes), *g* is the acceleration due to gravity, $\eta$ is the dynamic viscosity of the melt, and $\rho_s$ , $\rho_{gl}$ are the

densities of the particles and the glass melt, respectively. The calculation is performed in discrete time steps.

The model calculation of particle settling (and, consequently, retention) requires knowledge of the shape factor $f_G$ for each particle group. This factor can be estimated by image analysis using samples from gradient furnace testing, cold caps, melter suction samples, and discharged glass.

***Calculation of particle settling***

The particle settling is calculated by thick layer approximation (KLA). The base of KLA is the thin layer approximation (NLA) which is used at beginning of the process until the thin layer reaches the value of height of the first control volume above the bottom. At this moment, this first control volume is filled by particles (with prescribed VF concentration) and converted from glass to sludge. Then, the NLA is applied to the top surface of this new sludge control volume. This process is repeated and applied to each control volume which enables sludge layer growth at different rates at different positions on the bottom. The value of total layer height (thin portion plus height of the new sludge control volumes above bottom) is stored into the first bottom material point within the volume concentration field (in same manner as during NLA).
A thin layer algorithm for the particle settling calculation is described here in detail [2]. The Reynolds number of the particles in glass melt is very low, typically in the order of $10^{-8}$. Thus, the momentum of the particles is negligible and the velocity of the particles differs from the velocity of the glass melt only by the Stokes velocity in the vertical direction. The glass flow near the bottom is horizontal. The particles settle on the bottom only by gravitational force and with Stokes' velocity. The Stokes velocity depends on the size and the density of a particle. For one particle species, e.g., $RuO_2$, the density is constant, so the Stokes velocities $w_{si}$ are different for different size classes. In the case of a mixture of different particle species with significantly different densities, separate particle settling calculations must be executed.

In each volume element immediately above the bottom, a height $h_i$ is calculated for size class $i$ with a given time step $\Delta t$:

$$h_i = \Delta t . w_{si} \qquad (30)$$

All particles between the bottom and height $h_i$ above the bottom are falling fast enough to settle on the bottom during $\Delta t$. Thus, the fraction $s_i$ of particles settled from each volume element immediately above the bottom can be calculated as:

$$s_i = \frac{h_i}{\Delta z} \qquad (31A)$$

where $\Delta z$ is the height of a volume element. In the case that some kind of sticking between particles and the bottom surface is considered (caused by surface roughness, particle shape, and other effects), it is expressed by the entrapment distance $h_E$ given by user. This value must lie inside the control volume i.e., $h_E < \Delta z$ and it is added to the height $h_i$, so the resulting height is given by sum of $h_i$ and $h_E$. The fraction $s_i$ of

particles settled from each volume element immediately above the bottom can be now calculated as:

$$s_i = c_{in}\frac{h_i + h_E}{\Delta z} \qquad (31B)$$

Where $c_{in}$ is total volume fraction of particles of class $i$ entering the control volume from all directions. As a result, the number density $N_{V_i}$ decreases by a factor of $s_i$. The number of particles settled from time zero on is stored in the bottom volume elements of the respective number density field. This allows calculation of the height of the sludge layer as:

$$h = \frac{\Delta z \sum_{i=1}^{n} s_i N_{V_i} a_i^3}{C_{sl}} \qquad (32)$$

where $C_{sl}$ represents the volume fraction of the particles in the sludge, also known as the packing density or maximum volume fraction $VF_{NM}$ . $C_{sl}$ or $VF_{NM}$ must be determined experimentally. A typical value reported in the literature is 0.06 $m^3/m^3$ for noble metals.

***Approximation of long time simulation by extrapolation method***

During the calibration of case #B1 it was discovered that the calculation of NM settling (using thick layer approximation) using the reference noble metals concentration of 0.09 kg/kg and small entrapment (below 0.5 mm) would require extremely long computational time, which was not practical for the present effort. This was the basis for adopting a new indirect method that uses higher values of initial concentration and entrapment. These calculations are can be performed within reasonable computation times. Comparison of the settling trends calculated by the accelerated and original methods provided a basis for extrapolation of NM particle behavior and sludge growth.

We need to assume a similarity in settling behavior while using normal and 20-times higher initial concentration of NM, and by using entrapment in the range of 0.1 – 1 mm. The electrical conductivity of the sludge was set to a very high value (by using an electrical conductivity 50 times greater than that of the glass. See [4] and [7] for worst-case influence on melter operation.

## CALCULATION OF PARTICLES RETENTION IN THE MELTER

The key objective of noble metals behavior modeling is the determination of the mass fraction ($MF_{NM}$) of noble metal (in %) retained in the melter as a result of particle settling. $MF_{NM}$ can be calculated as a time dependent value during the model simulation. The model enables two methods of $MF_{NM}$ calculation:

$$MF_{NM}(t) = 100\frac{M(t)_{inj} - M(t)_{disch} - M(t)_{res}}{M(t)_{inj}} \qquad (33)$$

$$MF_{NM}(t) = 100\frac{M(t)_{settl}}{M(t)_{inj}} \quad (34)$$

where
$MF(t)_{NM}$ = is particle retention [%] in the melter until the time t
$M(t)_{inj}$ = is cumulative mass of injected particles until the time t
$M(t)_{disch}$ = is cumulative mass of discharged particles until the time t
$M(t)_{res}$ = is cumulative mass residue of particles in the glass until the time t
$M(t)_{settl}$ = is cumulative mass of settled particles (on the bottom) until the time t
Comparing these two results calculated by (eq.33) and (eq.34) gives us an indication of particle mass balance precision during modeling.

## PROGAM CODES

The semi-transient particle behavior in glass is calculated by a combination of steady states solvers HEART, ELECTRA, COMBUSTOR and transient solver PACO. The program PACO dynamically calculates particle concentration in glass melt. The program HEART calculates temperature and flow in the melter, the program ELECTRA calculates electrical fields in the melter and the program COMBUSTOR calculates the temperature and gas flow in the plenum space. The coupling of melter with plenum space is available by special program GM-CM COUPLE.

The coupling of temperature, flow and electric fields (HEART, ELECTRA) with particle concentration (PACO) in the melter is available by using the “GM-PC Coupling” section in the main Glass Furnace Model Window. There are two programs in this section: SETUP and PACO. The coupling parameters are specified by the SETUP in the “GM-PC Coupling” section and by the INPUT in GM section. Specifying the concentration parameters and calculation of concentration is made by PACO in the “GM-PC Coupling” section.

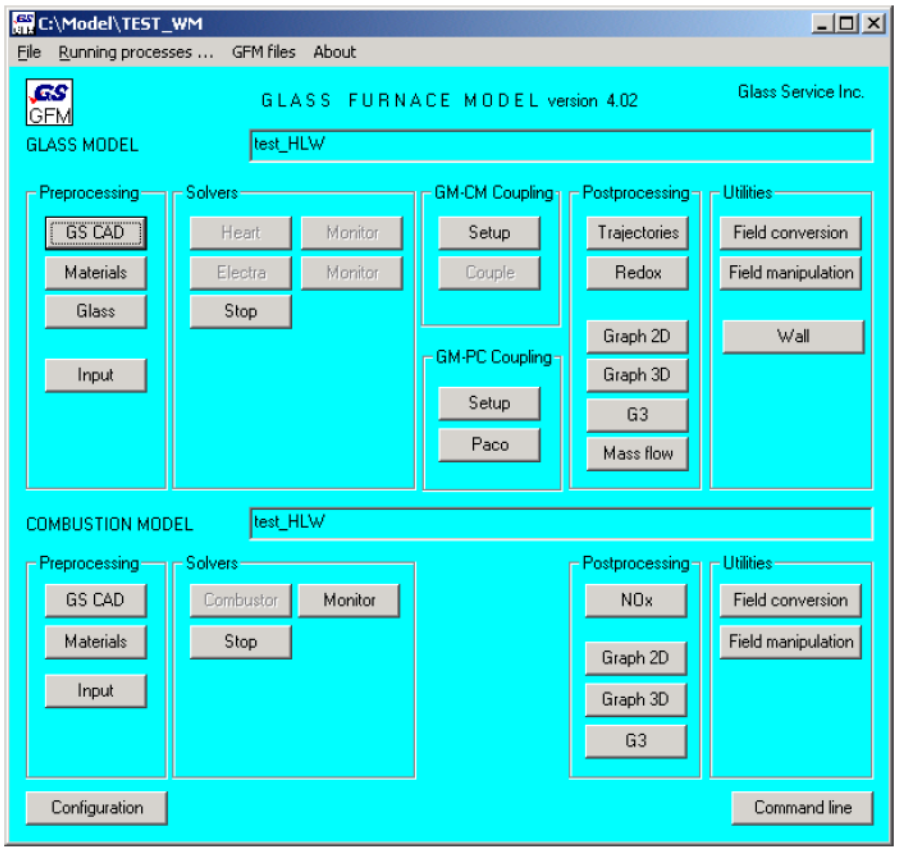


**Figure 1. Glass Furnace Model Operation Window**

***Description of the data files***

The user specifies the name of the project by characters $$$ (for example Ru1). The following data files are generated by the programs:

Computation parameters:
gda.d : binary file involving parameters set in GM INPUT program
gncda.d : binary file involving parameters set in SETUP program
$$$_iter.s : ASCII file involving actual number of iteration
$$$.spi : binary file involving parameters set in PACO program

Physical fields (3dim):
$$$tot.dir : binary file involving total mass concentration of particles
$$$totv.dir : binary file involving total volume fraction of particles [range from 0 to 1] and sludge layer thickness [m] stored in the first material grid below glass
$$$totn.dir : binary file involving total number density of particles
$$$#.dir : binary file involving mass concentration of particle class #
$$$n#.dir : binary file involving number density of particle class #

# MODELING RESULTS

## MODEL DESIGN AND DIMENSIONS

The model design, grid, boundary conditions were generated by GS-CAD program. Two separate models were created, one of glass space (GM) and second of plenum space (CM). The dimension are in [mm] unites. Axis orientation follows:

X: from North to South ; Y: from East to West ; Z: from top to bottom

Each space is displayed here in three cuts:

Horizontal view: XY ; Side view: XZ ; Side view: YZ

The design and dimensions of the WTP melter are based on Duratek WTP conceptual design for the HLW melter described in the Report "HLW Melter Thermal-Hydraulic Model" created by GS for Duratek in November 2001 [4]. The WTP melter differs from the WTP conceptual design HLW melter with a slightly higher position for the discharge throat opening (new center of opening is 13.22 in above the floor, this is a shift upward by 3.6 in), different bubbler assemblies five assemblies with 10 nozzles compared to five nozzles (see Table 1), removal of the bottom electrode, and a different computational grid.

The bubbling tubes were not modeled but approximated by boundary conditions (specifying the gas flow rate) at the position of the nozzles. The complicated pouring system with slanted and vertical canals was approximated by simple straight horizontal pouring canal at leading position of actual throat opening. This approximation has no influence on the NM settling process. The plenum space of WTP melter is identical with the plenum space of HLW melter, see [4].

**Design of the melter (down space, glass space):**

Number of computational grids: NX=66, NY=87, NZ=80,

459360 compu. cells, 1794 kB needed for one field

Inner dimensions [mm]: X=1524, Y=2438, z=1242

Outer dimensions [mm]: X=2895, Y=3352, z=1598

Batch thickness min, max [mm]: 41, 100

Side electrodes [mm]: thickness=152mm, height=330mm

Pouring exit canal: rectangular (Monofrax E), horizontal, center 335 mm above bottom, cross dimensions: y=100mm, z=94mm

Bubbler nozzles: at 51 mm above bottom, horizontal locations see table

**Design of the plenum space (upper space):**

Number of computational grids: NX=58, NY=70, NZ=36,

146160 compu. cells, 571 kB needed for one field

Inner dimensions [mm]: X=1828, Y=2742, z=870

Outer dimensions [mm]: X=3021, Y=3616, z=1224

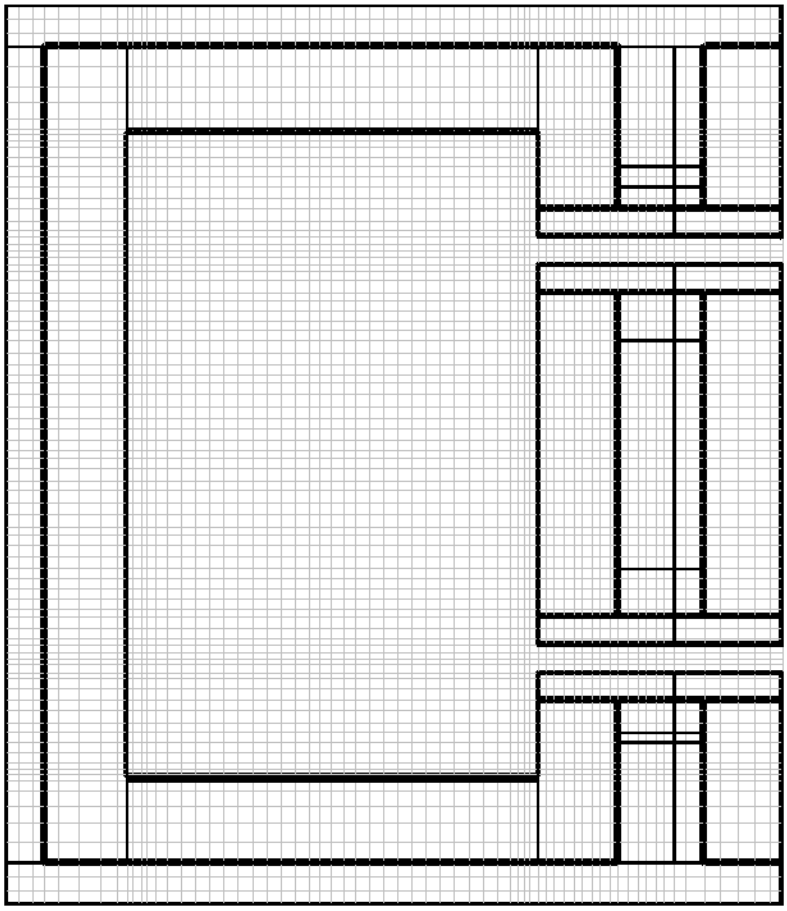

**Figure 2. Glass space: XY Horizontal view through horizontal discharge canals**

Figure 3. Glass space: YZ Side view through side electrodes, bottom electrode, and control thermocouples positions

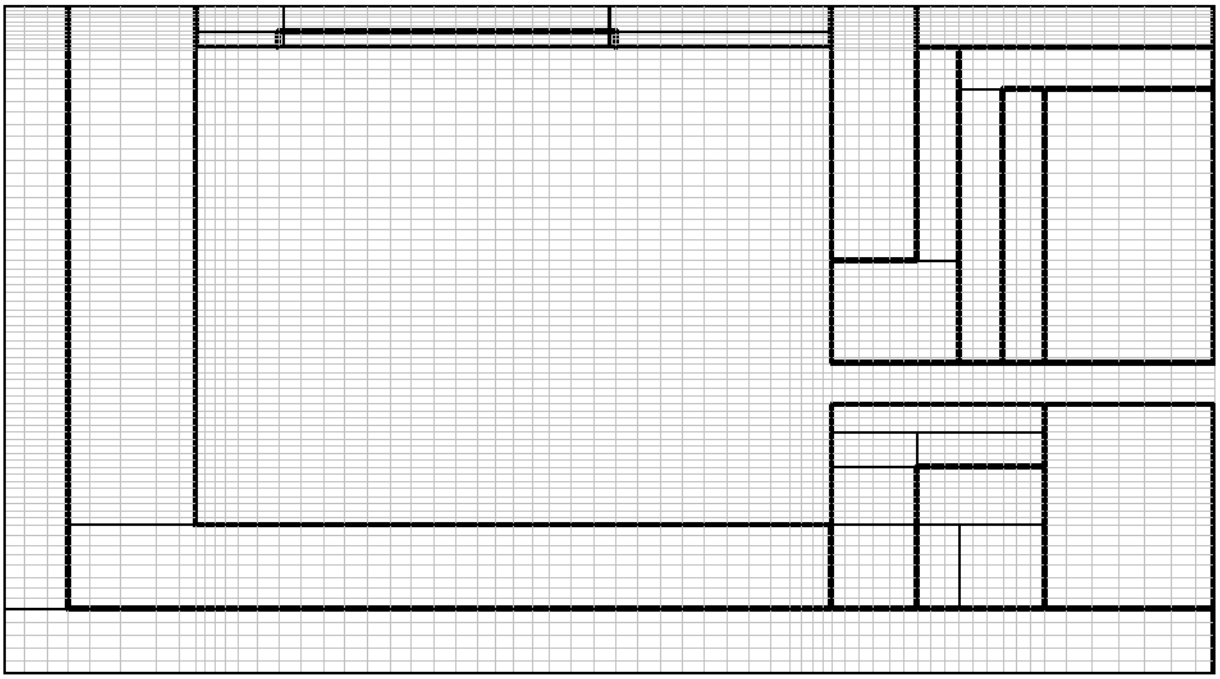

**Figure 4. Glass space: XZ Side view through horizontal discharge canal**

**Duratek WTP melter**
**Bubbler nozzles location [mm]**

| Nozzle No. | $X_{melter}$ | $X_{model}$ | $Y_{melter}$ | $Y_{model}$ | $X_{err}$, cm | $Y_{err}$, cm | $X_{err}$, in | $Y_{err}$, in |
|---|---|---|---|---|---|---|---|---|
| 1 | 863.0 | 842.5 | 1151.0 | 1156.5 | 2.1 | -0.6 | 0.8 | -0.2 |
| 2 | 1066.0 | 1054.5 | 1189.0 | 1192.0 | 1.2 | -0.3 | 0.5 | -0.1 |
| 3 | 863.0 | 842.5 | 2125.0 | 2122.0 | 2.1 | 0.3 | 0.8 | 0.1 |
| 4 | 1066.0 | 1054.5 | 2163.0 | 2160.0 | 1.2 | 0.3 | 0.5 | 0.1 |
| 5 | 1372.0 | 1383.5 | 701.0 | 699.0 | -1.2 | 0.2 | -0.5 | 0.1 |
| 6 | 1575.0 | 1595.5 | 739.0 | 741.0 | -2.1 | -0.2 | -0.8 | -0.1 |
| 7 | 1372.0 | 1383.5 | 1676.0 | 1676.0 | -1.2 | 0.0 | -0.5 | 0.0 |
| 8 | 1575.0 | 1595.5 | 1714.0 | 1712.0 | -2.1 | 0.2 | -0.8 | 0.1 |
| 9 | 1372.0 | 1383.5 | 2651.0 | 2653.0 | -1.2 | -0.2 | -0.5 | -0.1 |
| 10 | 1575.0 | 1595.5 | 2689.0 | 2694.5 | -2.1 | -0.6 | -0.8 | -0.2 |

**Table 1. Location of bubbler nozzles**

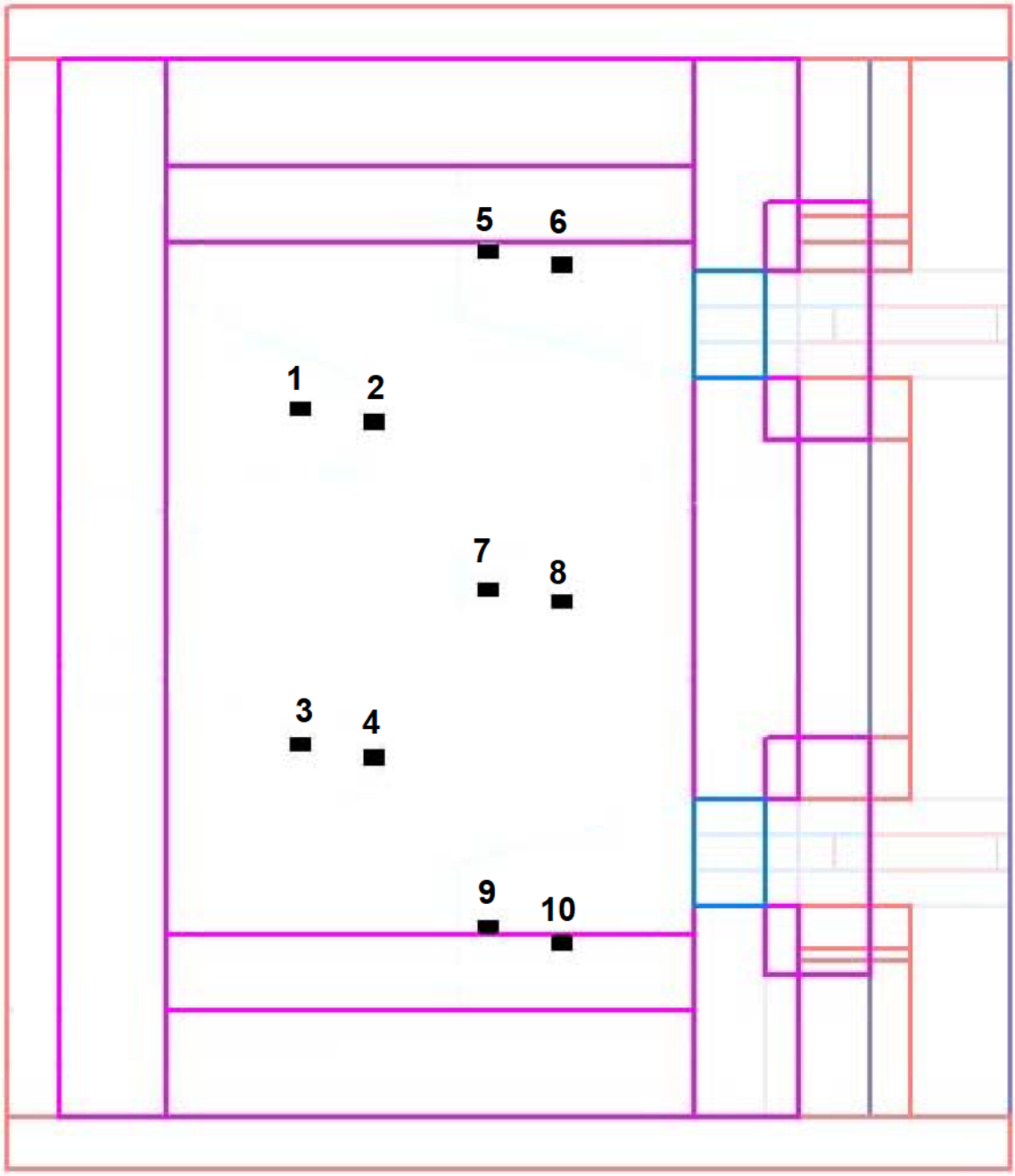


**Figure 5. Designation of the bubbler nozzles in the melter**

# MATERIAL PROPERTIES

Duraboard HD (insulation)

Thermal conductivity: $\lambda = A_\lambda + B_\lambda.T + C_\lambda.T^2$ ; $[\lambda] = W / (K.m)$ ; $T = K$

$A_\lambda$=0.06911445, $B_\lambda$= -3.9405.$10^{-5}$, $C_\lambda$1.2918.$10^{-7}$

Electrical conductivity : $\sigma = 0.001$ ; $[1 / (\Omega.m)]$

Density : $\rho = 416.5$ ; $[kg/m^3]$

Specific heat : $c_p = 1000.0$ ; [J / (kg.K)]

Castable dense (VERSFLOW 57A )

Thermal conductivity: $\lambda = 1.691$ ; [ W / (K.m)]

Electrical conductivity : $\sigma = 0.001$ ; $[1 / (\Omega.m)]$

Density : $\rho = 2550.0$ ; $[kg/m^3]$

Specific heat : $c_p = 1000.0$ ; [J / (kg.K)]

Castable insulated (KAOLITE 2300-li)

Thermal conductivity: $\lambda = A_\lambda + B_\lambda.T + C_\lambda.T^2$ ; $[\lambda] = W / (K.m)$ ; $T = K$

$A_\lambda$=0.221081, $B_\lambda$= 0.0000936236, $C_\lambda$= 0

Electrical conductivity : $\sigma = 0.001$ ; $[1 / (\Omega.m)]$

Density : $\rho = 1089.0$ ; $[kg/m^3]$

Specific heat : $c_p = 1000.0$ ; [J / (kg.K)]

MONOFRAX K3 (refractory block)

Thermal conductivity: $\lambda = A_\lambda + B_\lambda.T + C_\lambda.T^2 + D_\lambda.T^3$ ; $[\lambda] = W / (K.m)$ ; $T = K$

$A_\lambda$=6.04432, $B_\lambda$= -0.00165049, $C_\lambda$ = -1.34655.$10^{-6}$ , $D_\lambda$ = 7.11219.$10^{-10}$

Electrical conductivity : $\sigma = \exp\{A_\sigma + B_\sigma/(T + C_\sigma)\}$ ; $[\sigma] = 1 / (\Omega.m)$ ; $T = K$

$A_\sigma$=19.592, $B_\sigma$= -66507.1, $C_\sigma$= 1847.61

Density : $\rho = 4130.0$ ; $[kg/m^3]$

Specific heat : $c_p = 812.0$ ; [J / (kg.K)]

MONOFRAX H (refractory block)

Thermal conductivity: $\lambda = A_\lambda + B_\lambda.T + C_\lambda.T^2 + D_\lambda.T^3$ ; $[\lambda] = W / (K.m)$ ; $T = K$

$A_\lambda$=6.14209, $B_\lambda$= -0.00637191, $C_\lambda = 5.38874.10^{-6}$ , $D_\lambda = -1.25021.10^{-9}$

Electrical conductivity : $\sigma = \exp\{A_\sigma + B_\sigma/(T + C_\sigma)\}$ ; $[\sigma] = 1 / (\Omega.m)$ ; $T = K$

$A_\sigma$= -1.53722, $B_\sigma$= -2600.76, $C_\sigma$= -2346.02

Density : $\rho = 3350.0$ ; $[kg/m^3]$

Specific heat : $c_p = 659.0$ ; [J / (kg.K)]

MONOFRAX E (refractory block)

Thermal conductivity: $\lambda = A_\lambda + B_\lambda.T + C_\lambda.T^2$ ; $[\lambda] = W / (K.m)$ ; $T = K$

$A_\lambda$=11.3113, $B_\lambda$= -0.0158968, $C_\lambda = 8.48188.10^{-6}$

Electrical conductivity : $\sigma = \exp\{A_\sigma + B_\sigma/(T + C_\sigma)\}$ ; $[\sigma] = 1 / (\Omega.m)$ ; $T = K$

$A_\sigma$= 7.54177, $B_\sigma$= -5137.15, $C_\sigma$= -476.226

Density : $\rho = 4240$ ; $[kg/m^3]$

Specific heat : $c_p = 812.0$ ; [J / (kg.K)]

AZS - ZIRMUL (refractory brick)

Thermal conductivity: $\lambda = 1.89$ ; [ W / (K.m)]

Electrical conductivity : $\sigma = 0.0056$ ; [1 / ($\Omega$.m) ]

Density : $\rho = 3108.0$ ; $[kg/m^3]$

Specific heat : $c_p = 1000.0$ ; [J / (kg.K)]

INCONEL (electrodes)

Thermal conductivity: $\lambda = A_\lambda + B_\lambda.T$ ; $[\lambda] = W / (K.m)$ ; $T = K$

$A_\lambda$=6.64732, $B_\lambda$= 0.018548

Electrical conductivity : $\sigma = \exp\{A_\sigma + B_\sigma/(T + C_\sigma)\}$ ; $[\sigma] = 1 / (\Omega.m)$ ; $T = K$

$A_\sigma$= 13.5128, $B_\sigma$= 91.7459, $C_\sigma$= 228.782

Density : $\rho = 8190$ ; $[kg/m^3]$

Specific heat : $c_p = 371.885 + 0.266399*T$ ; [J / (kg.K)]

## GLASS AND BATCH PROPERTIES

The glass HLW98-31 was used and following properties were implemented:

Thermal conductivity: $[\lambda] = W / (K.m)$ ; $[T] = K$

$\lambda = 1.78 + 0.0004.T$ for $300K < T < 1000K$

$\lambda = 2.73746 - 0.00242144.T + 1.86384.10^{-6}.T^2$

Electrical conductivity : $\sigma = \exp\{A_\sigma + B_\sigma/(T + C_\sigma)\}$ ; $[\sigma] = 1 / (\Omega.m)$ ; $[T] = K$

$A_\sigma = 5.75735$, $B_\sigma = -1335.04$, $C_\sigma = -771.441$ for $1000K < T < 1700 K$

Density : $[\rho] = [kg/m^3]$ ; $[T] = K$

$\rho = 2750.28 - 0.249829. T$

Kinematic viscosity : $\nu = \exp\{A_\nu + B_\nu/(T + C_\nu)\}$ ; $[\nu] = m^2/s$ ; $[T] = K$

$A_\nu = -15.9565$, $B_\nu = 10772$, $C_\nu = -305.191$ for $1050K < T < 1600 K$

Specific heat : $c_p = 1350.0$ ; [J / (kg.K)] (a constant value approximation)

Feed and cold cap thermal conductivity:

$\lambda = 0.06571 + 0.002114.T$ for $300K < T < 1000K$

## NOBLE METAL AND SLUDGE PROPERTIES

The noble metals (NM) were considered to be particles of $RuO_2$, that represent the highest concentration of the noble metals and the most troublesome NM sludge component. The ruthenium oxide particles enter the glass space from bottom layer of the cold cap. The density of a pure particle ( $\rho_P$ ) is 6970 kg/m$^3$.

The particle volume fraction cV and mass fraction cM are recalculated by using reference glass density of $\rho G = 2395.0$ kg/m3 by a formula $cM = cV . (\rho P / \rho G)$, where $\rho P$ designates particle density.

The initial concentration of injected particles is given for each Test in Table 2 (nominal value is 0.09 wt%).

The maximum volume fraction of particles in the sludge layer is 6 vol % (a literature value).

The properties of a mixture of glass and noble metals are given by Eq.1 and Eq.2 in chapter 2.5.2. of [4]. The sludge is a mixture with maximum content of noble metals which is stated as C Vmax = 6 vol%. The coefficients of property formula follows:

| Property | A1 | A2 | B |
|---|---|---|---|
| Electrical Conductivity | 50.0 | 0 | 1.825 |
| Kinematic viscosity | 1014.95 | -0.609 | 1.5 |
| Thermal conductivity | 1.0 | 0 | 0 |

## BOUNDARY CONDITIONS

Thermal boundary conditions (TBC) and flow boundary conditions (FBC) were provided in both the glass space and plenum space.

### *Glass space – thermal boundary conditions*

South-wall:

The discharge chamber has not been modeled. The modeled south wall (discharge wall) is covered by 6 boundary planes where 6 boundary conditions are applied. At the position of the discharge chamber there is applied one TBC Type 3: Heat transfer, radiative, ambient tem. $T_a$ = 1100°C. Next to the discharge chamber there are applied 3 intermediate TBC Type 1: Constant heat flux $q_w$ = 0 kW/m$^2$ . On the outlet plane (pouring) there is applied TBC type 1: Constant heat flux $q_w$ = 0 kW/m$^2$ . The rest of south wall is covered by TBC Type 3: Heat transfer specified by ambient temperature 25 °C and heat transfer coefficient α = -6.57 + 0.053.$T_w$ , where $T_w$ is wall surface temperature.

North-, west-, east-wall and bottom:

On the north-, west-, east-walls and on the bottom there are applied TBC type 3: Heat transfer specified by ambient temperature 25 °C and heat transfer coefficient α = -6.57 + 0.053.$T_w$ where $T_w$ is wall surface temperature.

Top surface:

The top surface is covered by feed input, by batch, by glass or by walls. On the top boundary plane there is applied heat flux coming from plenum space according to the TBC generated by coupling procedure.

Feed input:

The feed is brought from the top using two imaginary streams coming through the plenum space. The input temperature of the feed at the batch surface is specified by a constant temperature of 40 ° C.

### *Glass space – FLOW boundary conditions*

Output:

Instead of the risers, a simple horizontal outlet canal approximations are used. A mass flow of average value of glass production 0.0347222 kg/s or 3,000 kg/day (total) is applied on the end canal plane (each exit 0.0173611 kg/s)

Input:

The feed is brought in from the top using two imaginary streams coming through the plenum space. The input flow BC (mass flow kg/s) is specified by the average value of the glass production rate. The water content of 70.05 wt% of $H_2O$ is specified within the input parameters using program INPUT.

### *Plenum space – thermal boundary conditions*

South-wall:

The discharge chamber is being not modeled and the same boundary condition system is applied as in the glass space.

North-, west-, and east-wall :

On the north-, west-, east-walls and on the bottom there are applied TBC type 3: Heat transfer specified by ambient temperature 25 °C and heat transfer coefficient $\alpha = -6.57 + 0.053.T_w$ where $T_w$ is wall surface temperature.

Bottom surface:

The bottom surface is covered by feed input, by batch, by glass or by walls. On the bottom boundary plane there is applied a temperature distribution coming from glass space according to the TBC generated by coupling procedure.

Top Surface:

Generally, the TBC type 3 is applied: Heat transfer specified by ambient temperature 25 °C and heat transfer coefficient $\alpha = -6.57 + 0.053.T_w$ , where $T_w$ is wall surface temperature.

### *Plenum space – FLOW boundary conditions*

Output:

The off gas exit is located on top surface and it covers summation of mass flows of evaporated water from feed and reaction gases from batch and of in-leakage air. The values are transferred from glass space by coupling procedure.

Inputs:

The gas input mass flow consists of evaporated water from feed and reaction gases from batch. The value is transferred from glass space by coupling procedure. Moreover, on in-leakage planes (air inputs) there are applied TBC type 2: Constant temperature of 32 o C.

### *$RuO_2$ particle size distribution*

The entering RuO2 particles are rectangular rods with average width b=0.7 μm and lengths L from 0.5 to 21 μm. The measured length distributions are displayed in Figure 30 and 31 in the report “Modeling the behavior of noble metals during HLW vitrification” [5]. Both the measurements were assembled together and an average resulting size distribution was calculated, see Table 7 of Report [5]. In order to accelerate the computation speed, only 3 new classes were created and their parameters needed for PACO program are listed in Table 2. Within Table 2, the rods were transformed into cubes of identical volume. The cube size *a* is given by the formula $a=b^{2/3}.L^{1/3}$

Table 2. Particle size distribution – class parameters for PACO program

DURATEK WTP MELTER

RuO2 particle class distribution for input cm-0.0009 kg/kg and 0.018 kg/kg

| | | | | | | For NM glass conc. of 0.09wt% | | For NM glass conc. of 1.8wt% | |
|---|---|---|---|---|---|---|---|---|---|
| class | length range | cube size range | central size | width | particle content | mass fraction. | number density | Mass fraction | density |
| | μm | μm | μm | μm | % | [kg/kg] | [1/m3] | [kg/kg] | [1/m3] |
| 1 | 0-1.5 | 0-0.9 | 0.45 | 0.9 | 8.4 | $7.56E^{-05}$ | $2.85E^{+14}$ | $1.51E^{-03}$ | $5.70E^{+15}$ |
| 2 | 1.5-6.5 | 0.9-1.5 | 1.2 | 0.6 | 73.4 | $6.61E^{-04}$ | $1.31E^{+14}$ | $1.32E^{-02}$ | $2.63E^{+15}$ |
| 3 | 6.5-16.5 | 1.5-2.0 | 1.75 | 0.5 | 18.2 | $1.64E^{-04}$ | $1.05E^{+13}$ | $3.28E^{-03}$ | $2.10E^{+14}$ |

## CALCULATED CASES

Using the GFM code, four different operating modes were simulated WTP tests #B1, #B5, #B6 and idling #B7. The modified model was calibrated on test #B1. The calibration was used to adjust the material properties to actual conditions, to find a steady state approximation of periodical feeding and pouring, to tune the evaporation of the water from the slurry surface, to adjust the PD constants of the electrical power control, and to estimate the entrapment distance during NM settling.

The electric heating was controlled by model PD controller of electrode potentials with constants: P=1.5, D=20 within 5 iteration period. The average value of 6 temperature points at the positions of the thermocouples was used with a control set-point of 1150 °C. An example of the course of PD controller function is displayed on Figure 6, where the total electrical power Qgl (inside glass) and Qtot (inside glass and materials) oscillates with high intensive damping. The steady constant value has been reached after 10000 iterations.

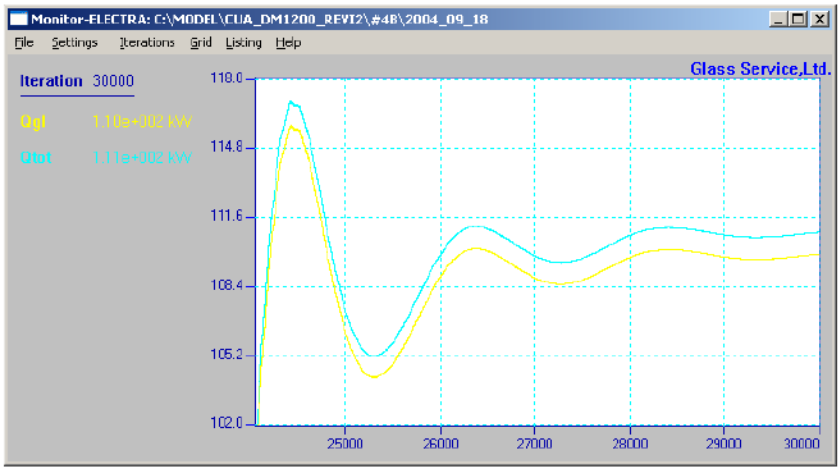


Figure 6. PD automatic model control of electrical power in the melter.

The input and operation melter parameters of calculated cases are listed in Table 3. During each test several runs were calculated.

| DURATEK WTP MELTER : CALCULATED CASES | | | | | | | | | | |
|---|---|---|---|---|---|---|---|---|---|---|
| | NM | Entrap | No.of | Prop.factor | | | | Common display time | | |
| Case designation | Injection | ment | Bubbler | of sludge | Simulated actual time | | | of sludge layer pattern | | |
| | wt% | mm | nozzles | El.condu. | sec | min | hr | min | min | min |
| #B1C1,8E1,0 | 1.8 | 1 | 10 | 1 | 241200 | 4020 | 67 | 1380 | 2000 | |
| #B1C1,8E0,5 | 1.8 | 0.5 | 10 | 1 | 121200 | 2020 | 33.67 | | 2000 | |
| #B1C1,8E0,1 | 1.8 | 0.1 | 10 | 1 | 220800 | 3680 | 61.33 | | 2000 | |
| #B1C1,8E1,0EL2x | 1.8 | 1 | 10 | 2 | 237600 | 3960 | 66 | | 2000 | |
| #B1C1,8E1,0EL5x | 1.8 | 1 | 10 | 5 | 168000 | 2800 | 46.67 | | 2000 | |
| #B1C0,09E0,1 | 0.09 | 0.1 | 10 | 1 | 337800 | 5630 | 93.83 | | | |
| #B1C0,09E1,0 | 0.09 | 1 | 10 | 1 | 793200 | 13220 | 220.33 | | | 10200 |
| #B5C1,8E1,0 | 1.8 | 1 | 8 | 1 | 129600 | 2160 | 36 | 1380 | | |
| #B5C0,09E1,0 | 0.09 | 1 | 8 | 1 | 662400 | 11040 | 184 | | | 10200 |
| #B6C1,8E1,0 | 1.8 | 1 | 6 | 1 | 828000 | 1380 | 23 | 1380 | | |
| #B6C0,09E1,0 | 0.09 | 1 | 6 | 1 | 620400 | 10340 | 172.33 | | | 10200 |
| #B7C0,09E1,0 | 0.09 | 1 | 10 | 1 | 962400 | 16040 | 267.33 | | | |

The different case designations used the following flow and temperature assumptions.

| **Characteristic of modeling (all case designations beginning with)** | **WTP Case** | ***Glass Service Case*** | **Number of Nozzles** | **Nozzle Flow Rate, ACFM** | **Setpoint Temperature[#], C** | **Average Glass Temperature[#], C** | **Specific Bubbling Rate, ACFM / $m^2$** | **Specific Bubbling Rate, SCFM / $m^2$** |
|---|---|---|---|---|---|---|---|---|
| **#B1** | 1 | B2 | 10 | 1.15 | 1150 | 1139 | 3.09 | 1.10 |
| **#B5** | 2 C | B5 | 8 | 1.15 | 1150 | 1141 | 2.47 | 0.88 |
| **#B6** | 2 D | B6 | 6 | 1.15 | 1150 | 1139 | 1.85 | 0.66 |
| **#B7** | 2 E | B7-0.1 | 10 | 0.1 | 1050 | 1022 | 0.27 | 0.10 |

Table 3. Modeled cases input parameters and total simulated time summary

### *Coupled model calculation results*

The results for the coupled model for four different bubbler conditions are cases #B1, #B5, #B6, and #B7, which modeled the nominal, nominal with one failed bubbler, nominal with two failed bubblers, and idling at a reduced bubbling rate, respectively. The respective results are presented in Figures 7, 8, 9, 10 where the same temperature and flow scales are used.

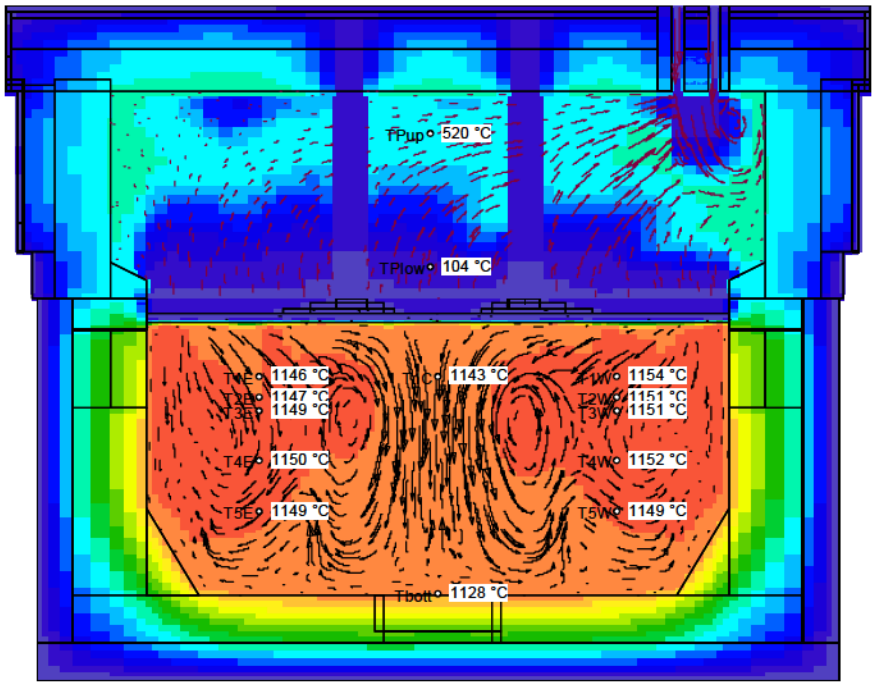


Figure 7a. Flow (streamlines) and temperature (color) distribution in YZ central cut of WTP melter, case #B1 (WTP case 1)

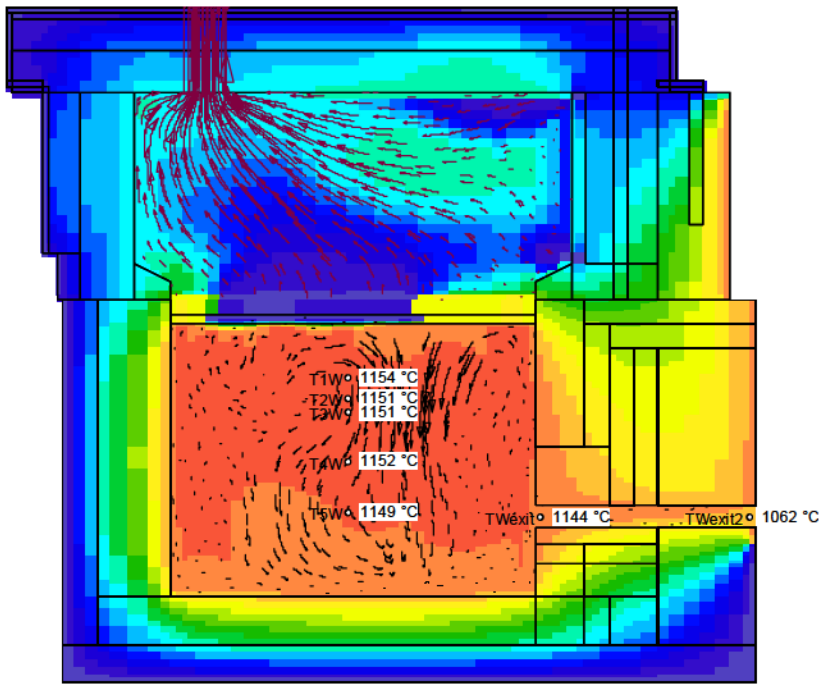


Figure 7b. Flow (streamlines) and temperature (color) distribution in XZ cut through the west pouring canal of WTP melter, case #B1 (WTP case 1)

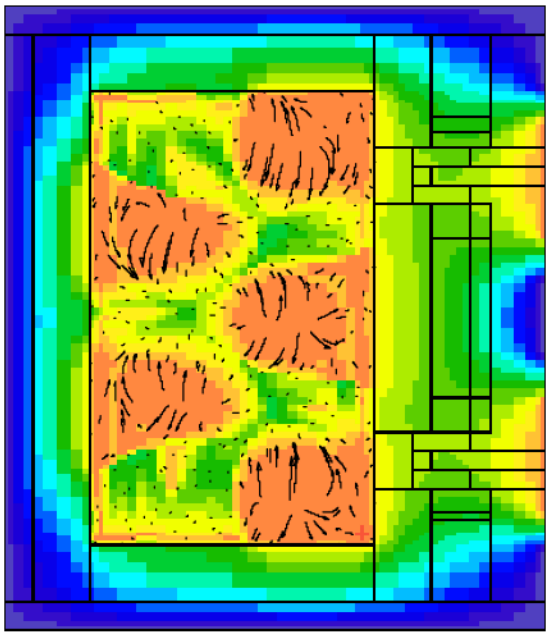

Figure 7c. Flow (streamlines) and temperature (color) distribution in XY cut at the first layer below the cold cap of WTP melter, case #B1 (WTP case 1)

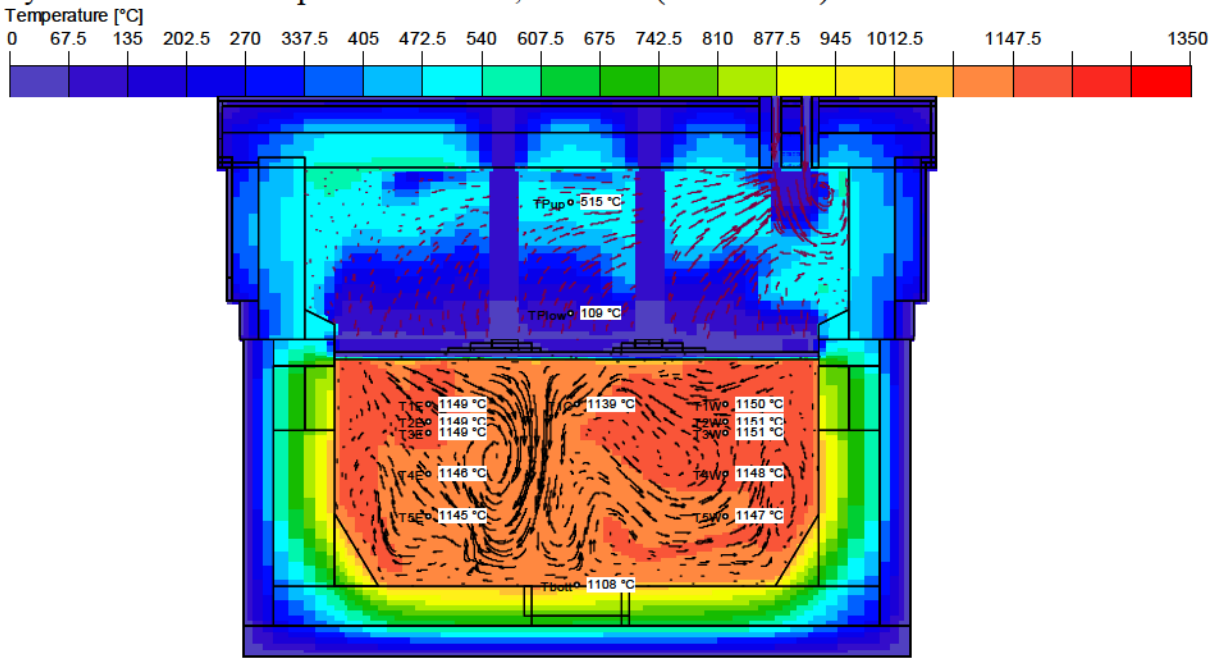


Figure 8a. Flow (streamlines) and temperature (color) distribution in YZ central cut of WTP melter, case #B5 (WTP case 2C)

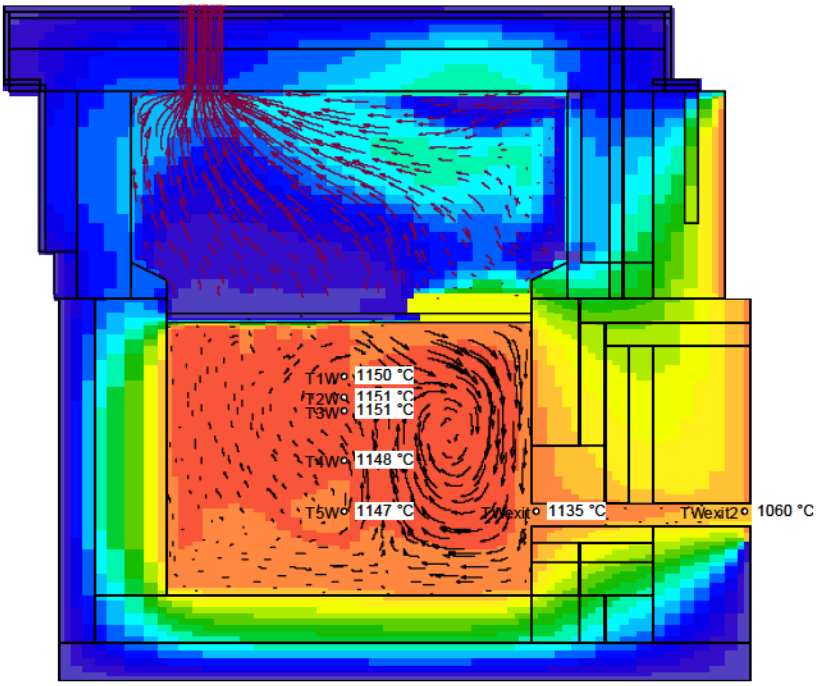


Figure 8b. Flow (streamlines) and temperature (color) distribution in XZ cut through the west pouring canal of WTP melter, case #B5 (WTP case 2C)

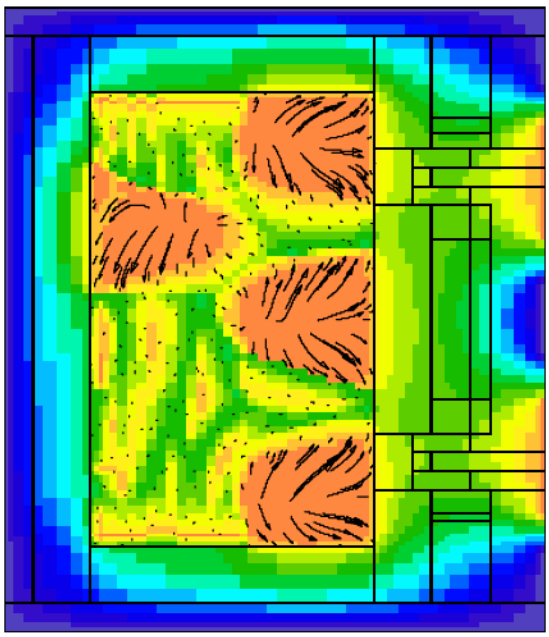

Figure 8c. Flow (streamlines) and temperature (color) distribution in XY cut at the first layer below the cold cap of WTP melter, case #B5 (WTP case 2C)

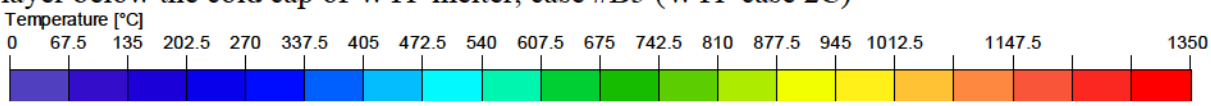

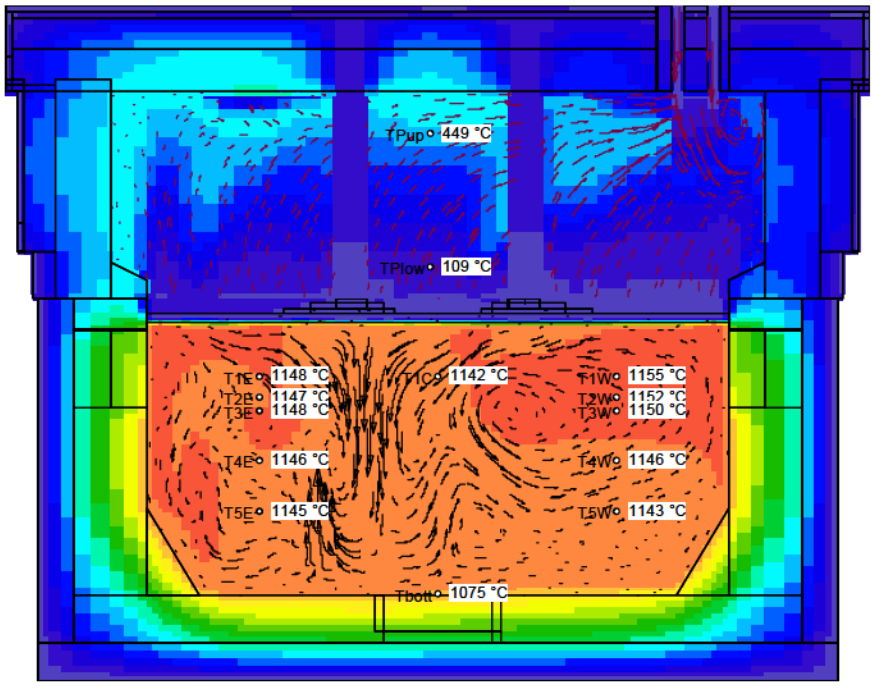


Figure 9a. Flow (streamlines) and temperature (color) distribution in YZ central cut of WTP melter, case #B6 (WTP case 2D)

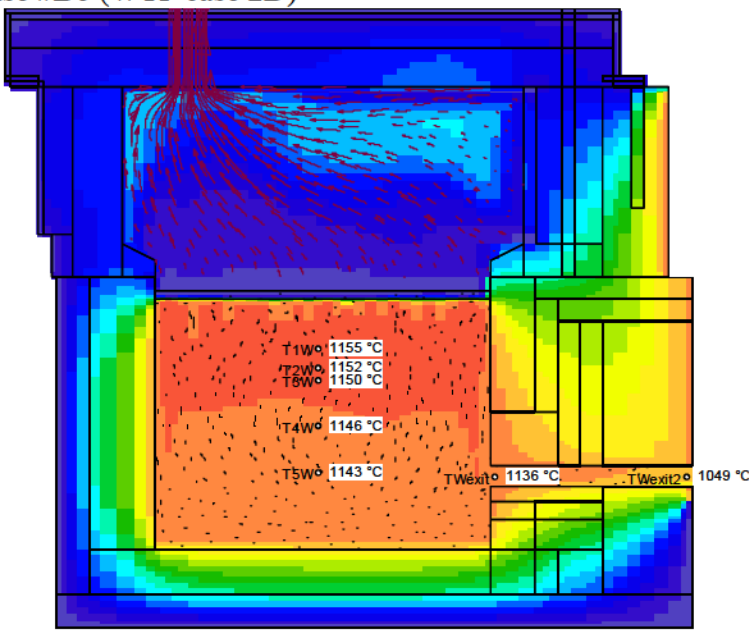


Figure 9b. Flow (streamlines) and temperature (color) distribution in XZ cut through the west pouring canal of WTP melter, case #B6 (WTP case 2D)

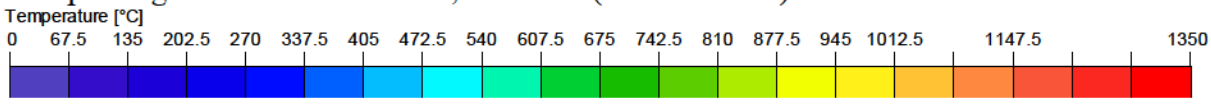

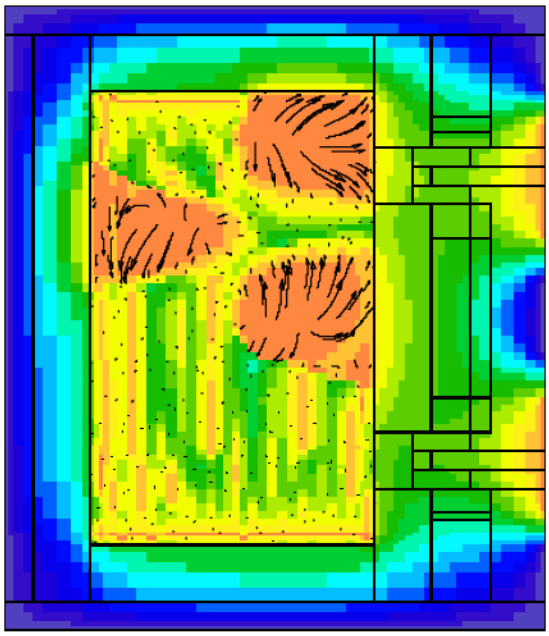

Figure 9c. Flow (streamlines) and temperature (color) distribution in XY cut at the first layer below the cold cap of WTP melter, case #B6 (WTP case 2D)

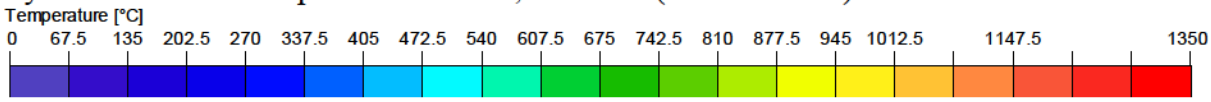

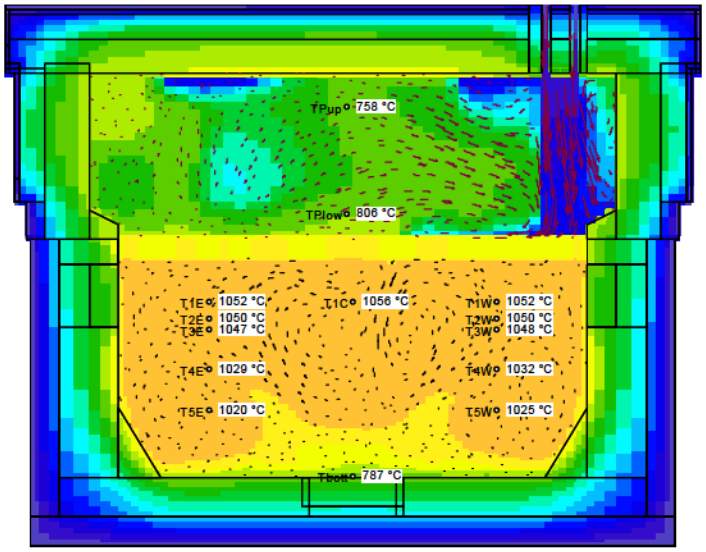


Figure 10a. Flow (streamlines) and temperature (color) distribution in YZ central cut of WTP melter, case #B7 (WTP case 2E idling)

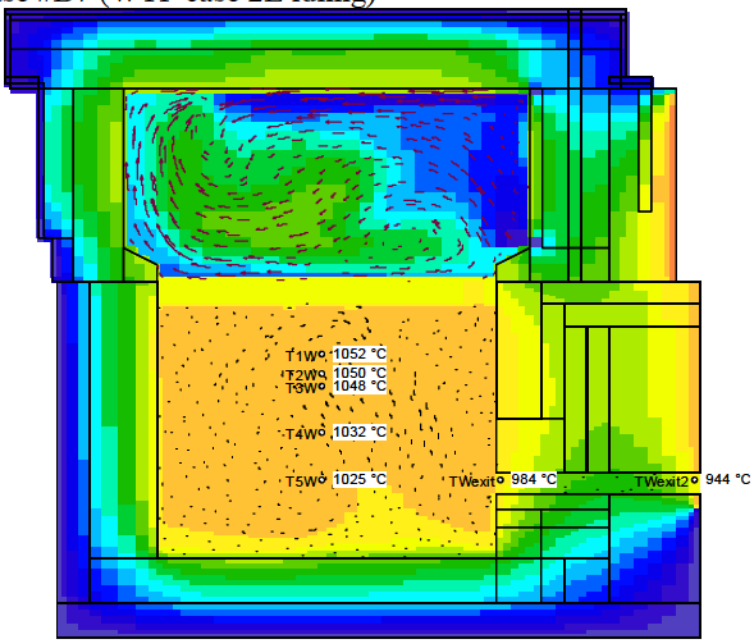


Figure 10b. Flow (streamlines) and temperature (color) distribution in XZ cut through the west pouring canal of WTP melter, case #B7 (WTP case 2E idling)

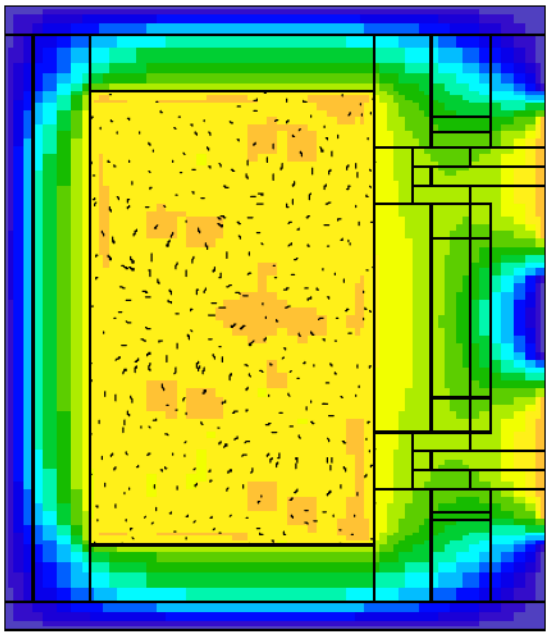

Figure 10c. Flow (streamlines) and temperature (color) distribution in XY cut at the first glass layer of WTP melter, case #B7 (WTP case 2E idling)

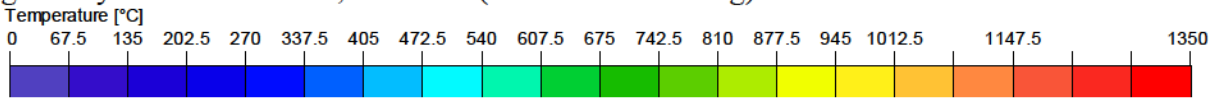


***Graphical display of melter flow, temperature, electrical quantities, and NM settling calculation results***

The 2-D graphs show combinations of 2 or 3 physical quantities in each slide at the final times (see simulated actual time in Table 3) in Figure 11- Figure 16.

Figure 11a shows color fill of temperature, velocity streamlines, and sludge layer isolines in the middle YZ cut. Figure 11b shows Joulean heat and temperature isolines in the middle YZ cut. Figure 11c displays the electrical current density (color fill), vector of electrical current and isolines of electrical potential in the middle YZ cut. Figure 11d shows color fill of NM concentration and vector of electrical current on horizontal XY cut at one grid above the bottom. Figure 11e shows color fill of NM sludge layer height [m] above the bottom using horizontal XY projection view.

It was found that the noble metals did not settle uniformly but settled in separate piles located around the bubbler nozzles, see Figure 11d and Figure 11e. The slanted bottom is covered rather deeply by NM. In case of specifying fast settling (high NM injection of 1.8 wt% and high entrapment of 1mm) tall NM columns rise in some positions (see Figure 11a and Figure 11c). This phenomenon could be caused by numerics of the settling algorithm or by the fact there is no feedback of unlimited growth inside the program PACO algorithm (that is there is no numeric method for piles to collapse, slump or otherwise approximate reality within the subroutine). The generation of a more sophisticated algorithm (considering particle agglomeration, hindered settling, piles interaction and collapsing, etc.) is outside the scope of this project.

Because there was no sludge measurements in test melters, the entrapment parameter is given by simple a constant without any dependency on glass velocity, surface

conditions (refractory, existing flat or wavy or slanted sludge), or other conditions. The lack of experimental knowledge of the entrapment parameter might also be the cause of the columns rising. Fortunately, it is evident form the cumulative and settling curves (see Figure 20 – Figure 23) that the existence of NM columns does not change the global settling quantities very much (the curves are continuous).

Figure 17a, Figure 17b, and Figure 17c show sludge layer height distribution (by color fill) in the vertical projection through XY planes above the flat and slanted bottom for case #B1, #B5, #B6 for 20-times enhanced RuO2 concentration of 1.8wt% and entrapment=1.0mm at the same time =1380 min = 23 hr. The influence of the missing bubbler(s) in cases #B5 and #B6 is quite evident.

Figure 18a, Figure 18b, and Figure 18c show sludge layer height distribution (by color fill) in the vertical projection through XY planes above the flat and slanted bottom of the cases #B1, #B5, #B6 for actual RuO2 concentration of 0.09wt% and entrapment=1.0mm at same time=10200 min = 170 hr. The influence of the missing bubblers in cases #B5 and #B6 is clearly indicated The character of sludge piles development in both the initial RuO2 high concentrations of 1.8 wt% and 0.09wt% is practically the same. Since the results are nearly the same between the two concentrations but for different times, this allows us to accelerate the calculation of noble metal settling through extrapolations as described in Chapter 3.6.4.

Figure 19a, Figure 19b, Figure 19c, Figure 19d, and Figure 19e show sludge layer height distribution (by color fill) in vertical projection through XY planes above flat and slanted bottom of the case #B1 for 20-times enhanced RuO2 concentration of 1.8wt% and various entrapment heights (1.0, 0.5, and 0.1 mm) at the same time=2000 min = 33.33 hr. The character of sludge piles for all cases is practically identical which also supports the use of extrapolations described in chapter 3.6.4.

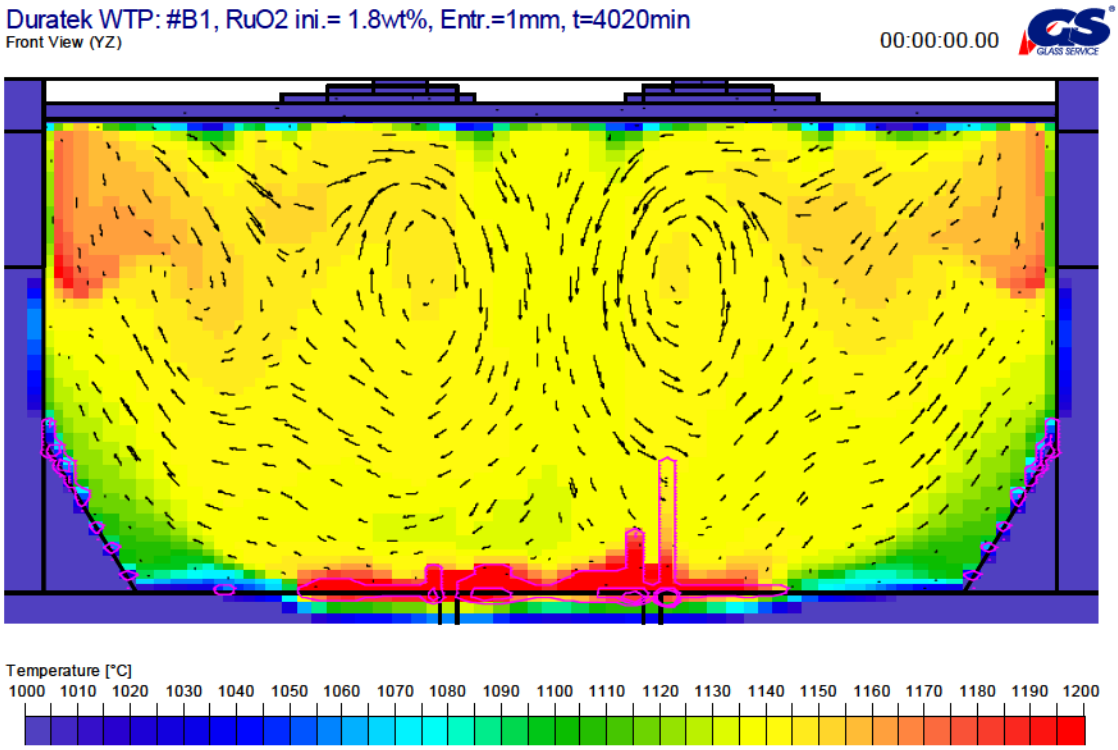


Figure 11a. Temperature distribution (color fill), velocity streamlines, and isolines of NM sludge concentration in the middle YZ cut of case #B1C1,8E1,0 (WTP case 1)

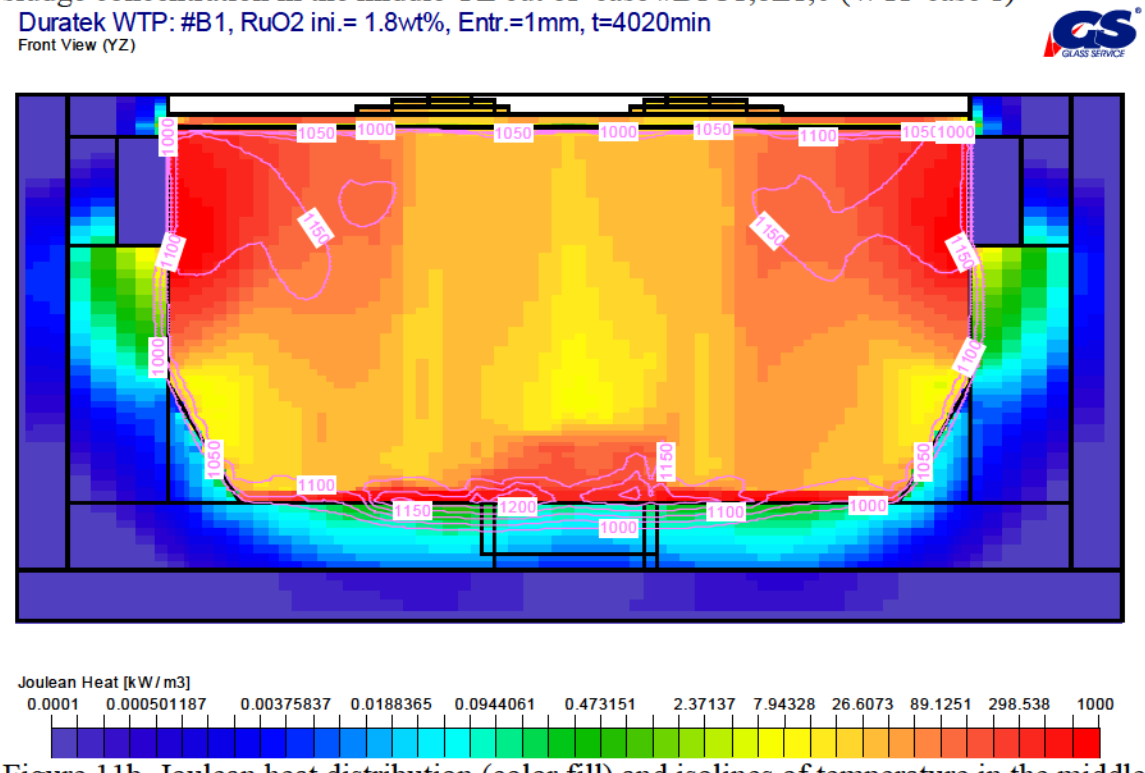


Figure 11b. Joulean heat distribution (color fill) and isolines of temperature in the middle YZ cut of case #B1C1,8E1,0 (WTP case 1)

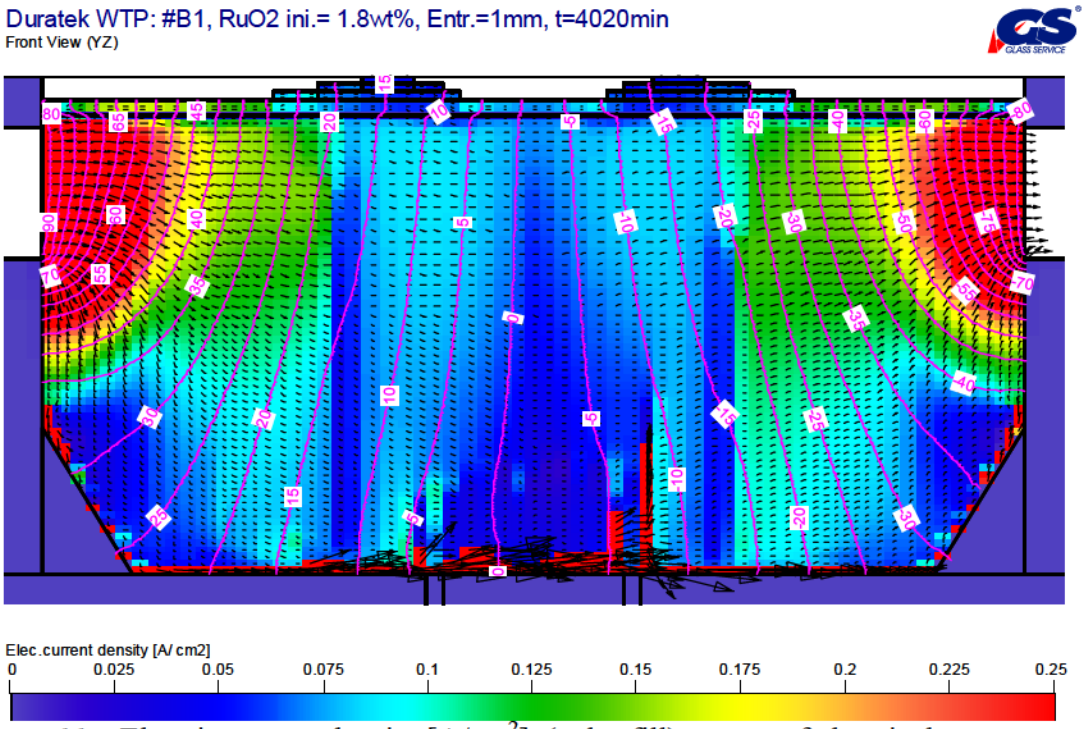


Figure 11c. Electric current density [A/cm$^2$] (color fill), vector of electrical current, and electrical potential isolines in the middle YZ cut of the case #B1C1,8E1,0 (WTP case 1)

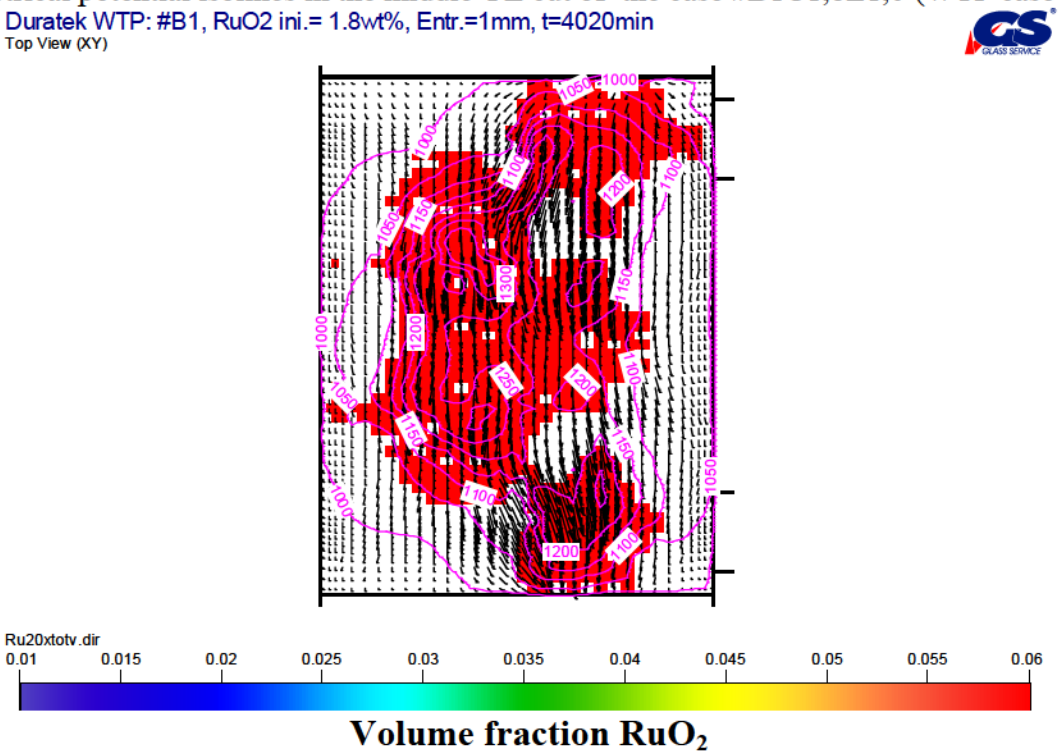


Figure 11d. Sludge layer pattern (color fill), isolines of temperature, and vector of electrical current in horizontal cut XY at one grid above bottom of the case #B1C1,8E1,0 (WTP case 1)

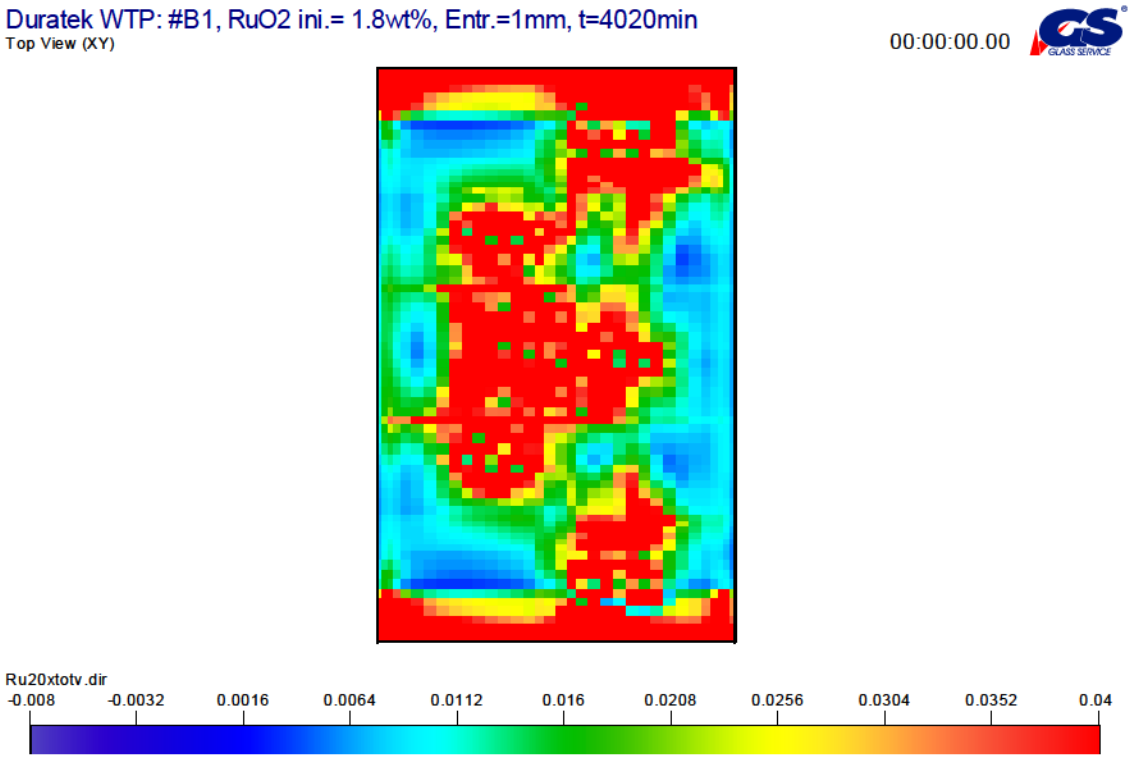


Figure 11e. Sludge layer height distribution (color fill) in vertical projection through XY planes above flat and slanted bottom of the case #B1C1,8E1,0 (WTP case 1)

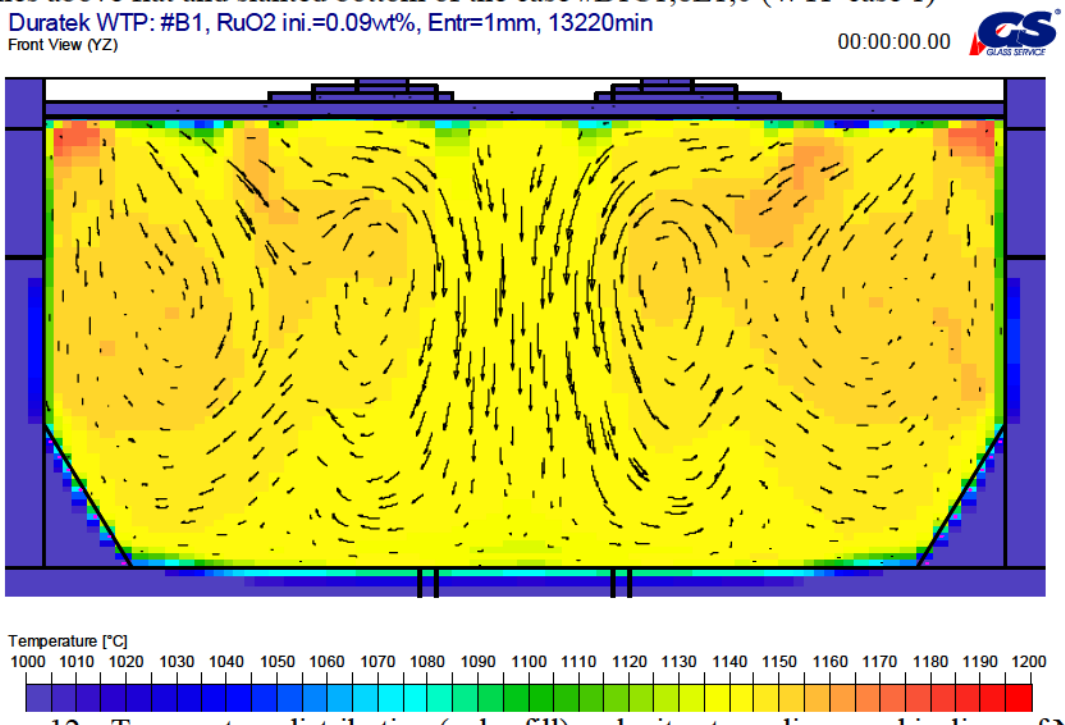


Figure 12a. Temperature distribution (color fill), velocity streamlines, and isolines of NM sludge concentration in the middle YZ cut of case #B1C0,09E1,0 (WTP case 1)

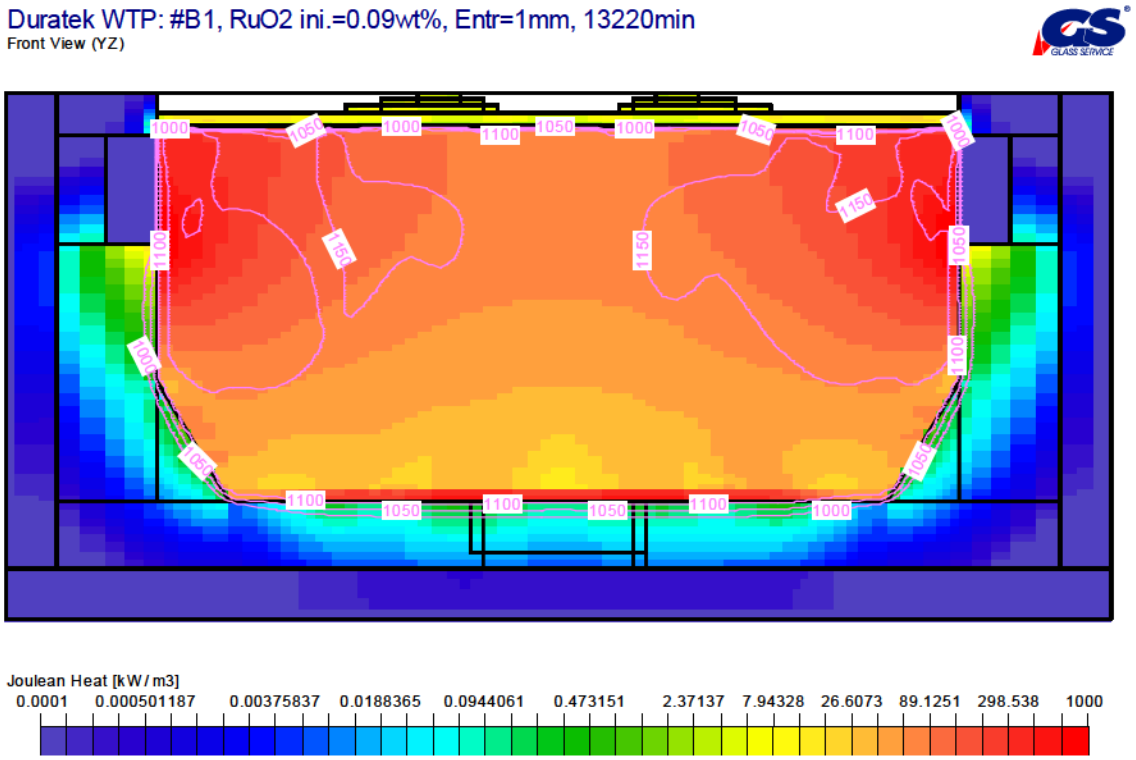


Figure 12b. Joulean heat distribution (color fill) and isolines of temperature in the middle YZ cut of case #B1C0,09E1,0 (WTP case 1)

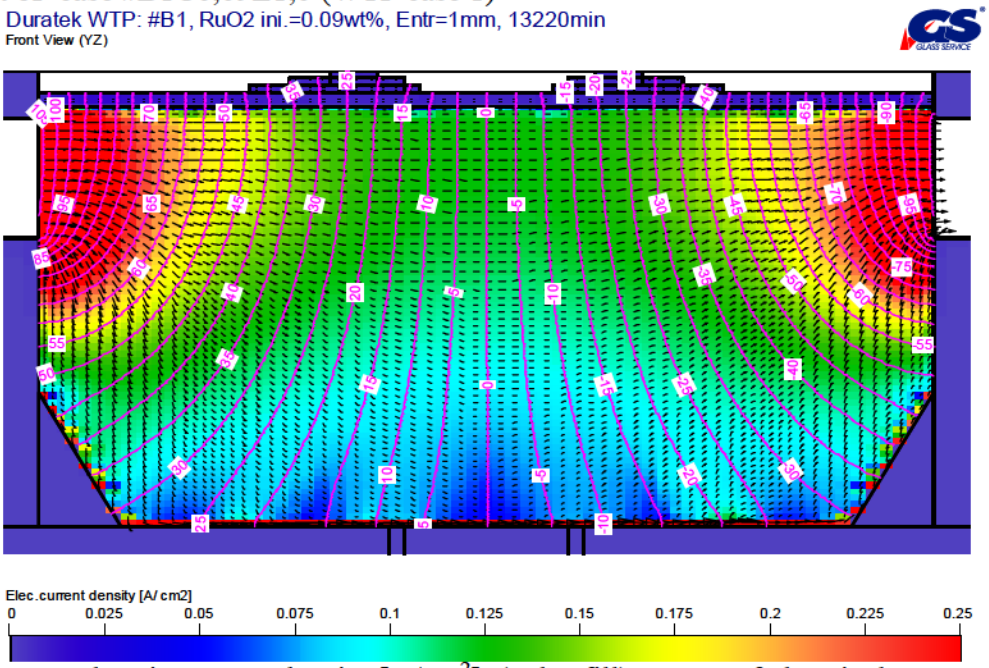


Figure 12c. Electric current density [A/cm$^2$] (color fill), vector of electrical current, and electrical potential isolines in the middle YZ cut of the case #B1C0,09E1,0 (WTP case 1)

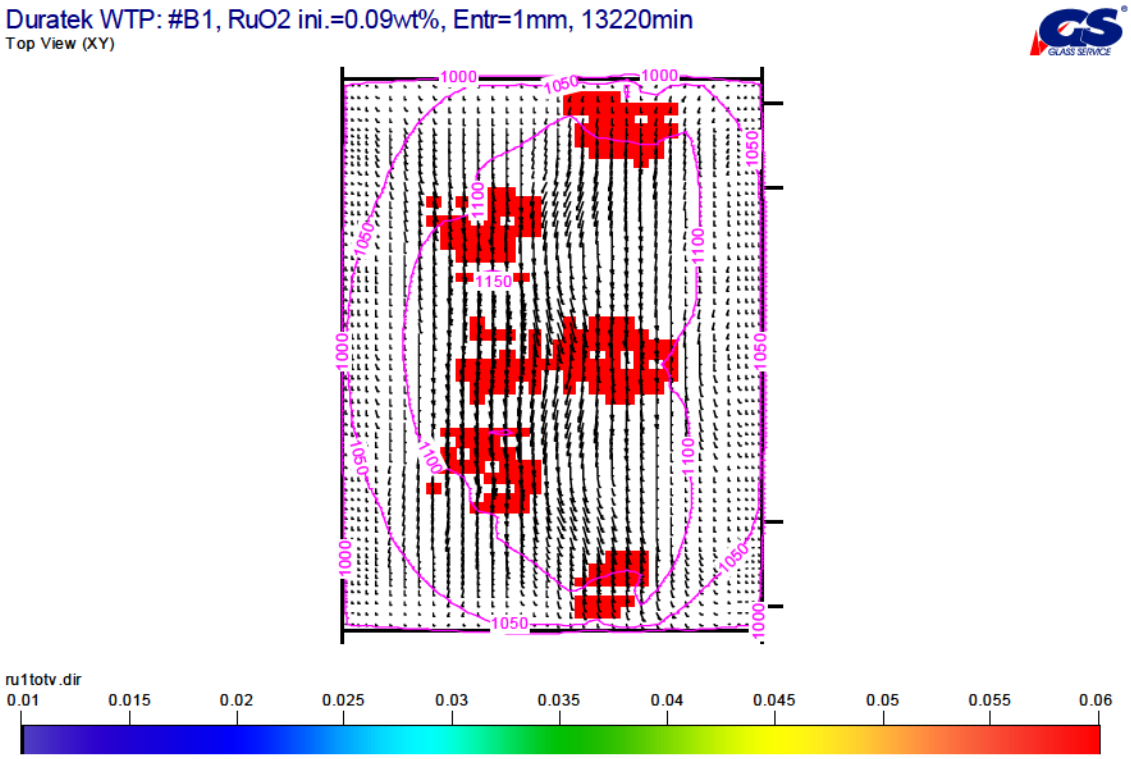


Figure 12d. Sludge layer pattern (color fill), isolines of temperature, and vector of electrical current in horizontal cut XY at one grid above bottom of the case #B1C0,09E1,0 (WTP case 1)

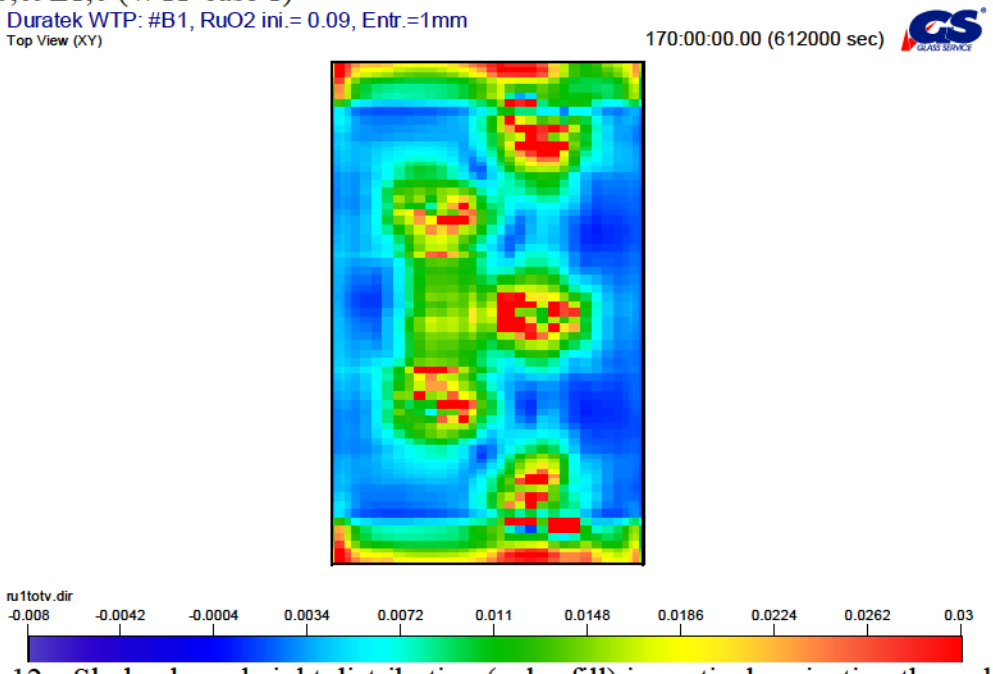


Figure 12e. Sludge layer height distribution (color fill) in vertical projection through XY planes above flat and slanted bottom of the case #B1C0,09E1,0 (WTP case 1)

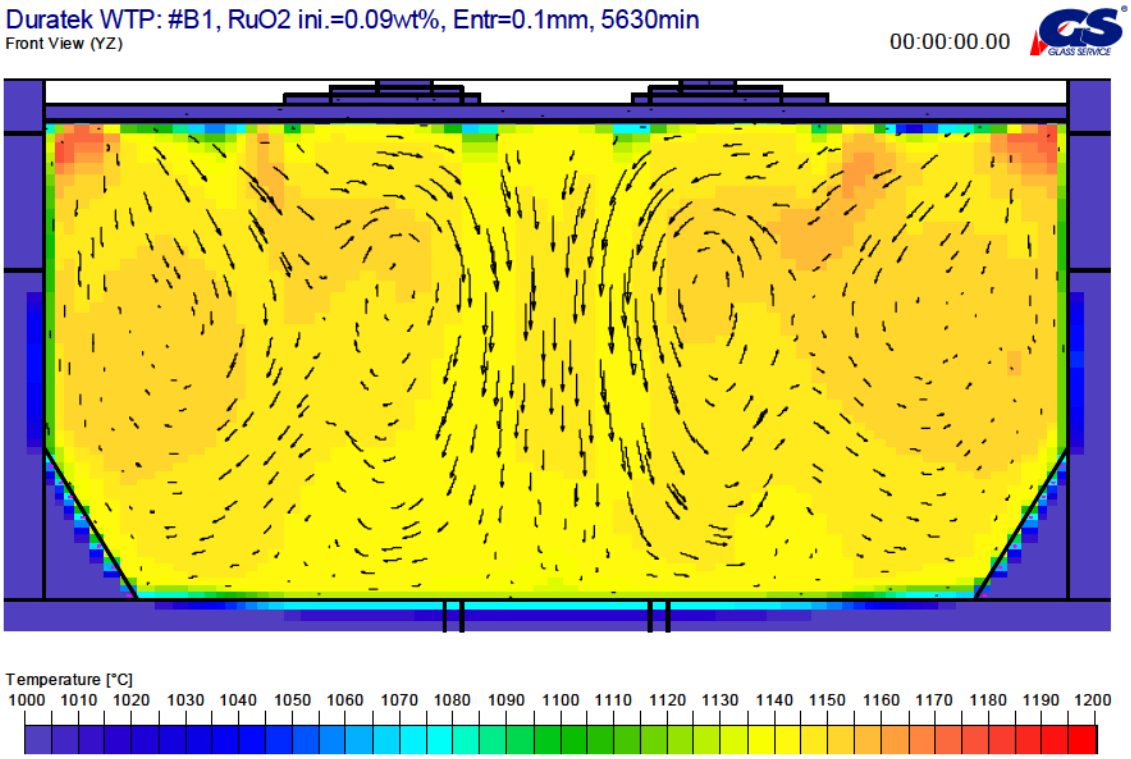


Figure 13a. Temperature distribution (color fill), velocity streamlines, and isolines of NM sludge concentration in the middle YZ cut of case #B1C0,09E0,1 (WTP case 1)

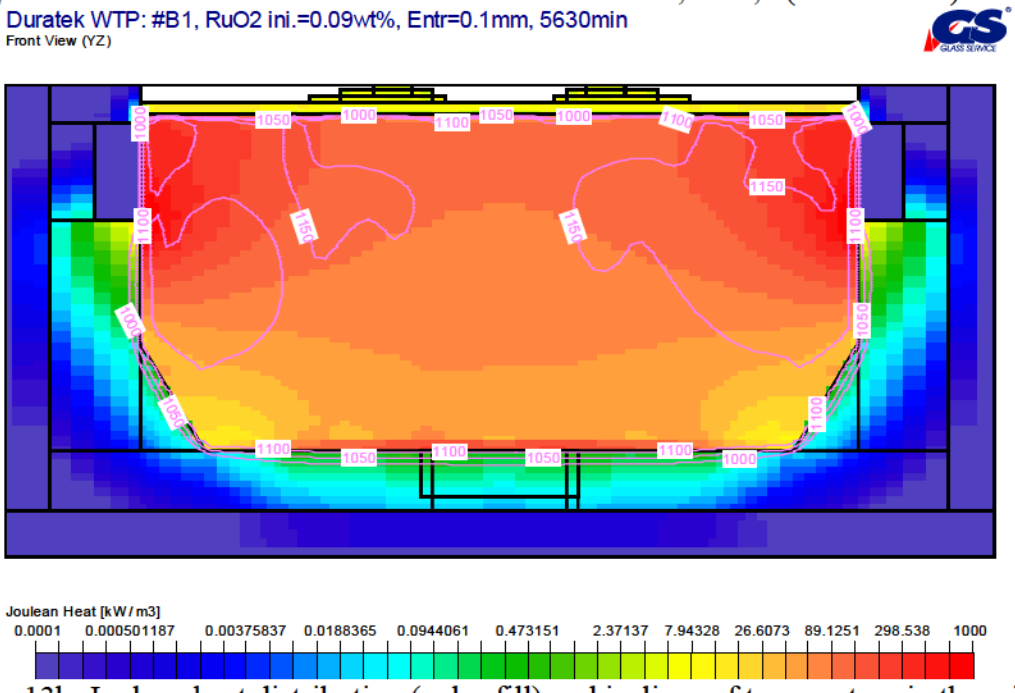


Figure 13b. Joulean heat distribution (color fill) and isolines of temperature in the middle YZ cut of case #B1C0,09E0,1 (WTP case 1)

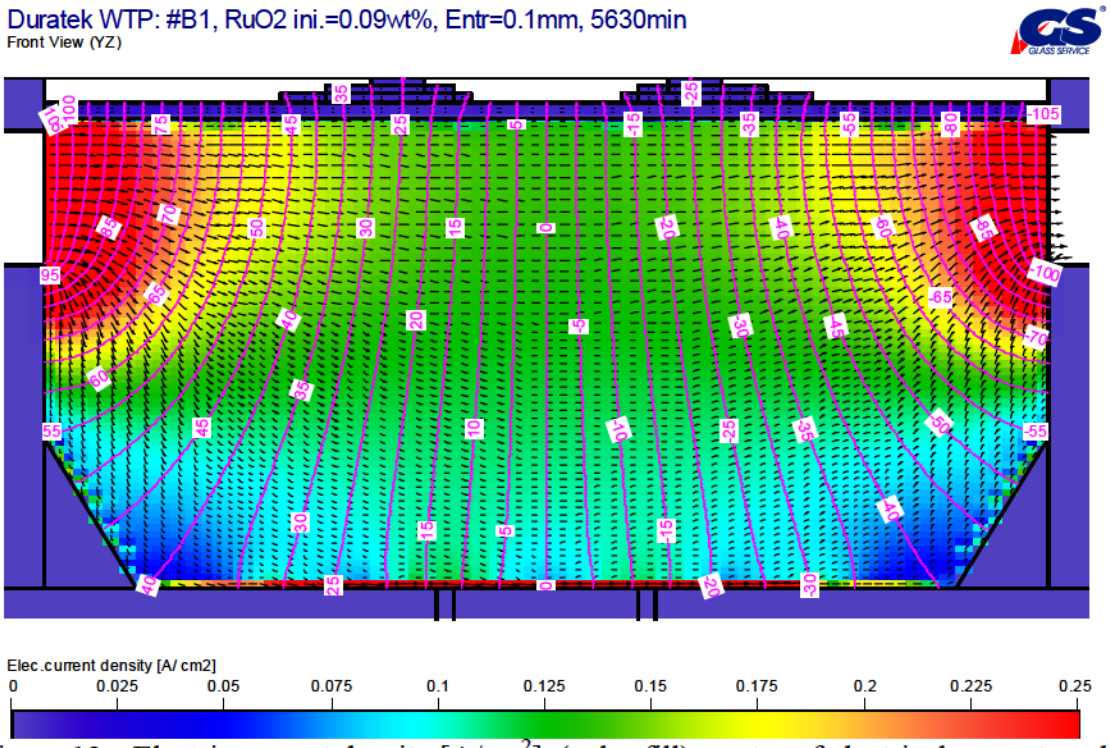


Figure 13c. Electric current density [A/cm$^2$] (color fill), vector of electrical current, and electrical potential isolines in the middle YZ cut of the case #B1C0,09E0,1 (WTP case 1)

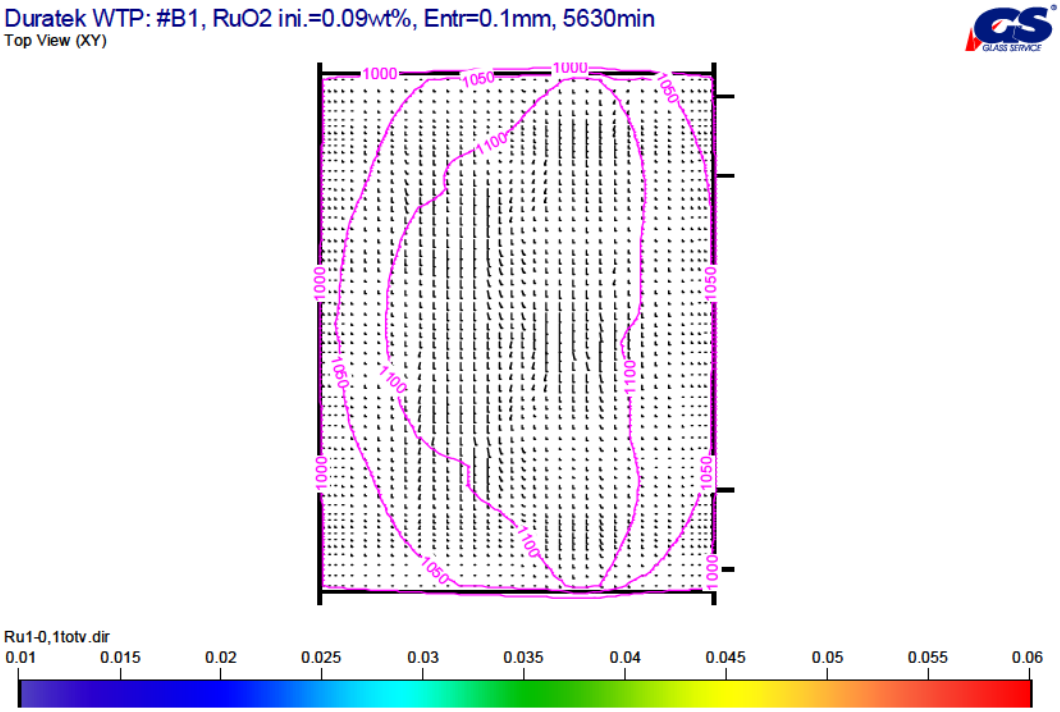


Figure 13d. Sludge layer pattern (color fill), isolines of temperature, and vector of electrical current in horizontal cut XY at one grid above bottom of the case #B1C0,09E0,1 (WTP case 1)

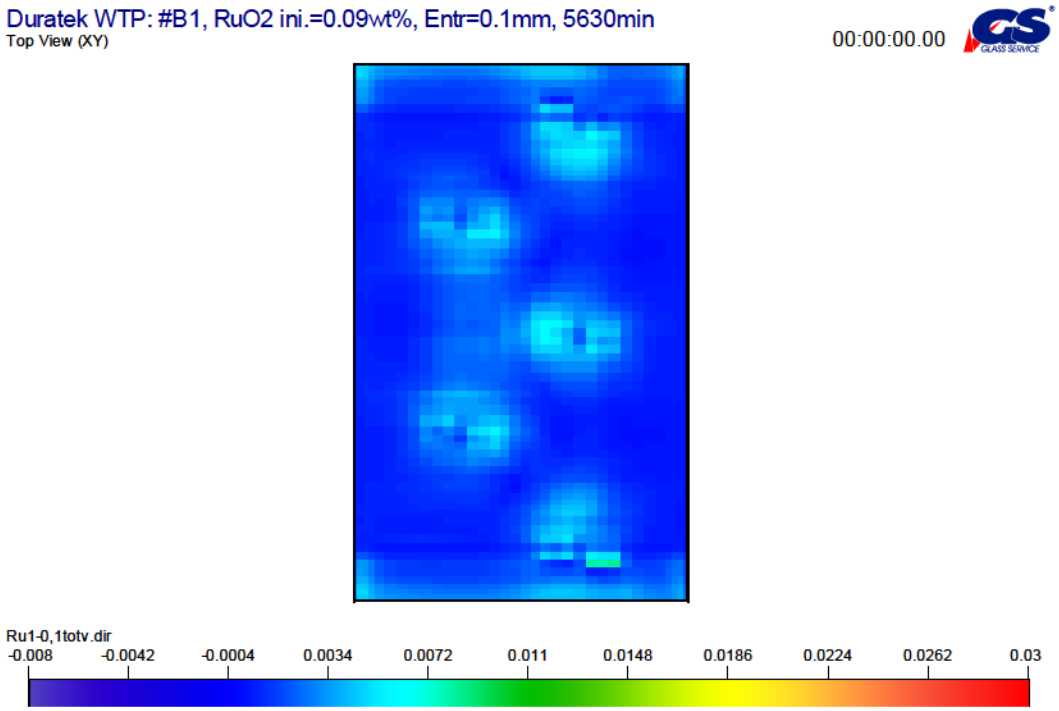


Figure 13e. Sludge layer height distribution (color fill) in vertical projection through XY planes above flat and slanted bottom of the case #B1C0,09E0,1 (WTP case 1)

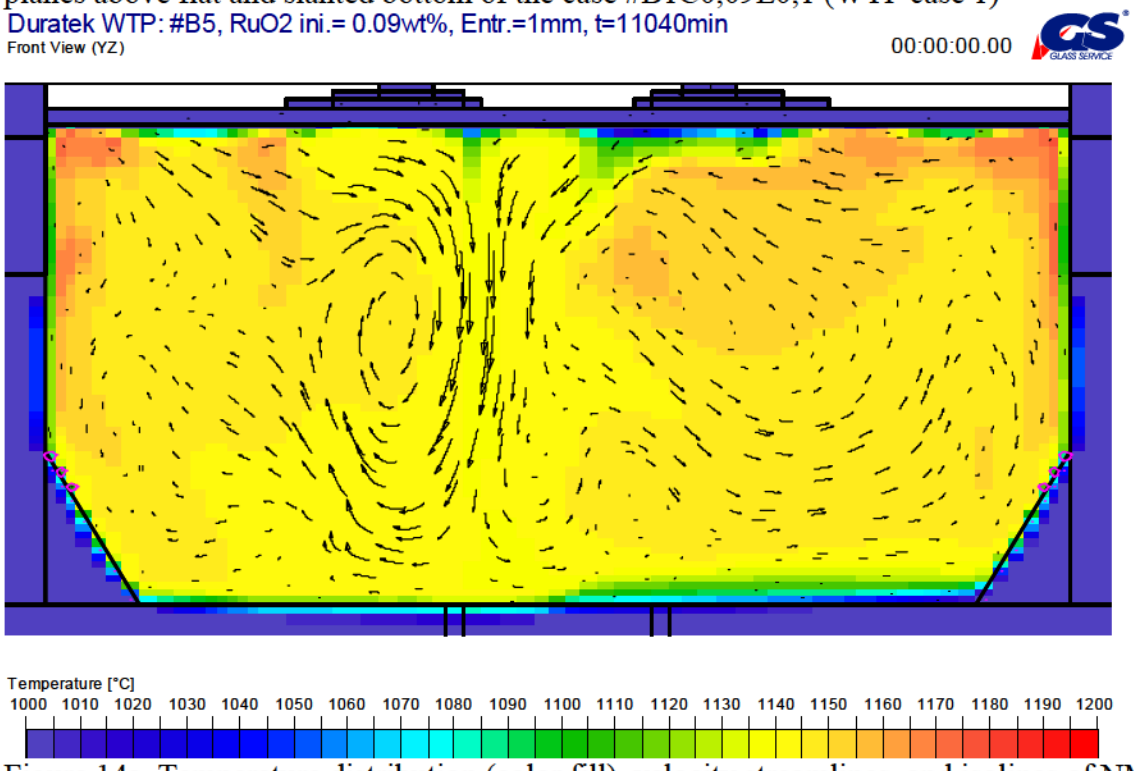


Figure 14a. Temperature distribution (color fill), velocity streamlines, and isolines of NM sludge concentration in the middle YZ cut of case #B5C0,09E1,0 (WTP case 2C)

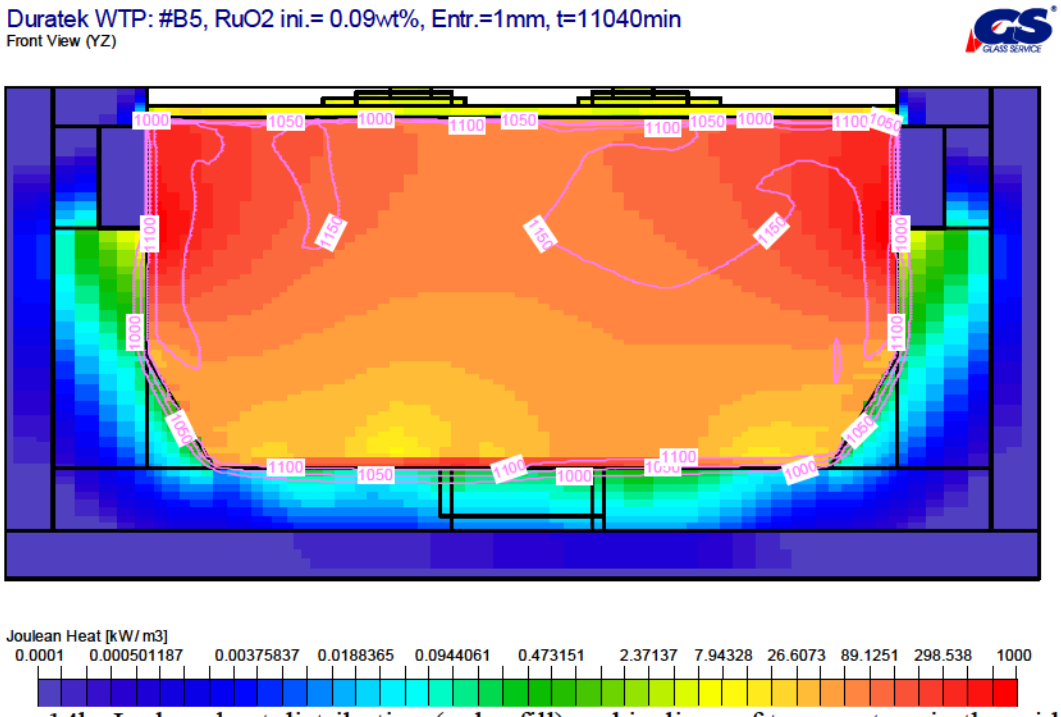


Figure 14b. Joulean heat distribution (color fill) and isolines of temperature in the middle YZ cut of case #B5C0,09E1,0 (WTP case 2C)

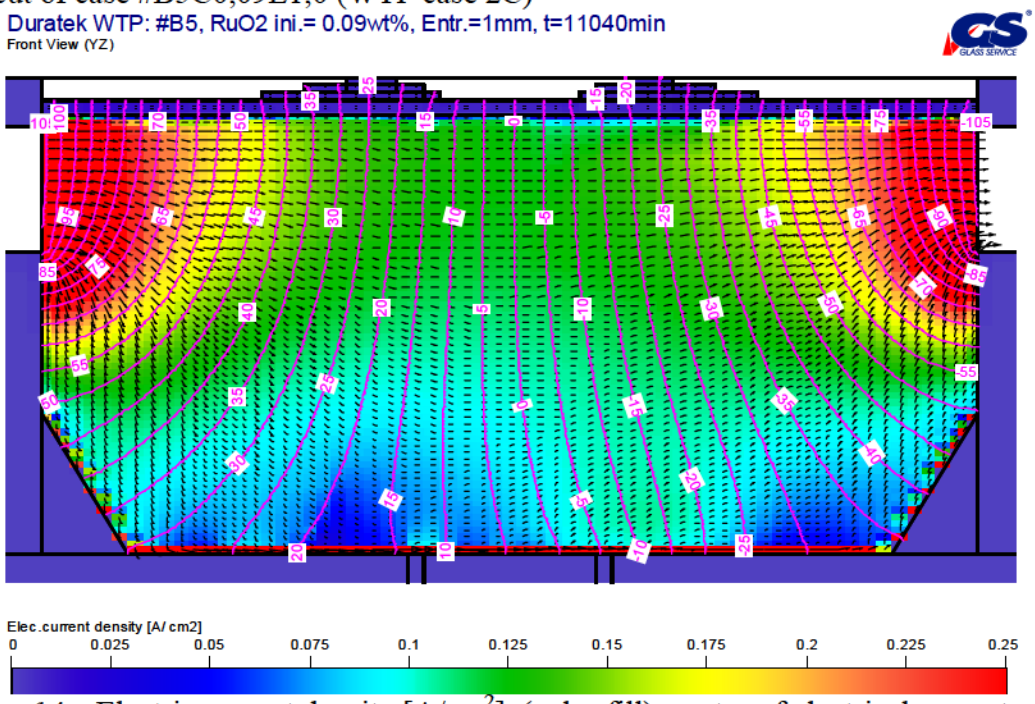


Figure 14c. Electric current density [A/cm$^2$] (color fill), vector of electrical current, and electrical potential isolines in the middle YZ cut of the case #B5C0,09E1,0 (WTP case 2C)

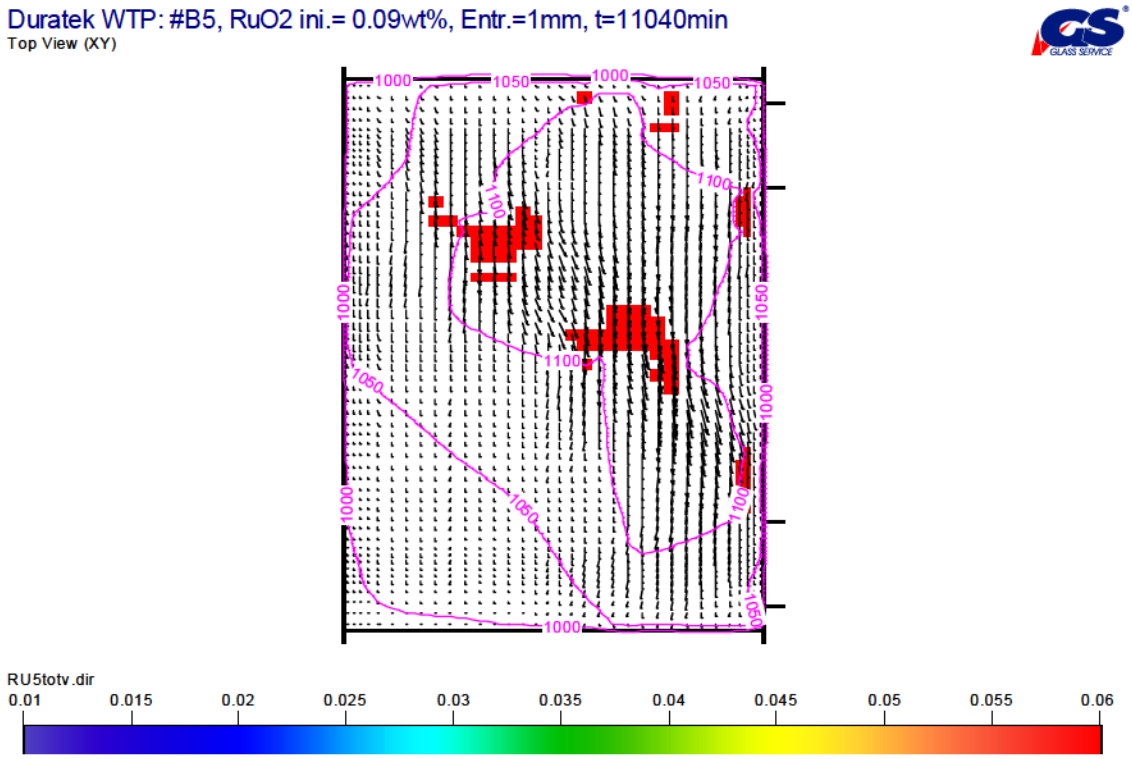


Figure 14d. Sludge layer pattern (color fill), isolines of temperature, and vector of electrical current in horizontal cut XY at one grid above bottom of the case #B5C0,09E1,0 (WTP case 2C)

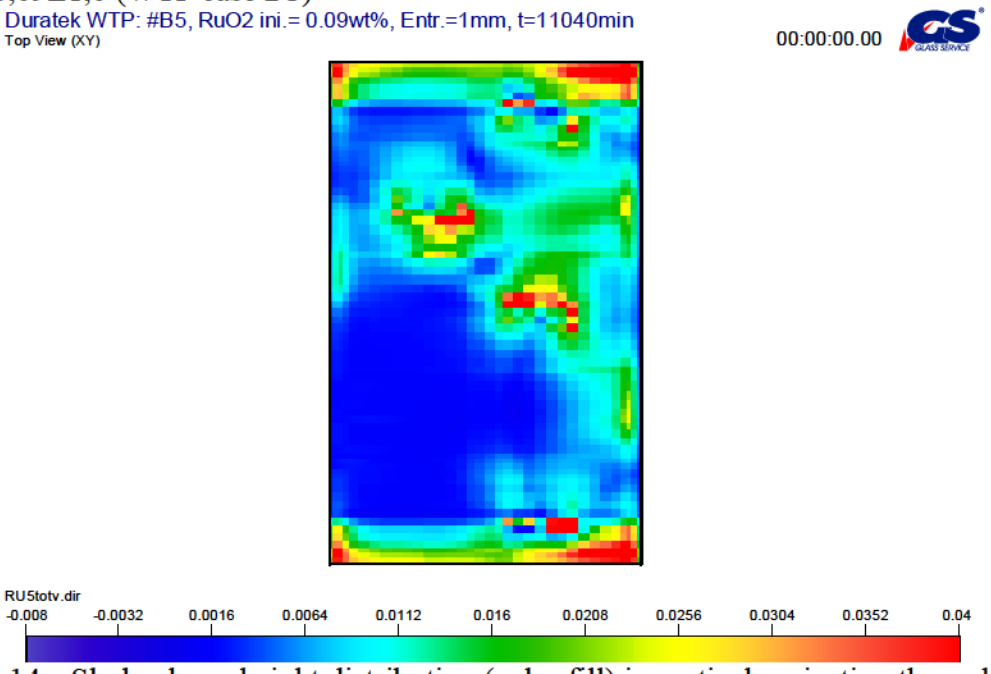


Figure 14e. Sludge layer height distribution (color fill) in vertical projection through XY planes above flat and slanted bottom of the case #B5C0,09E1,0 (WTP case 2C)

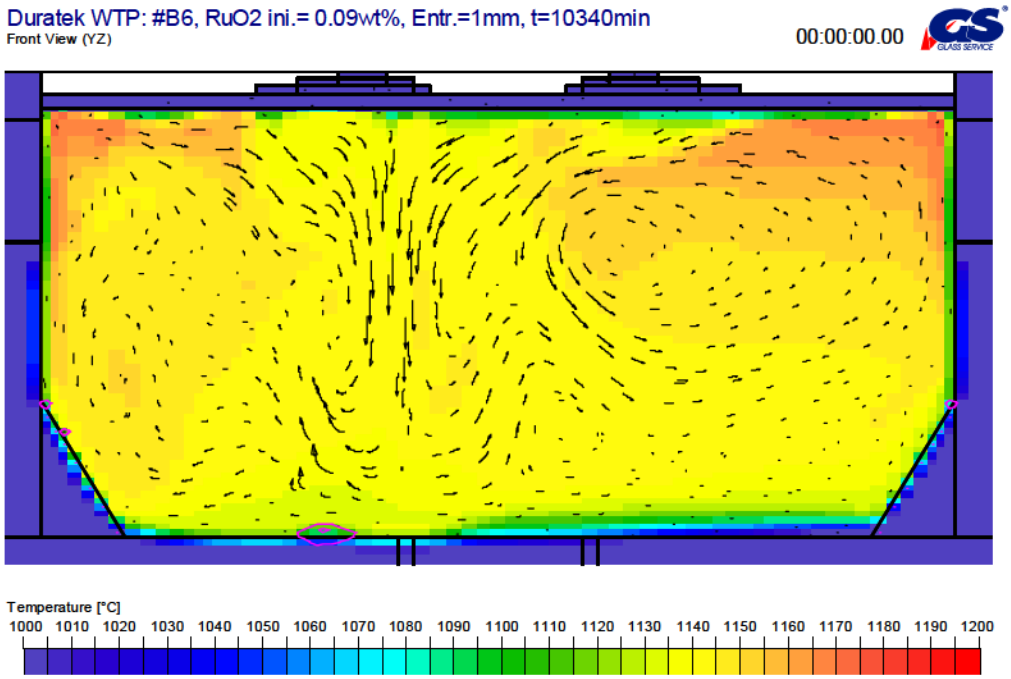


Figure 15a. Temperature distribution (color fill), velocity streamlines, and isolines of NM sludge concentration in the middle YZ cut of case #B6C0,09E1,0 (WTP case 2D)

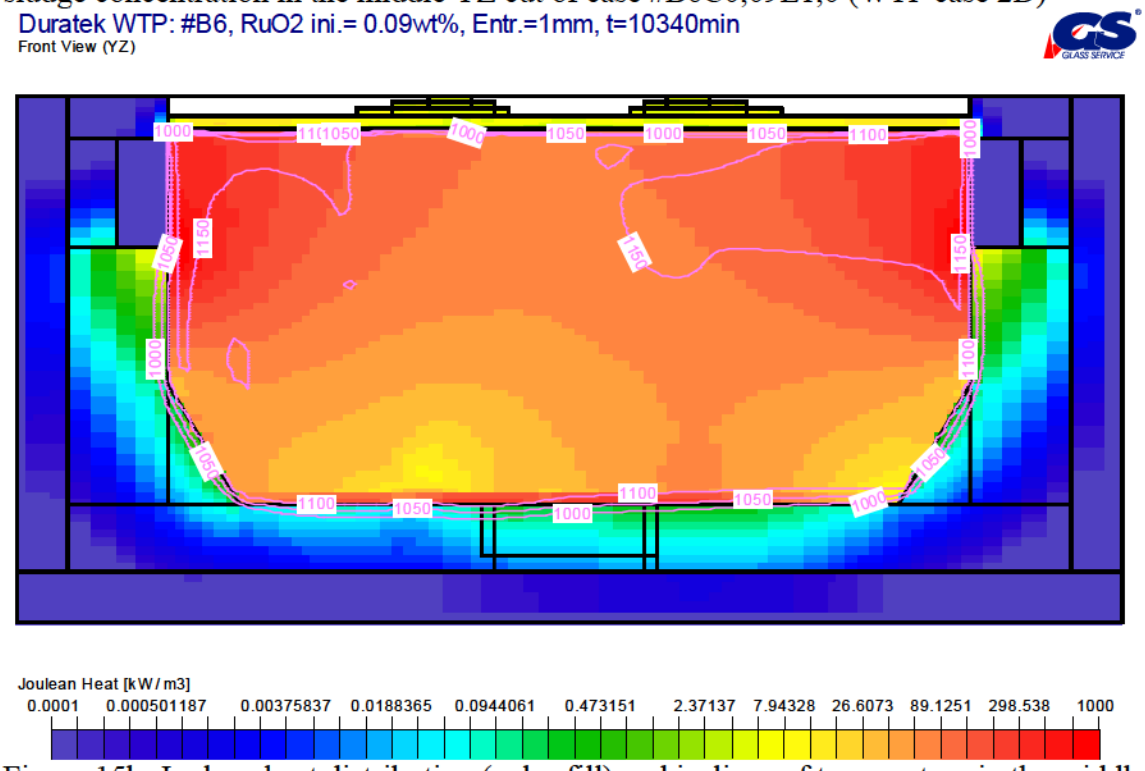


Figure 15b. Joulean heat distribution (color fill) and isolines of temperature in the middle YZ cut of case #B6C0,09E1,0 (WTP case 2D)

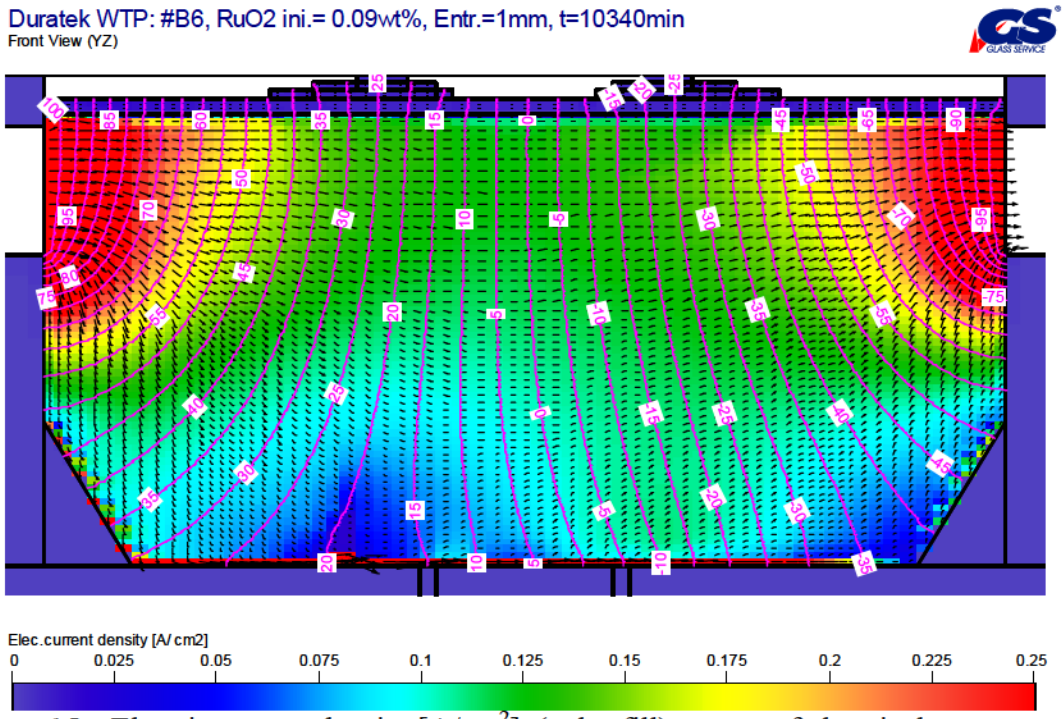


Figure 15c. Electric current density [A/cm$^2$] (color fill), vector of electrical current, and electrical potential isolines in the middle YZ cut of the case #B6C0,09E1,0 (WTP case 2D)

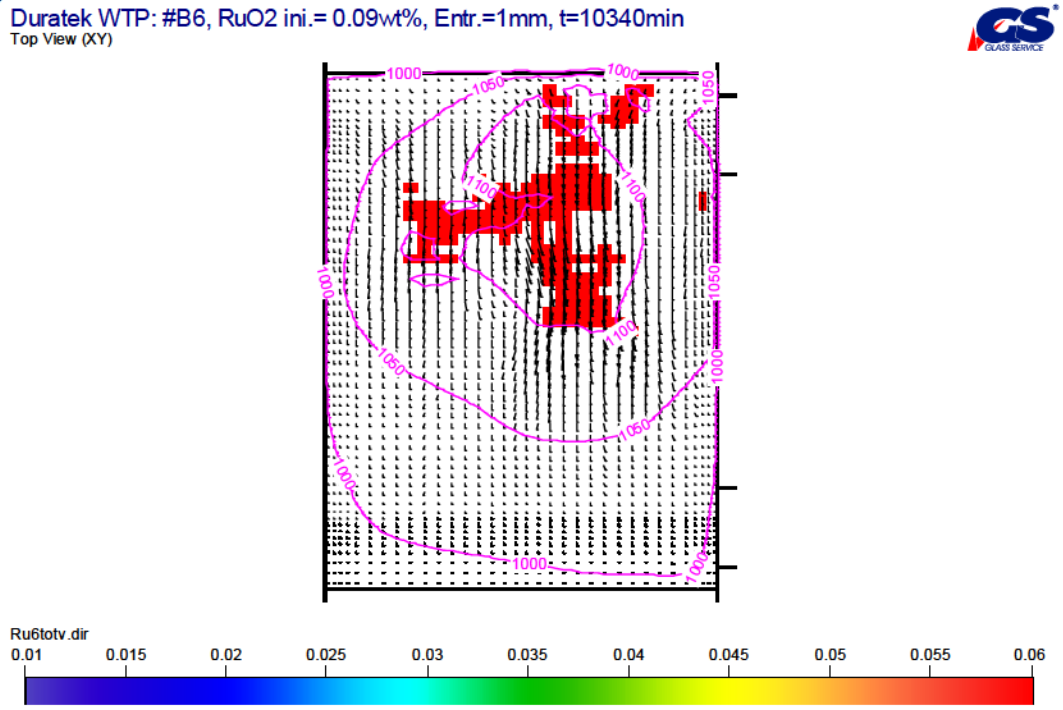


Figure 15d. Sludge layer pattern (color fill), isolines of temperature, and vector of electrical current in horizontal cut XY at one grid above bottom of the case #B6C0,09E1,0 (WTP case 2D)

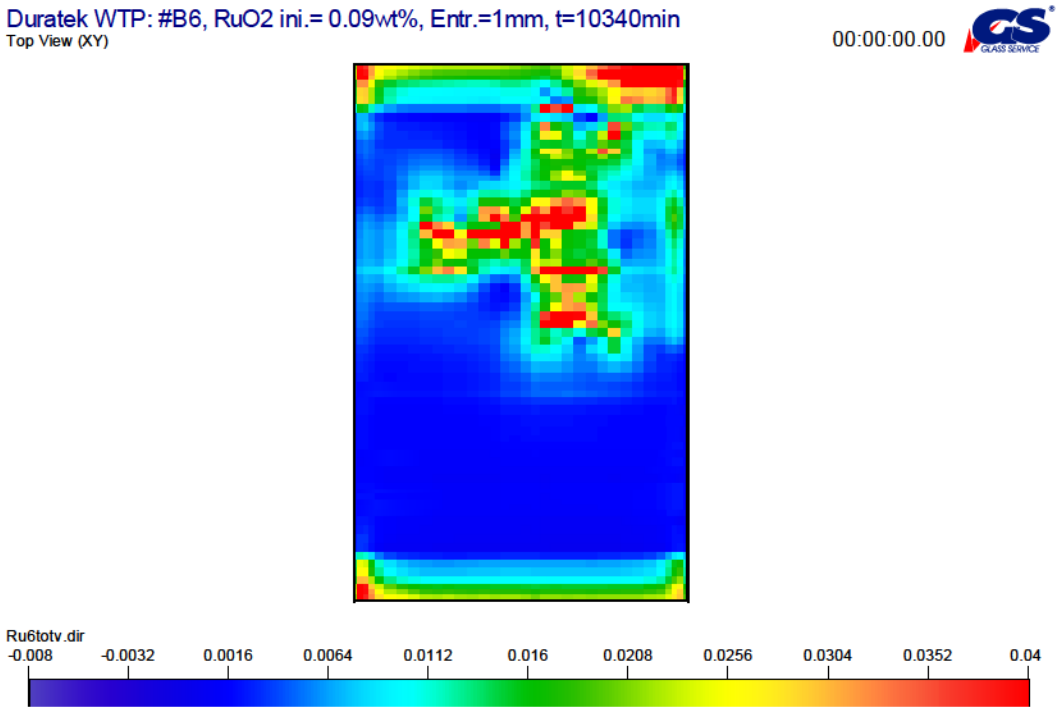


Figure 15e. Sludge layer height distribution (color fill) in vertical projection through XY planes above flat and slanted bottom of the case #B6C0,09E1,0 (WTP case 2D)

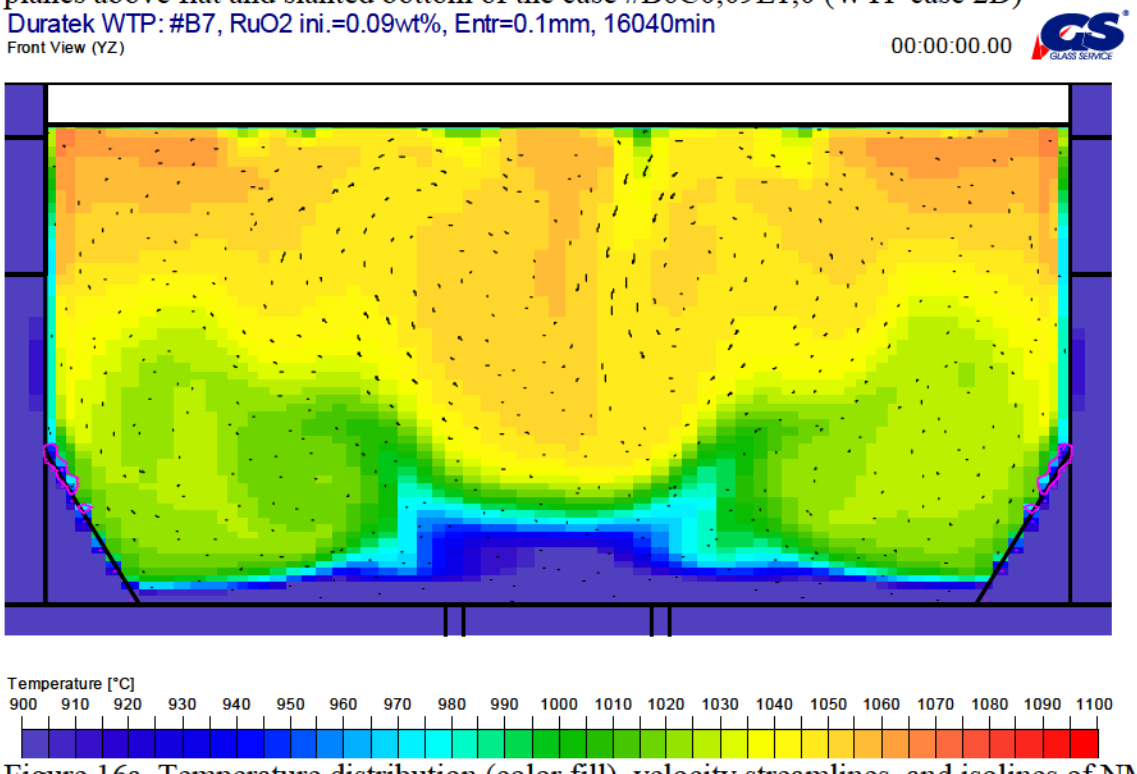


Figure 16a. Temperature distribution (color fill), velocity streamlines, and isolines of NM sludge concentration in the middle YZ cut of case #B7C0,09E1,0 (WTP case 2-idling)

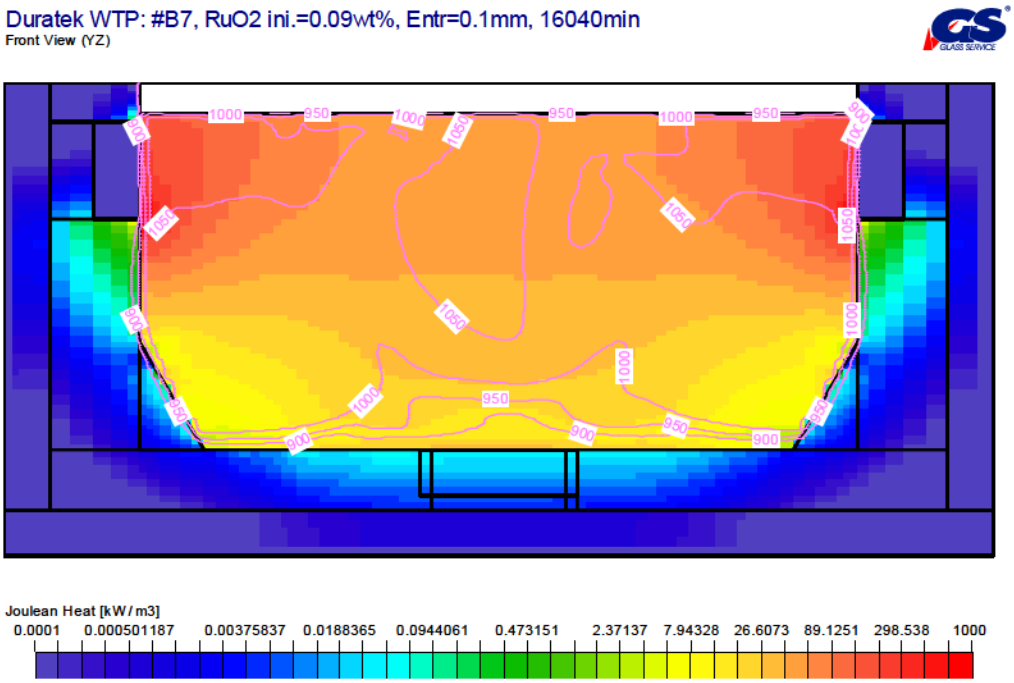


Figure 16b. Joulean heat distribution (color fill) and isolines of temperature in the middle YZ cut of case #B7C0,09E1,0 (WTP case 2-idling)

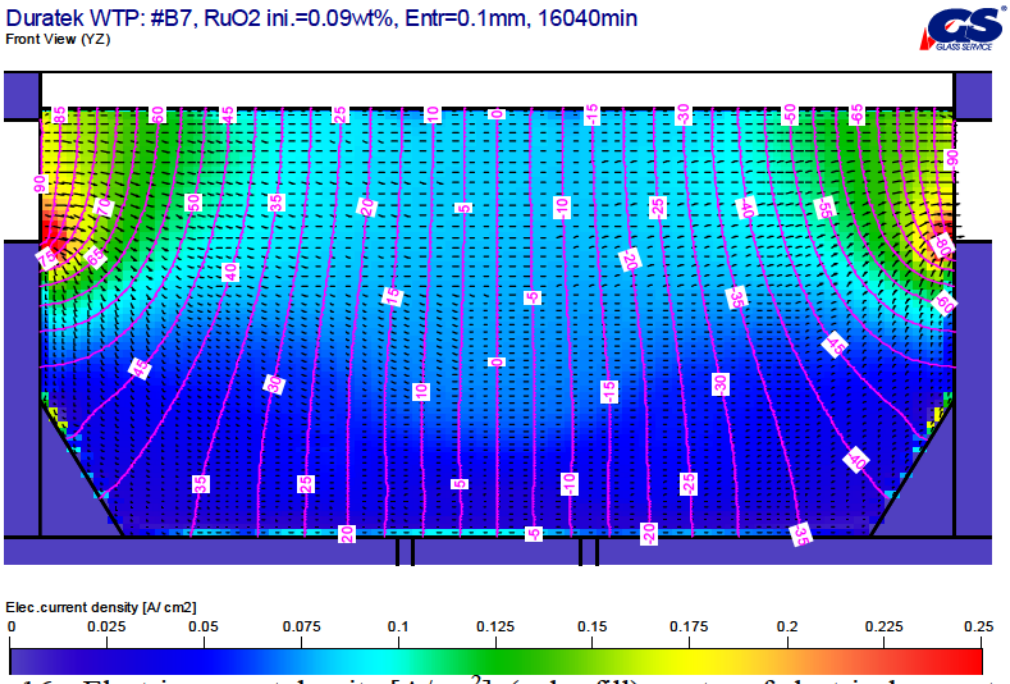


Figure 16c. Electric current density [A/cm$^2$] (color fill), vector of electrical current, and electrical potential isolines in the middle YZ cut of the case #B7C0,09E1,0 (WTP case 2-idling)

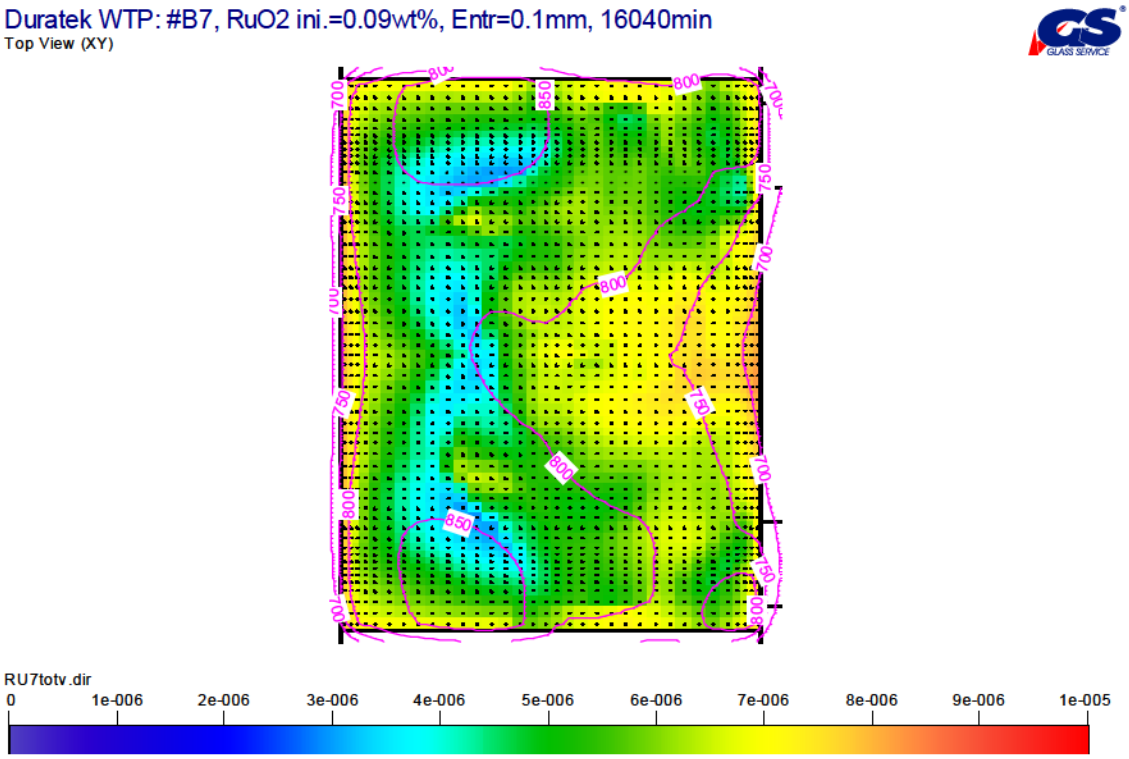


Figure 16d. Sludge layer pattern (color fill), isolines of temperature, and vector of electrical current in horizontal cut XY at one grid above bottom of the case #B7C0,09E1,0 (WTP case 2-idling)

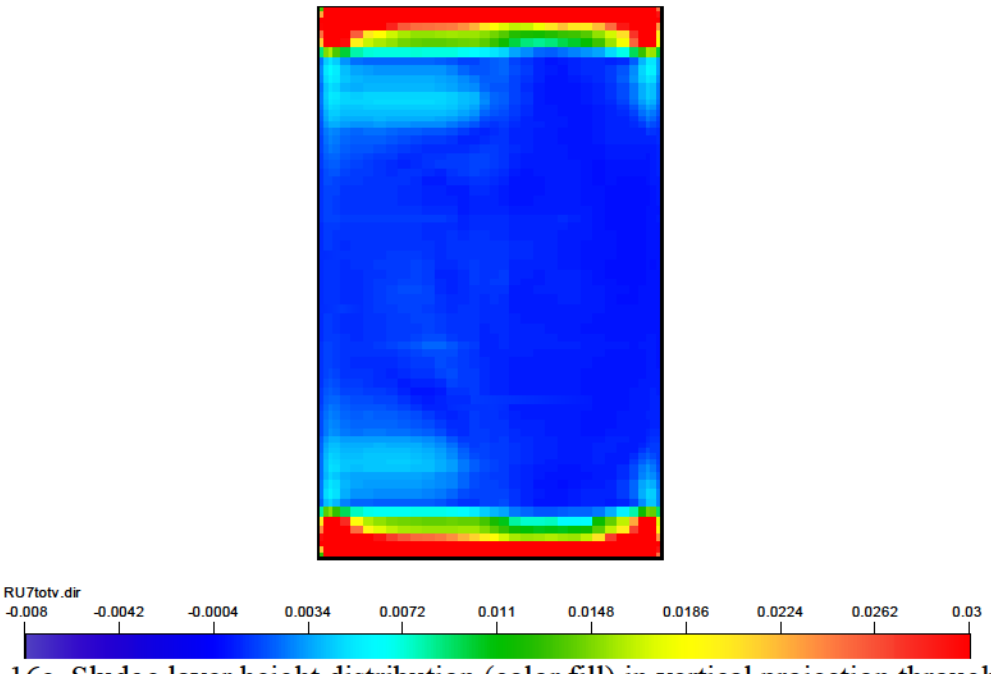


Figure 16e. Sludge layer height distribution (color fill) in vertical projection through XY planes above flat and slanted bottom of the case #B7C0,09E1,0 (WTP case 2-idling)

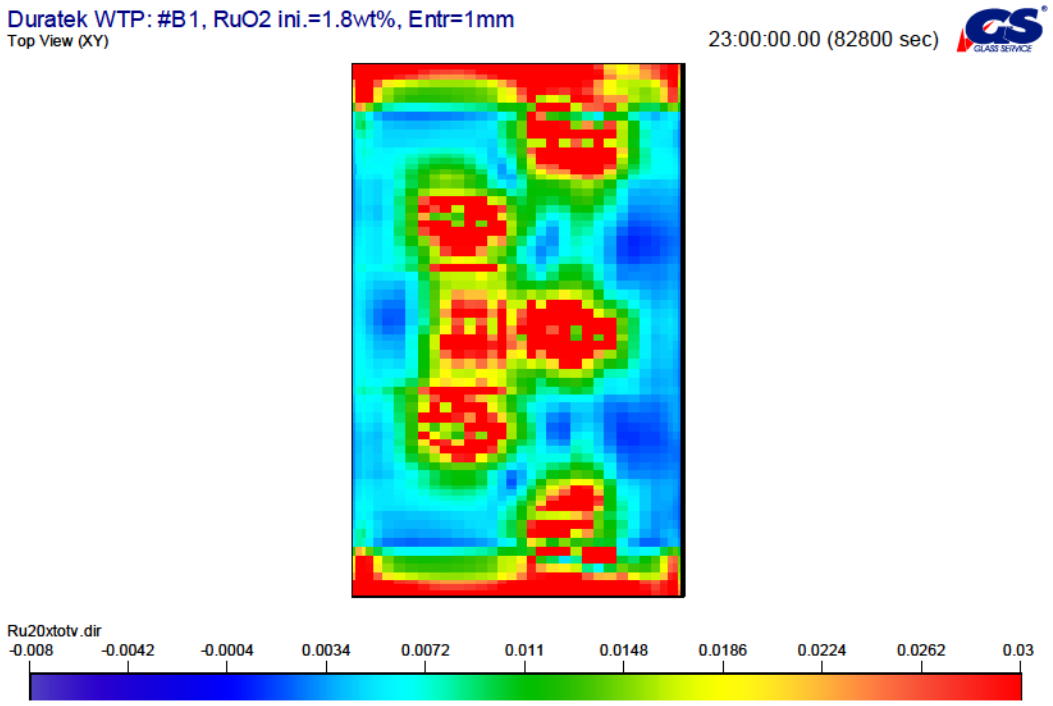


Figure 17a. Sludge layer height distribution (color fill) in vertical projection through XY planes above flat and slanted bottom of the case #B1C1,8E1,0 at time=1380 min = 23 hr (WTP case 1)

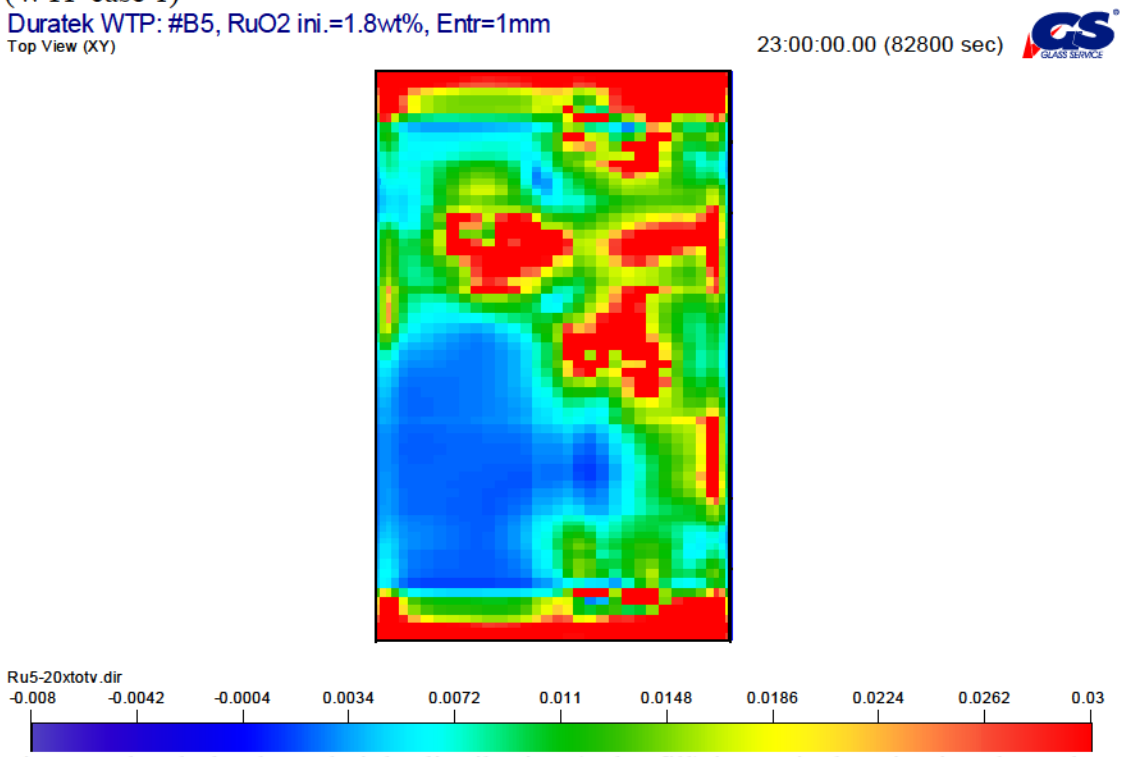


Figure 17b. Sludge layer height distribution (color fill) in vertical projection through XY planes above flat and slanted bottom of the case #B5C1,8E1,0 at time=1380 min = 23 hr (WTP case 2C)

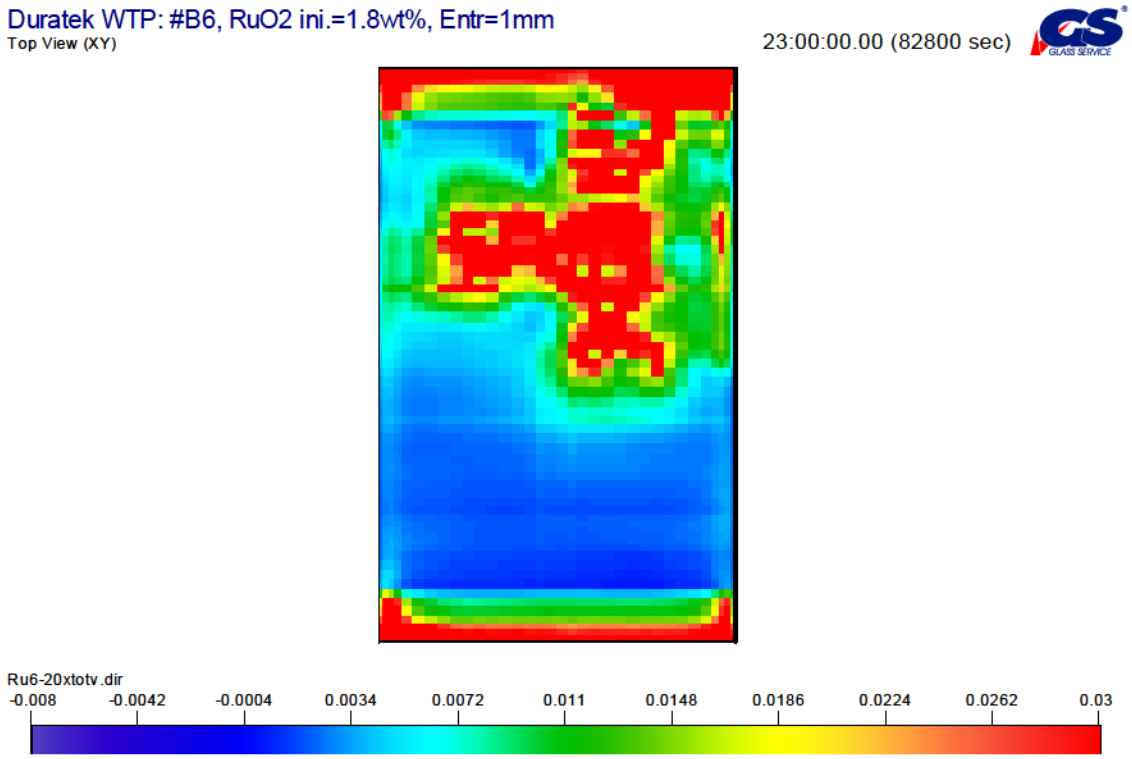


Figure 17c. Sludge layer height distribution (color fill) in vertical projection through XY planes above flat and slanted bottom of the case #B6C1,8E1,0 at time=1380 min = 23 hr (WTP case 2D)

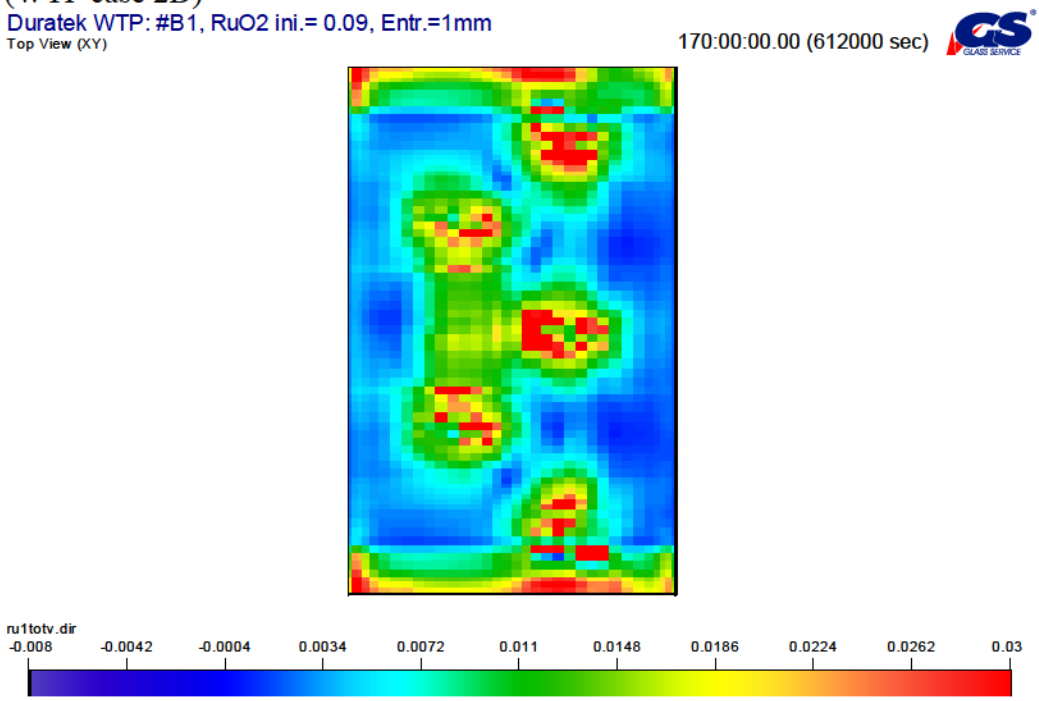


Figure 18a. Sludge layer height distribution (color fill) in vertical projection through XY planes above flat and slanted bottom of the case #B1C0.09,8E1,0 at time=10200 min = 170 hr (WTP case 1)

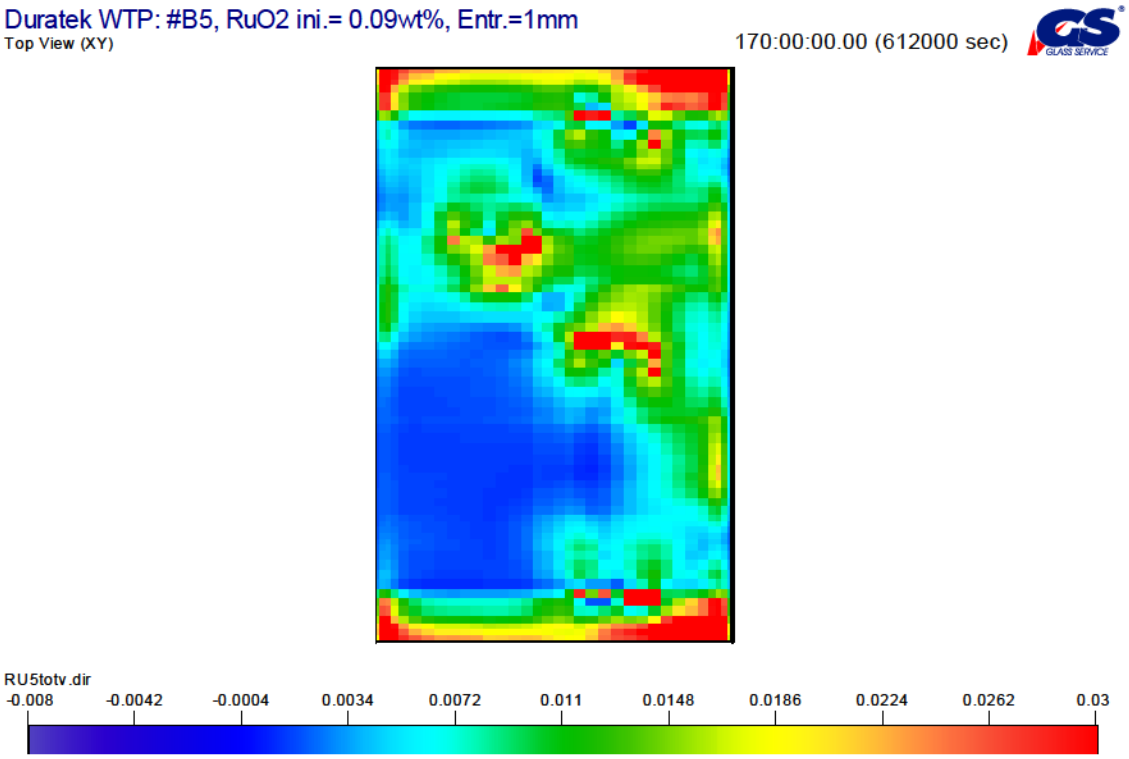


Figure 18b. Sludge layer height distribution (color fill) in vertical projection through XY planes above flat and slanted bottom of the case #B5C0.09,8E1,0 at time=10200 min = 170 hr (WTP case 2C)

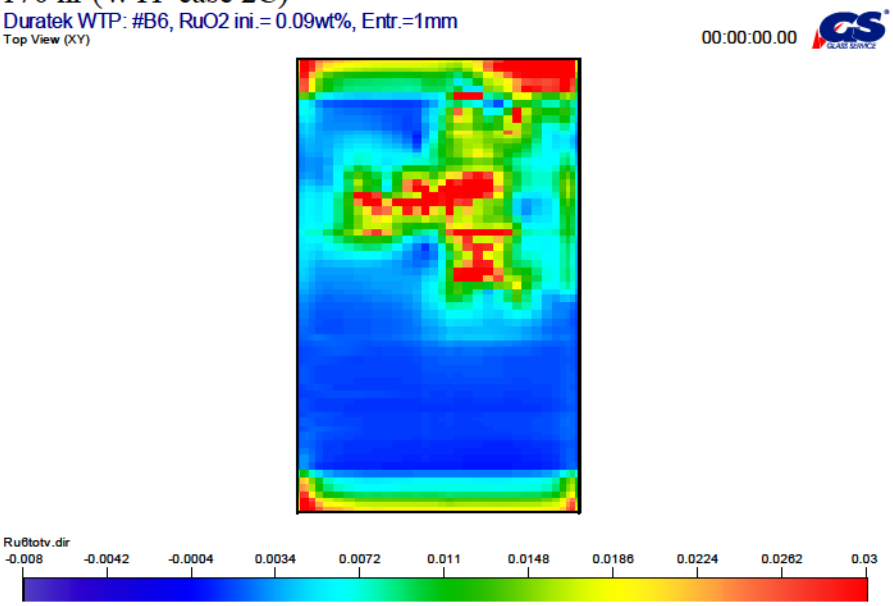


Figure 18c. Sludge layer height distribution (color fill) in vertical projection through XY planes above flat and slanted bottom of the case #B6C0.09,8E1,0 at time=10200 min = 170 hr (WTP case 2D)

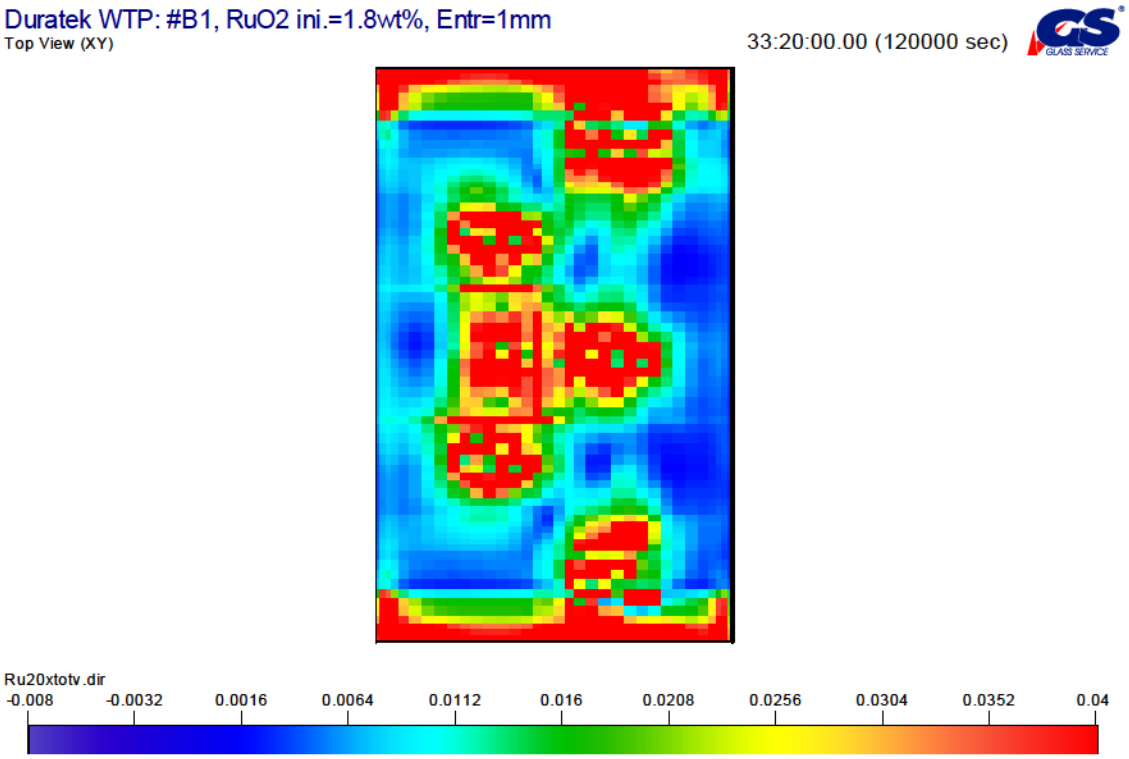


Figure 19a. Sludge layer height distribution (color fill) in vertical projection through XY planes above flat and slanted bottom of the case #B1C1.8,E1,0 at time=2000 min = 33.33 hr (WTP case 1)

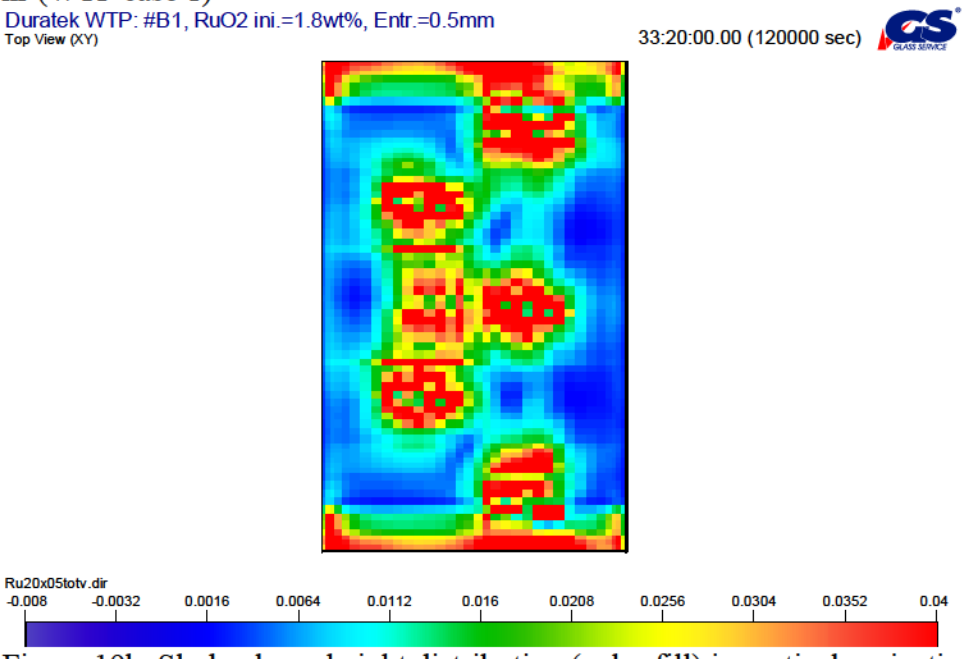


Figure 19b. Sludge layer height distribution (color fill) in vertical projection through XY planes above flat and slanted bottom of the case #B1C1.8,E0.5 at time=2000 min = 33.33 hr (WTP case 1)

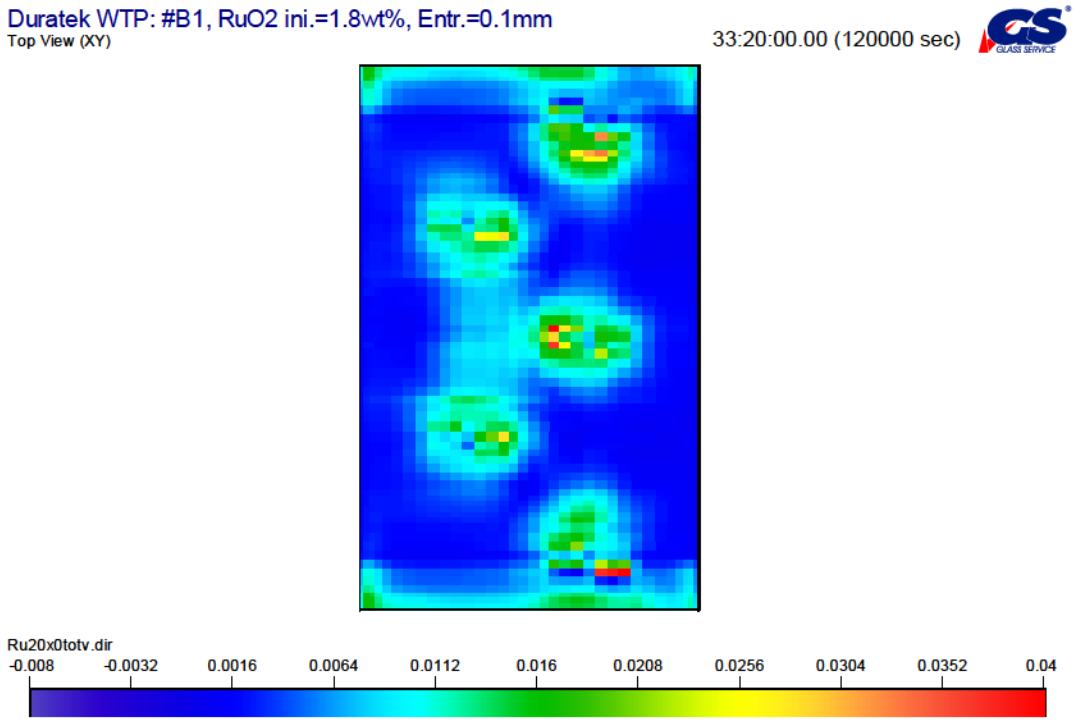


Figure 19c. Sludge layer height distribution (color fill) in vertical projection through XY planes above flat and slanted bottom of the case #B1C1.8,E0.1 at time=2000 min = 33.33 hr (WTP case 1)

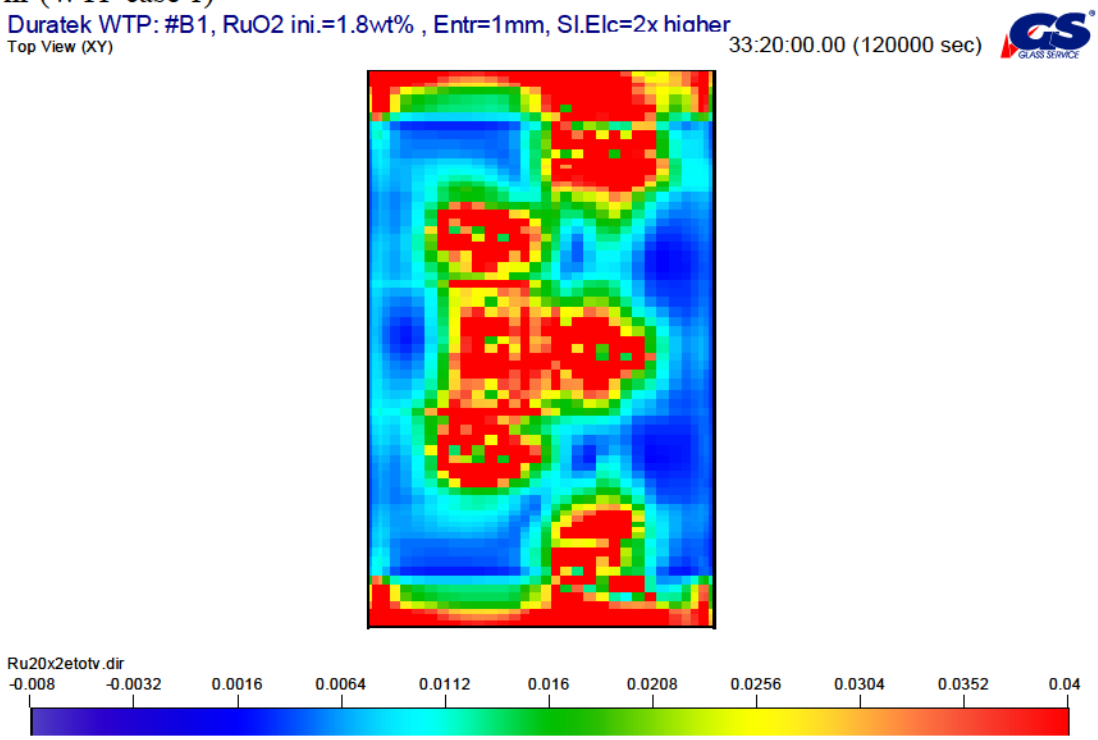


Figure 19d. Sludge layer height distribution (color fill) in vertical projection through XY planes above flat and slanted bottom of the case #B1C1.8,E1,0 EL2x at time=2000 min = 33.33 hr (WTP case 1)

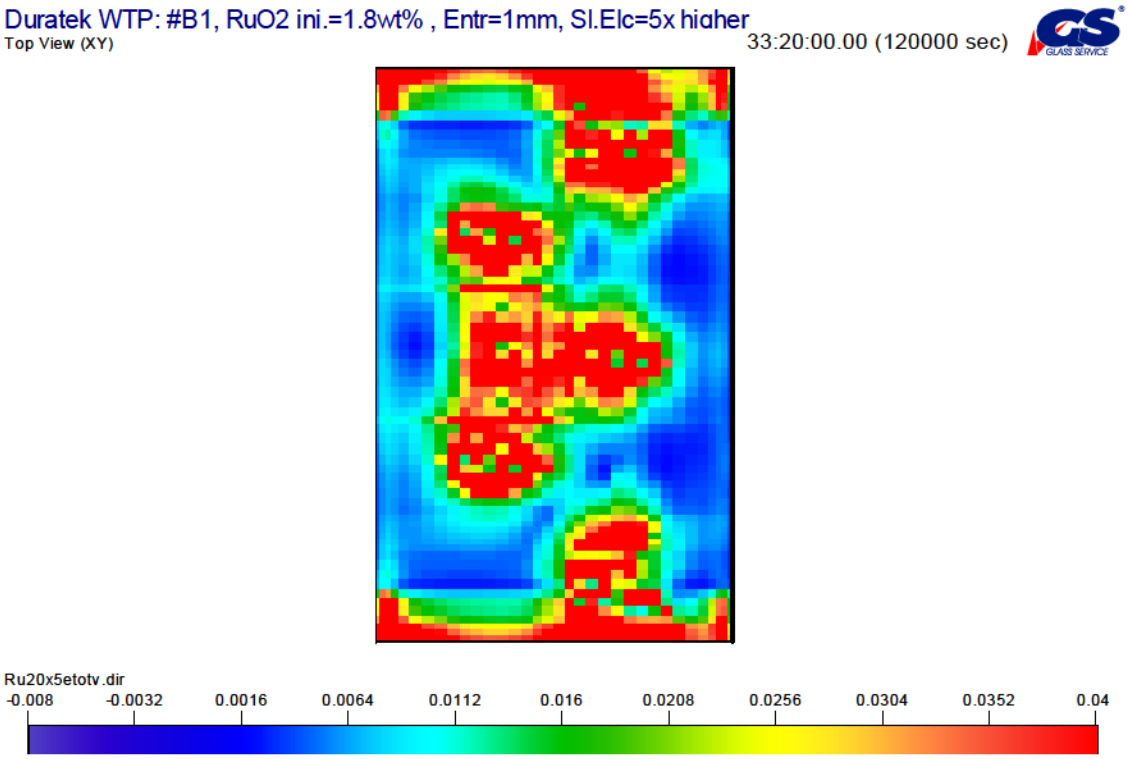


Figure 19e. Sludge layer height distribution (color fill) in vertical projection through XY planes above flat and slanted bottom of the case #B1C1.8,E1,0 EL5x at time=2000 min = 33.33 hr (WTP case 1)

### *Quantitative analysis of NM settling in the melter*

Several cumulative quantities were calculated during time settling process: mass of NM discharged from the melter, mass of NM settled on the bottom, mass of NM remaining in the melter glass, and retention according to eq.(33). The time developments of the cumulative masses are displayed on Figure 20- Figure 23. These retention curves show high retention values of approx. 90 % for the first step of parameters of high injected concentration of 1.8 wt% (20 times higher than the prescribed value of 0.09 wt%) and high entrapment=1mm. This high retention has been stabilized after approx. 70 hrs of the settling process. These extreme first step parameters (injection=1.8wt%, entrapment=1mm) were used for fast investigation of sludge layer generation. It is supposed that the fast settling process is of same character as slower settling at second step of parameters (normal injection=0.09wt%, high entrapment=1mm). The stabilizing period of this second step is higher, approx. 200 hrs but the retention is still very high, approx 85%. We can conclude the next third step of parameters (normal injection=0.09wt%, entrapment=0.1mm) will be close to reality for the actual melter but the calculation is very time consuming so it is not possible to reach a stabilized stage in reasonable computational time. For now, we have no direct proof of this conclusion because we have not made any measurements of the entrapment parameter and no literature values were found. On the other hand, we have some indication of sludge layer growth from other sources [5], [6], [7] which entitle us (by relative comparisons of the layer growth rate) to accept this third step of parameters as a reasonable one.

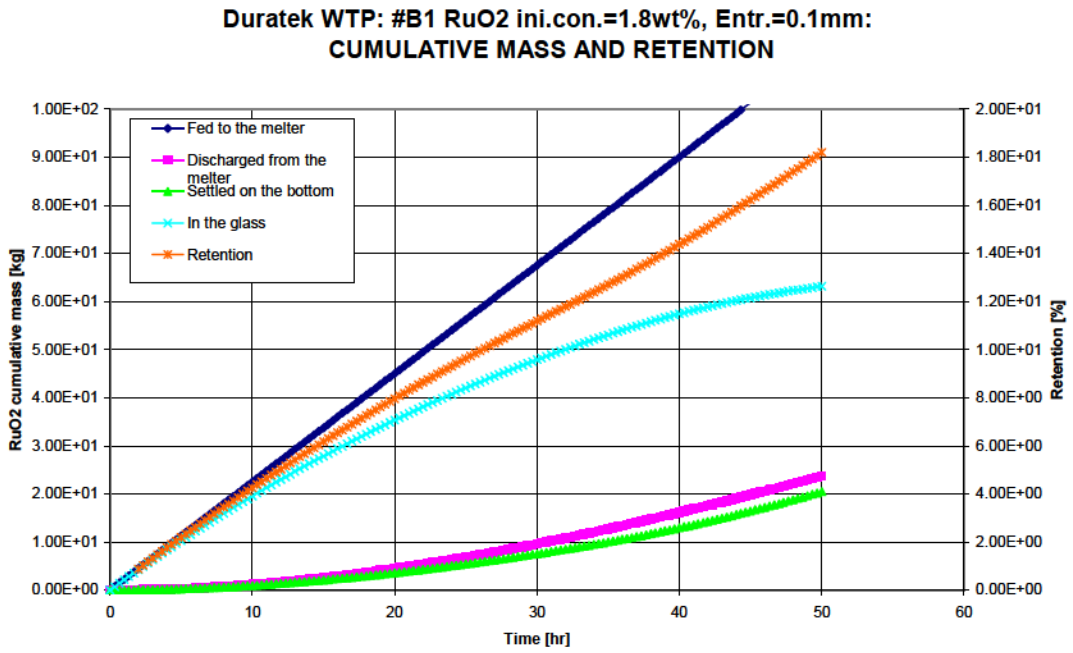


Figure 20a. Cumulative mass time development in case #B1C1,8E1,0 for $RuO_2$ initial concentration=1.8wt% and entrapment=1mm (WTP case 1)

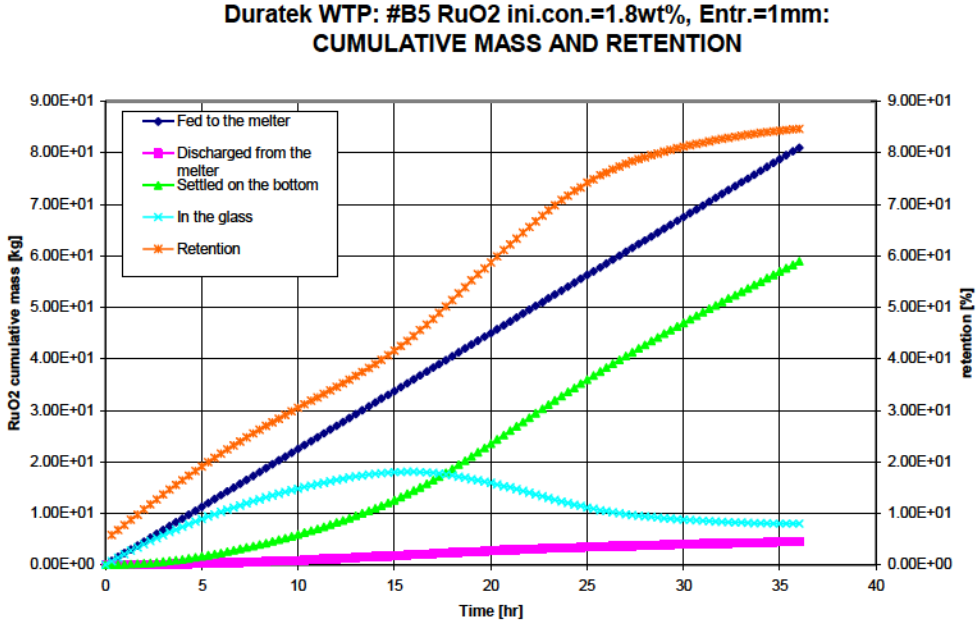


Figure 20b. Cumulative mass time development in case #B5C1,8E1,0 for $RuO_2$ initial concentration=1.8wt% and entrapment=1mm (WTP case 2C)

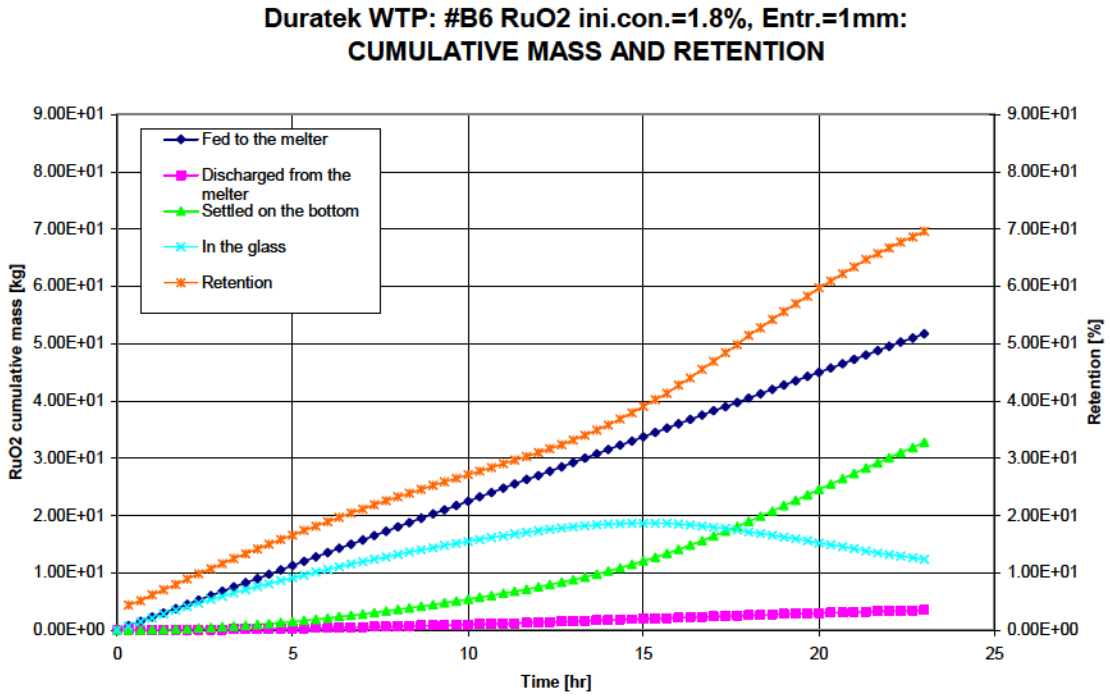


Figure 20c. Cumulative mass time development in case #B6C1,8E1,0 for $RuO_2$ initial concentration=1.8wt% and entrapment=1mm (WTP case 2D)

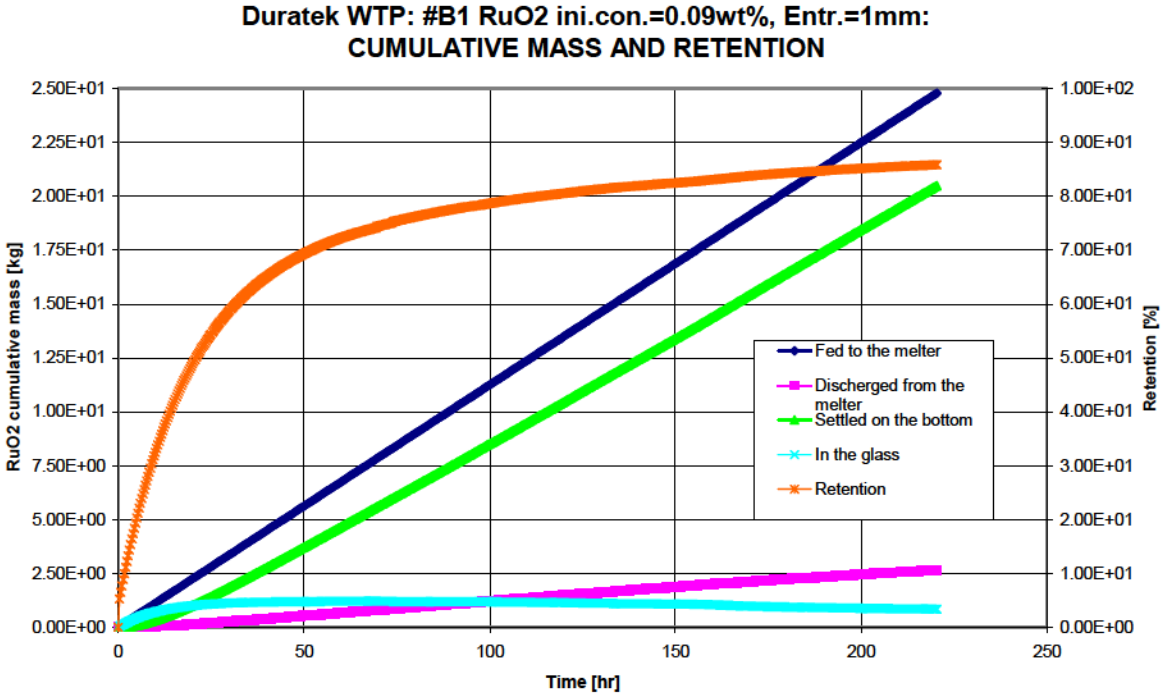


Figure 21a. Cumulative mass time development in case #B1C0,09E1,0 for $RuO_2$ initial concentration=0.09wt% and entrapment=1mm (WTP case 1)

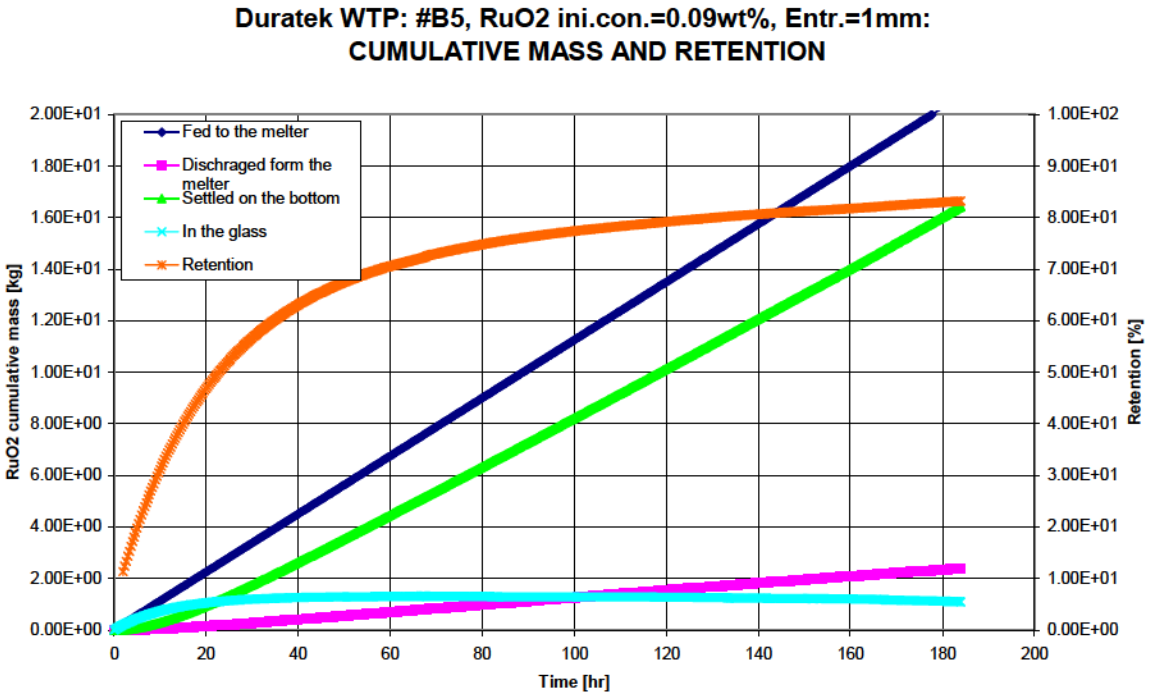


Figure 21b. Cumulative mass time development in case #B5C0,09E1,0 for $RuO_2$ initial concentration=0.09wt% and entrapment=1mm (WTP case 2C)

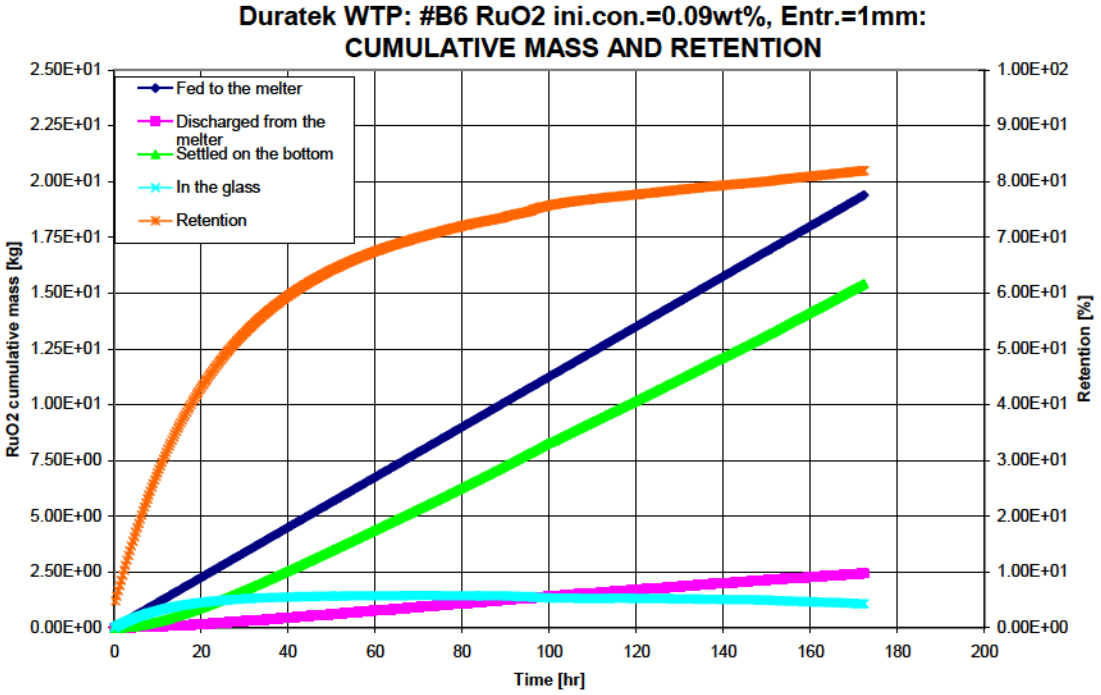


Figure 21c. Cumulative mass time development in case #B6C0,09E1,0 for $RuO_2$ initial concentration=0.09wt% and entrapment=1mm (WTP case 2D)

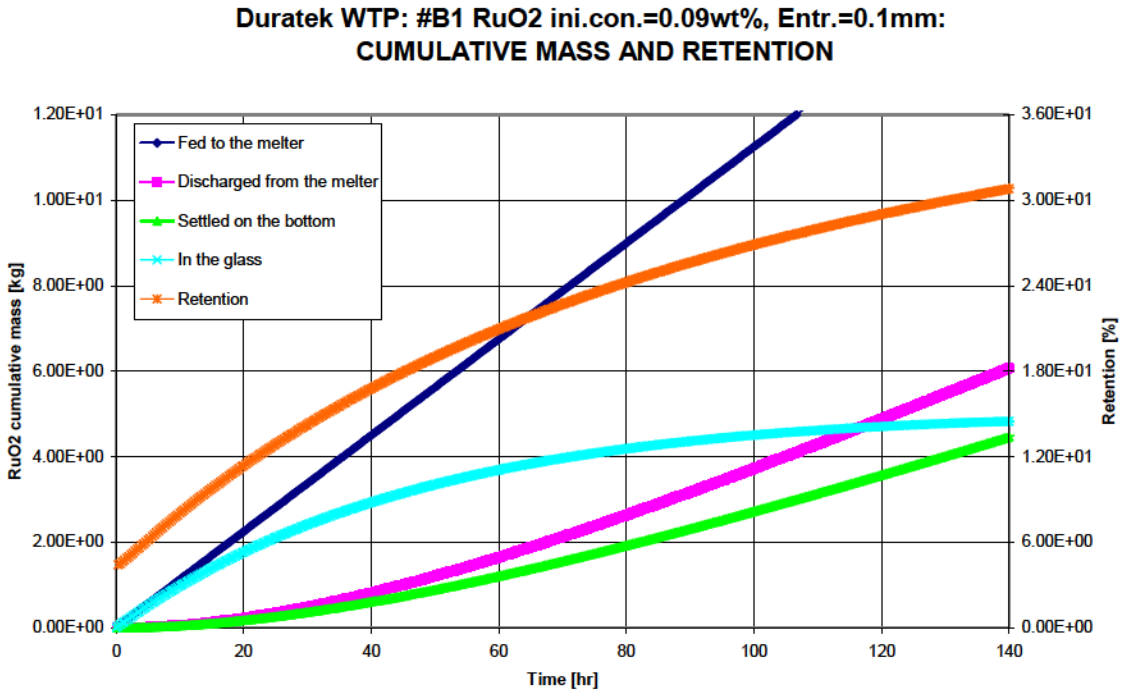


Figure 22. Cumulative mass time development in case #B1C0,09E0,1 for $RuO_2$ initial concentration=0.09wt% and entrapment=0.1mm (WTP case 1)

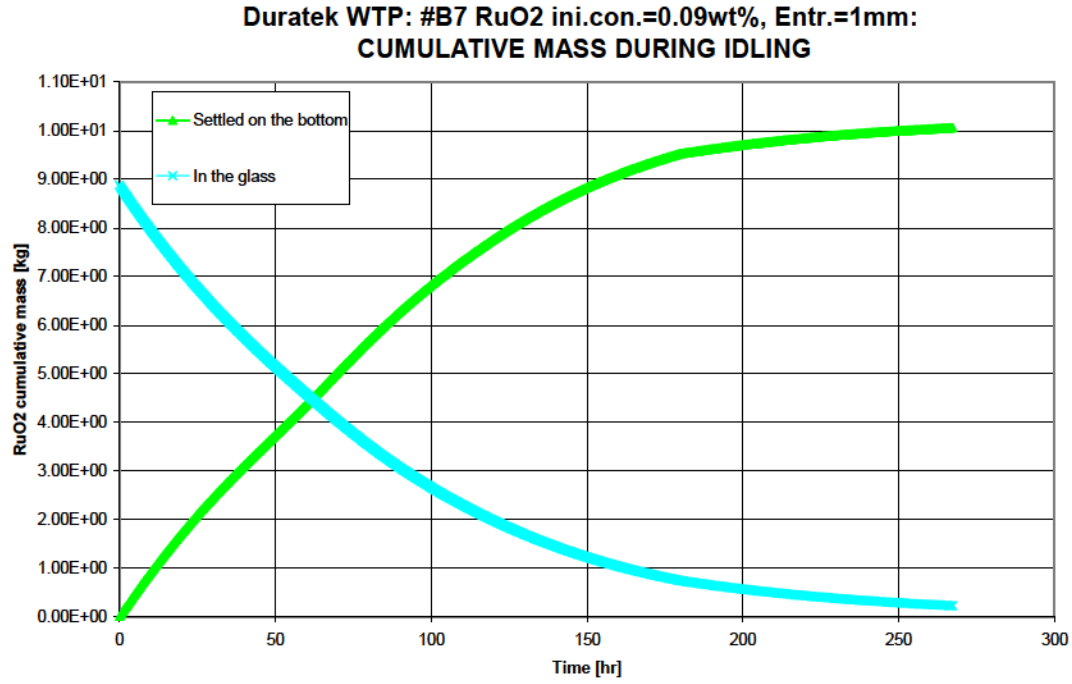


Figure 23. Cumulative mass time development in case #B7C0,09E1,0 (idling) for $RuO_2$ initial concentration=0.09wt% in the glass of the whole melter and entrapment=1mm (WTP case 2E)

Figure 24 shows mass balance error during dynamic (time transient) calculation of NM settling in all cases. This error is given by formula

$$M(t)_{err} = 100.\frac{M(t)_{out} - M(t)_{inj}}{M(t)_{inj}} \text{ where } M(t)_{out} = M(t)_{settl} + M(t)_{res} + M(t)_{disch} \qquad (35)$$

The variable meaning is same as in eq.33) and (34). The error does not exceed 12 % which can be considered as a good simulation precision. All the cases with initial NM concentration 0.09 wt% (prescribed value) show the error below 6% which is twice lower than in cases with initial concentration of 1.8 wt% (20 times higher than prescribed value).

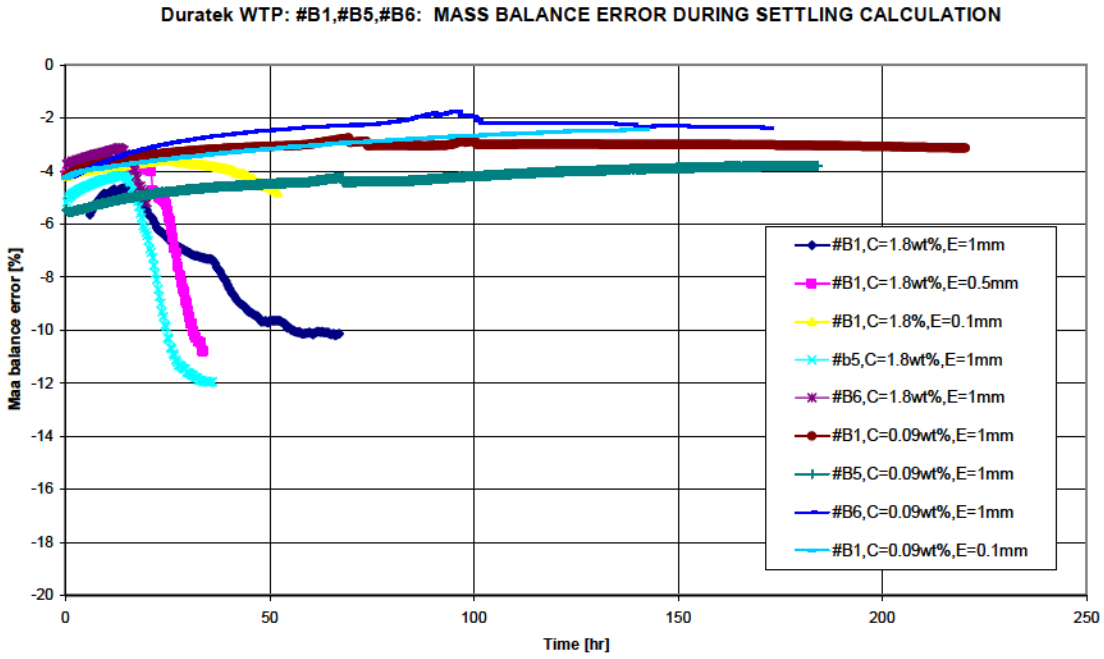


Figure 24. Mass balance error during transient settling calculation

### *Estimation of time to beginning of melter hot spots*

The goal of this study was to estimate the conditions at which the operation of melter begins to show adverse behavior due to noble metals. This situation is caused by the growth of the sludge layer which is more electrically conductive than the glass. When the layer of noble metals grows sufficiently, a change in the distribution of electrical values (potential, current, Joulean heat) will occur in the melter. During the calibration calculation a parameter was found which indicated the beginning of this process. This parameter is simply the time development of maximal temperature ($T_{max}$) in the melter inside or near the sludge layer. $T_{max}$ starts to rise at the time when the sludge layer starts

to become significant. The increase of $T_{max}$ is caused by the increase of Joulean heat generation due to higher electrical current passing through a significant height of sludge layer (see Figure 11c,d – Figure 15c,d). If the sludge layer is thin enough, $T_{max}$ remains essentially constant with time until hotspot are developed with temperature, $T_{max}$. This behavior is shown in Figures 25 through 29 for two different entrapment heights and two different noble metals concentrations.

Unfortunately, the computation time for actual melter settling conditions is too long to develop a significantly thick sludge layer. To overcome this excessively long computational time, a new approximation method was used: The input concentration of NM was increased 20-times (from 0.09 to 1.8 wt %) and entrapment was increased 10-times (from 0.1 to 1.0 mm). The sludge layer generation is not uniform but collects rapidly in piles located near or at the position of the bubbler nozzles, see Figure 19d and Figure 19e. Due to the non-uniformity of sludge accumulation, a simple value of average sludge thickness could not be used for quantitative analysis. Instead, a new parameter – the relative [%] bottom coverage by several thickness classes was introduced. The bottom coverage (given by % of total bottom surface) of NM layer not less than 5, 8, 17, 34, and 51 mm was calculated during the NM settling simulation. This quantity is designated as Cover>5mm, Cover>8mm, Cover>17mm, Cover>34mm, and Cover>51mm in the graphs on Figure 25 - Figure 29 or as time functions fc5(t), fc17(t) [%;hr] in Table 4.

The approximation method consisted of 3 steps:

1. Display calculated bottom cover [%] for the given thickness classes with maximum temperature, $T_{max}$. Estimate the critical time $t_{cr}$ for the initial departure of $T_{max}$ above the average bulk glass temperature and calculate the cover values $fc5_{cr} = fc5(t_{cr})$ and $fc17_{cr} = fc17(t_{cr})$ (which were chosen as being representative) for case #B1, #B5, and #B6 at high conditions of input NM concentration of 1.8 wt% and entrapment height of 1mm at which the maximum temperature breaks away from the average (see Figure 25a, 26a, 27a, 28a, 29a).
2. Calculate bottom cover [%] course fc5(t) and fc17(t) for case #B1, B5, and #B6 at actual input NM concentration 0.09 wt% and enhanced entrapment 1mm. (see Figure 25b,26b, 27b). Find the extrapolation of cover functions fc5(t) and fc17(t) up to the critical values $fc5_{cr}$ and $fc17_{cr}$ and calculate the $T_{max}$ rise critical time $t_{cr}$ which is supposed to be valid for the given settling conditions (C=0.09 wt%, E=1mm), see Table 4. We need to suppose the character of bottom cover process is analogous for both values of NM concentration (1.8, and 0.09 wt%). This can be estimated by comparing the curves in Figures 25a – 27a and Figures 25b – 27b.
3. Calculate the time dependent development of cumulative mass of settled NM for input concentrations C=1.8 wt% and C=0.09 wt% and for entrapment E=1mm and E=0.1mm (see Figure 30). This mass accumulation function is linear (except for the starting period), as indicated in Figure 30. Now, using this linearity, we can suppose the critical time $t_{cr}$ at actual conditions (C=0.09wt%, E=0.1mm) is proportional to the entrapment value: We are able to calculate the critical time $t_{cr}$ for actual entrapment=0.1mm from knowledge of the $t_{cr}$ for entrapment=1mm by using the proportionality factor, the slope of the line for an entrapment of 1 mm compared to 0.1 mm from figure 30 as = 0.1004/0.0367 = 2.7357. The time development on Figure 30 indicates that this proportionality is practically the same for all the cases #B1, #B5, and #B6.

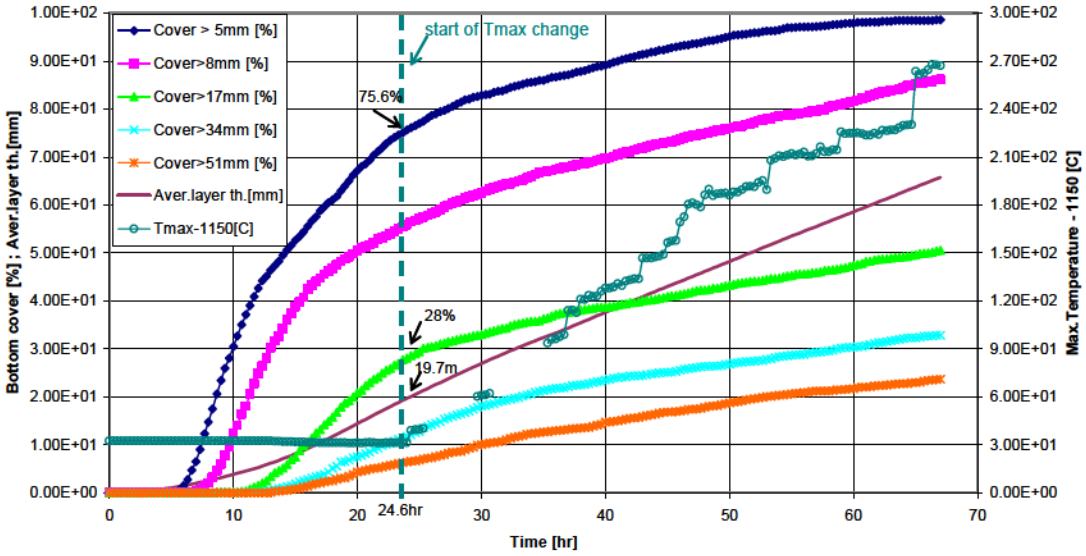


Figure 25a. Time development of bottom cover by NM sludge and melter max. temperature Tmax and estimation of critical time $t_{cr}$ in cases #B1C1,8E1,0 for $RuO_2$ initial concentration=1.8wt% and entrapment=1mm (WTP case 1)

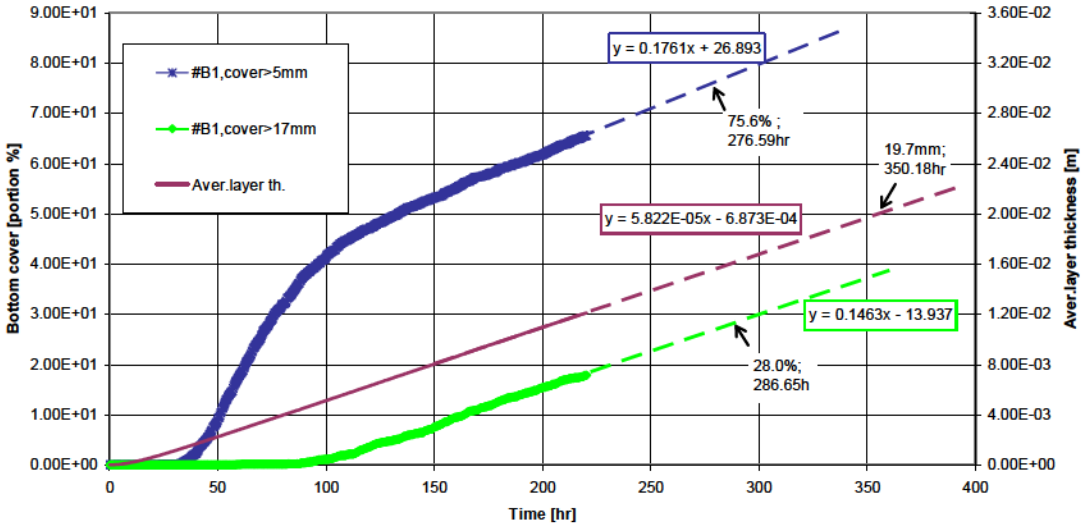


Figure 25b. Time development fc5(t) and fc17(t) of bottom cover by NM sludge including extrapolation and estimation of critical time $t_{cr}$ of Tmax rise in case #B1C0,09E1,0 for $RuO_2$ initial concentration=0.09wt% and entrapment=1mm (WTP case 1)

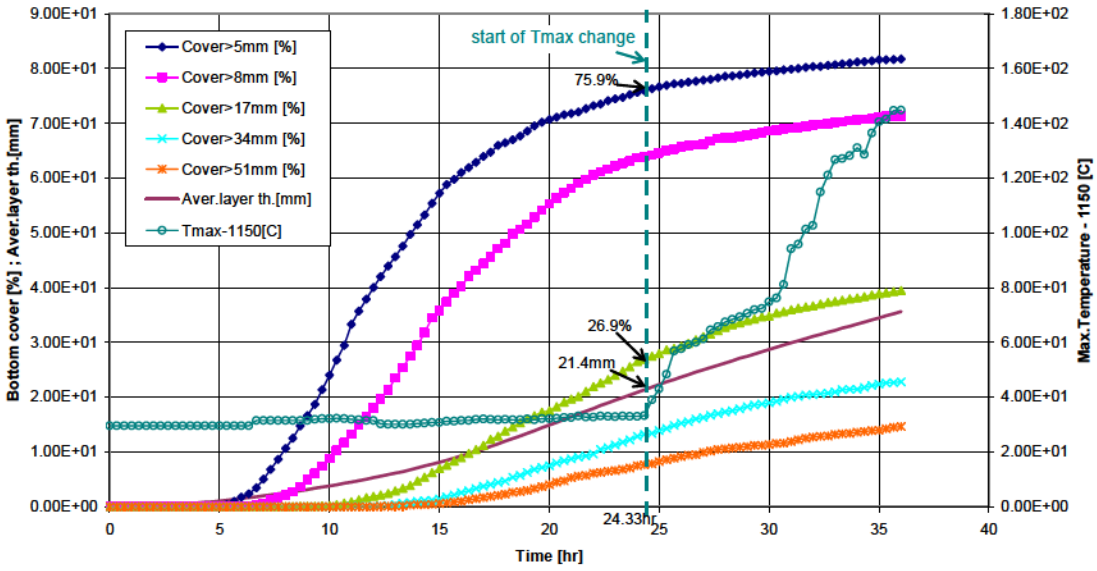


Figure 26a. Time development of bottom cover by NM sludge and melter max. temperature Tmax and estimation of critical time $t_{cr}$ in case #B5C1,8E1,0 (one bubbler off) for $RuO_2$ initial concentration = 1.8wt% and entrapment=1mm (WTP case 2C)

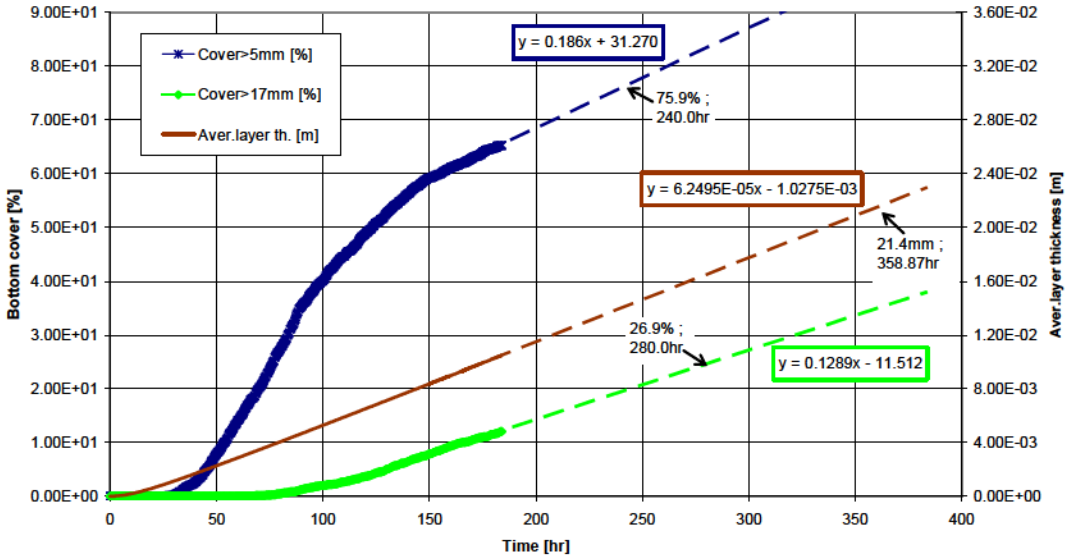


Figure 26b. Time development fc5(t) and fc17(t) of bottom cover by NM sludge including extrapolation and estimation of critical time $t_{cr}$ of Tmax rise in case #B5C0,09E1,0 (one bubbler off) for $RuO_2$ initial concentration=0,09wt% and entrapment=1mm (WTP case 2C)

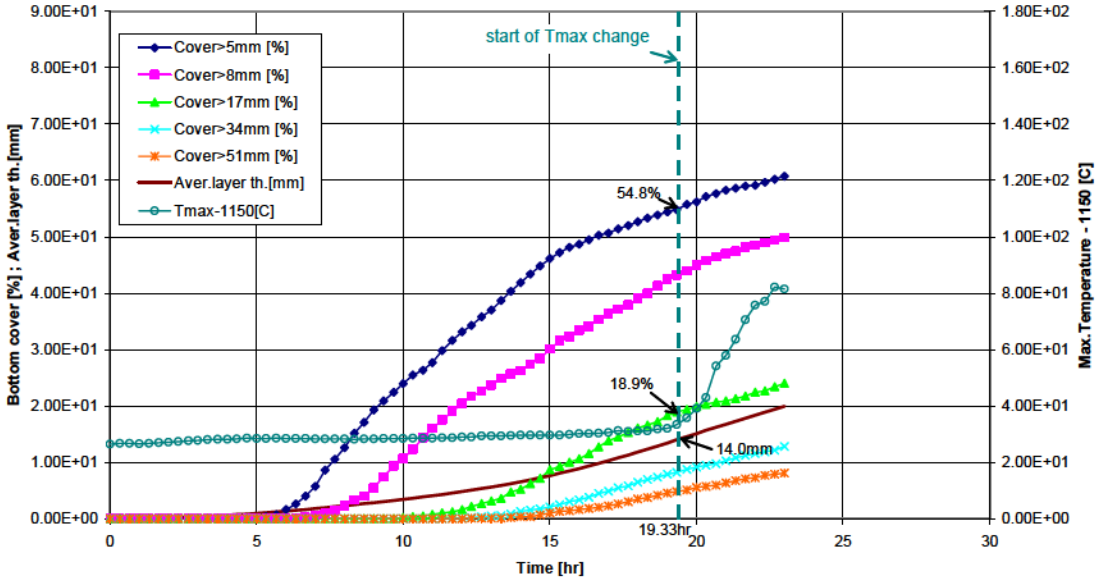


Figure 27a. Time development of bottom cover by NM sludge and melter max. temperature Tmax and estimation of critical time $t_{cr}$ in case #B6C1,8E1,0 (two bubblers off) for $RuO_2$ initial concentration=1.8wt% and entrapment=1mm (WTP case 2D)

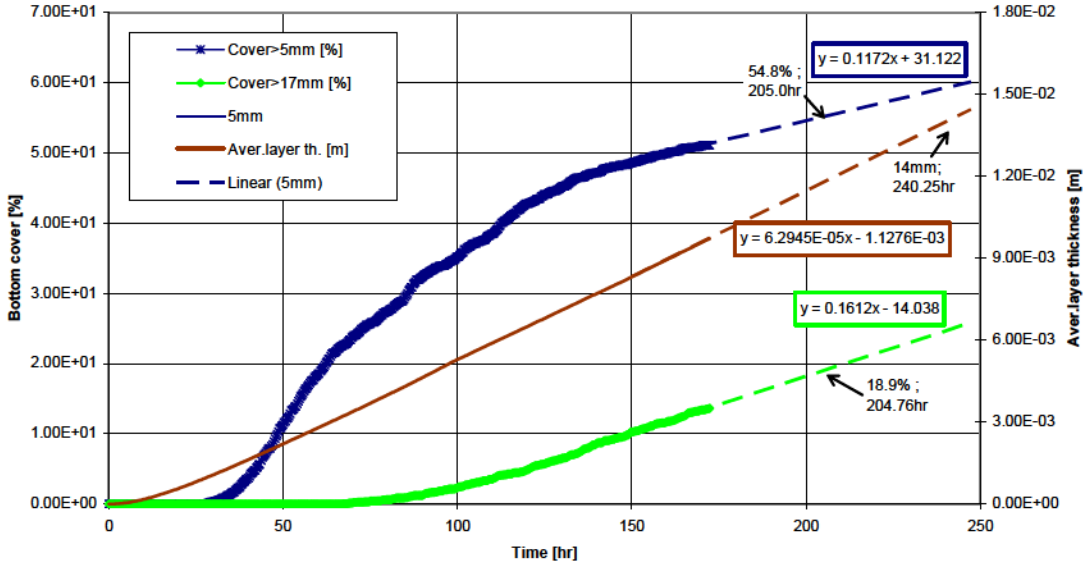


Figure 27b. Time development fc5(t) and fc17(t) of bottom cover by NM sludge including extrapolation and estimation of critical time $t_{cr}$ of Tmax rise in case #B6C0,09E1,0 (two bubblers off) for $RuO_2$ initial concentration=0,09wt% and entrapment=1mm (WTP case 2D)

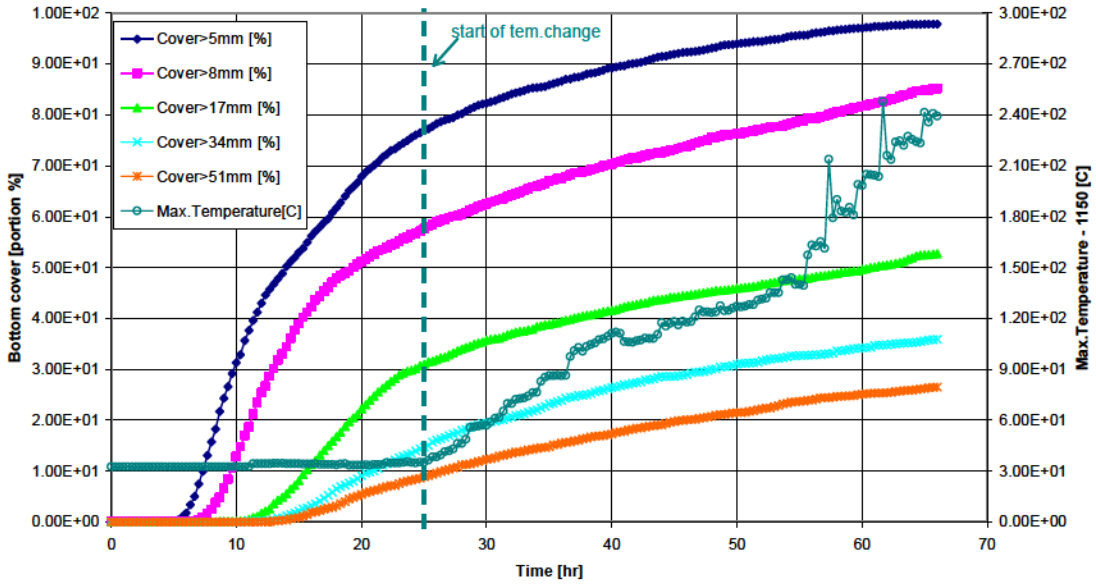


Figure 28a. Time development of bottom cover by NM sludge and melter max. temperature Tmax and estimation of critical time $t_{cr}$ in case #B1C1,8E1,0EL2x for $RuO_2$ initial concentration=1.8wt%, entrapment=1mm, and 2-times higher sludge electrical conductivity (WTP case 1)

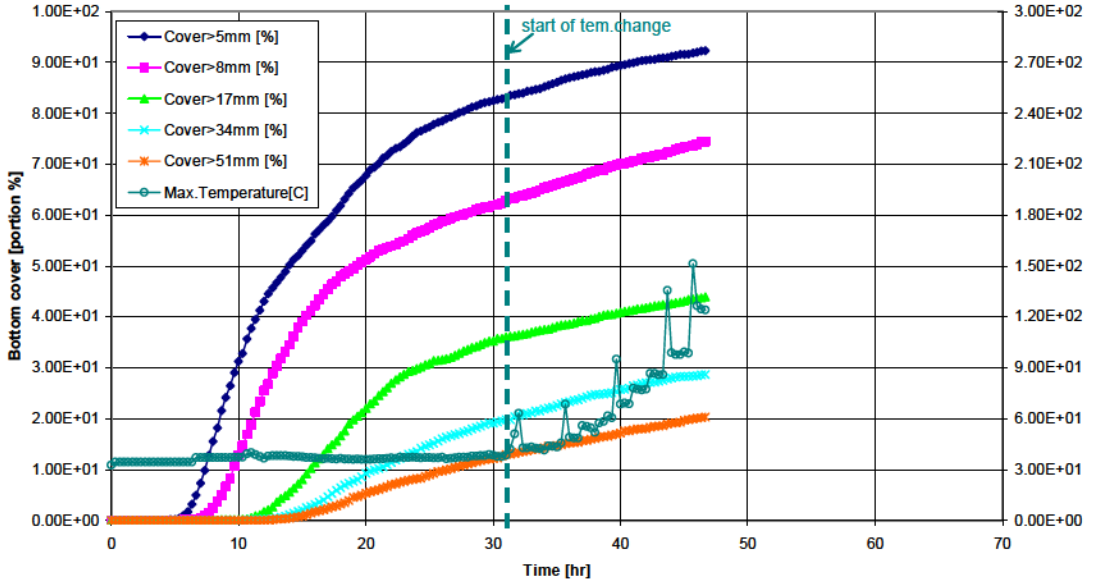


Figure 29a. Time development of bottom cover by NM sludge and melter max. temperature Tmax and estimation of critical time $t_{cr}$ in case #B1C1,8E1,0EL5x for $RuO_2$ initial concentration=1.8wt%, entrapment=1mm, and 5-times higher sludge electrical conductivity (WTP case 1)

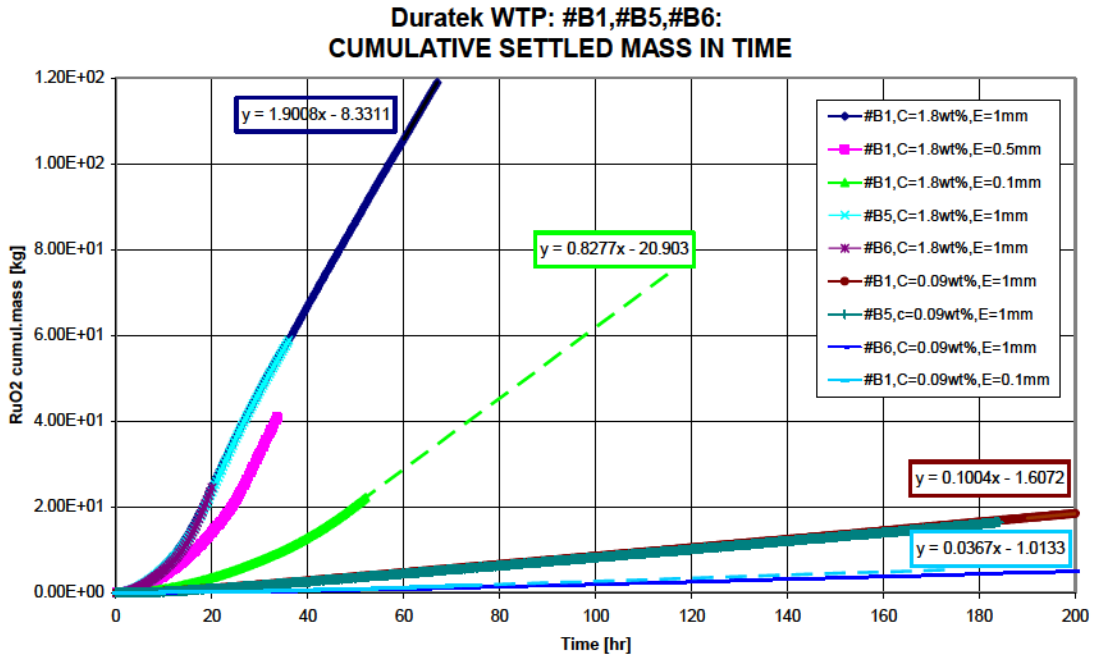


Figure 30. Time development of NM cumulative settled mass including extrapolations for all cases #B1, #B5, #B6 for $RuO_2$ initial concentration=0.09 wt% and 1.8wt% , and entrapment=1mm and 0.1 mm

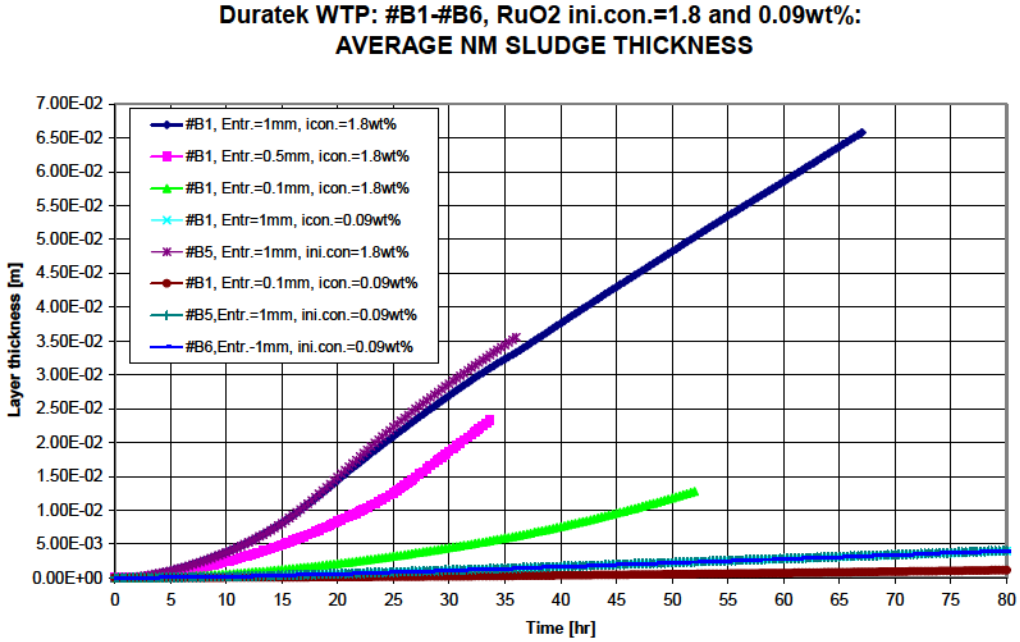


Figure 31. Time development of NM average thickness of sludge layer in all cases #B1, #B5, #B6 for $RuO_2$ initial concentration=0.09 wt% and 1.8wt% , and entrapment=1mm and 0.1 mm

## Table 4. Estimation of critical time for onset of hot spots for cases #B1, #B5, #B6

| Case # | Bottom cover at Tmax jump | | Aver.layer | Bottom cover > 5 mm | | Bottom cover > 17 mm | | Average layer thickness | |
|---|---|---|---|---|---|---|---|---|---|
| C=ini.con.[wt%] | Cover>5mm | Cover>17mm | thickness | Cover function | Tmax jump | Cover function | Tmax jump | function | Tmaxjump |
| E=entrap[mm] | fc5 [%] | fcl7 [%] | [mm] | fc5(t) ; [%]; [hr] | time [hr] | fc17(t) ;[%];[hr] | time [hr] | atl(t) ; [m];[hr] | time [hr] |
| #B1C1,8E1,0 | calcul.=75.6 | catcul.=28.0 | cal =197 | graphical | cat =246 | graphical | cal.=24.6 | graphical | Cal.=24.6 |
| #B1C0·09E1,0 | extrapo.=75.6 | extrapo.=28.0 | ex.=19.7 | 0.1761t+26.893 | ex.=276.59 | 0.1463(t)-13.937 | ex.=286.6 | 5.82E-5(t)-6.87E-4 | ex.=350. |
| #B1C0,09E0,1 | extrapo.=75.6 | extrapo.=28.0 | ex.=19.7 | pro.fac.= 2.7357 | ex.=756.67 | pro.fac.= 2.7357 | ex.=784.2 | pro.fac.= 2.7357 | ex.=958 |
| #B5C1,8E1,0 | calcul.75.9 | cafcul.=26.9 | cal.=21.4 | graphical | cal.=24.33 | graphical | cal.=24.33 | graphical | cal.=24.33 |
| #B5C0,09E1,0 | extrapo.=75.9 | extrapo.=26.9 | ex.=21.4 | 0.186t+31.270 | ex.=240.0 | 0.1289(t)-11.512 | ex.=280.0 | 6.249E-5(t)-1.027E-3 | ex.=359 |
| #B5C0·09E0,1 | extrapo.=75.9 | extrapo.=26.9 | ex.=21.4 | pro.fac.= 2.7357 | ex.=656.57 | pro.fac.= 2.7357 | ex.=766.0 | pro.fac.= 2.7357 | ex.=982 |
| #86C1,8E1,0 | calcul.=54.8 | calcuL=18.9 | cal.=14.0 | graphical | cal =19.33 | graphical | cal.=19.33 | graphical | cal=19.33 |
| #3600,09E1,0 | extrapo.=54.8 | extrapo.=18.9 | ex.=14.0 | 0.1101t+32.23 | ex.=205.0 | 0.1601(t)-13.833 | ex.=204.76 | 6.300E-5(t)-1.137E-3 | ex.=240. |
| #B6CO$^{3}$09E0,1 | extrapo.=54.8 | extrapo.=18.9 | ex.=14.0 | pro.fac.= 2.7357 | ex.=560.82 | pro.fac.= 2.7357 | ex.=560.2 | pro.fac.= 2.7357 | ex.=657. |

# SUMMARY AND CONCLUSIONS

## CHARACTER OF GLASS FLOW IN MELTER

The glass flow in the melter can be characterized as strongly circulated, more than was the case for the calculations for the DM1200 melter [5] because there are more bubbling nozzles and the bubbling rate per nozzle is higher. It can be assumed (based on comparison of retention values for various melters, [5], [6], [7]) that the entrapment height is a lower value (E=0.1mm) in the cases with stronger flow circulation than in cases of weaker flow circulation (E=1.0mm). The general flow in cases #B1,#B5, #B6 is essentially not influenced by the growing piles of sludge within the calculated settling times, see Figure 11a - Figure 16a.

## CHARACTER OF NM SETTLING IN MELTER

It was found that noble metals settling was not uniform but developed separate piles located at and around the nozzles, see Figure 11e, Figure 12e, Figure 13e, Figure 14e, Figure 15e, and Figure 16e. The sloped wedges at either end of the cavity beneath the electrodes had relatively high thickness of settled noble metals. When noble metals settling was modeled at an accelerated rate (high NM injection of 1.8 wt% and high entrapment height of 1mm) tall NM columns rose in some positions, see Figure 11a, Fig11c. This phenomenon could be caused by numerics of the settling algorithm or by the fact there is no feedback for unlimited growth such as a criteria for collapsing unstable piles, etc. inside the program, see analysis in chapter 3.6.2.

## PREDICTION FOR THE ONSET OF HOT SPOTS

The goal of this study was to estimate the conditions at which the operation of melter begins to move into a fault regime. This situation is caused by growing an electrically conductive sludge layer of non-uniform shape. It was found that a jump in the maximum melter temperature (Tmax) may be the first indication of the challenge of noble metals settling. However this localized influence does not flag eminent melter failure. This localized phenomena may take years to manifest itself from a macro influence into a global impact typically recognized by significant increases in electrode current. However, this observation may be an excellent parameter for identifying preferred melter designs with a modest amount of computer modeling, see Figure 25 – Figure 29. A double extrapolation technique was used to estimate the critical time $t_{cr}$ for the jump in the maximum temperature (initial concentration 0.09wt% and entrapment=0.1mm) for all cases #B1, #B5, #B6, see chapter 3.6.4.
It should be noted that the estimation for the onset in the jump of local temperature is more comparative than quantitative because of uncertainties of several properties (entrapment $h_E$, geometrical settling factor of particles $f_G$ (eq.29), sludge volume

fraction $VF_{NM}$) that have not been measured and the existing computer model settling algorithm which does not include feedback of unlimited growth, particle agglomeration, hindered settling, interaction of piles and collapsing, etc., see chapter 3.6.2. The height of the sludge layer is proportionately dependent on the value of the volume fraction for noble metals, $VF_{NM}$, and on the entrapment, $h_E$, for which the fundamental mechanisms are unknown, and less dependent on the value of $f_G$.

However, calculations presented herein are based on the most precise existing model for noble metals properties and parameters that are currently available. The presented computer model is universal and can be used directly in future applications by applying more precise parameters and properties if they become available.

## SENSITIVITY STUDY

A comparison between the reference conductivity of the noble metal sludge and ones with higher electrical conductivity were calculated. From the comparison of the sludge layer accumulated shown in Figures 25a, 28a, and 29a with normal, 2-times higher, and 5-times higher electrical conductivity, we conclude that sludge electrical conductivity does not appear to influence sludge accumulation.

## REFERENCES

[1] S.V.Patankar, "Numerical heat transfer and fluid flow", Hemisphere Publishing Corporation, 1980

[2] P.Schill, M.Trochta, J.Matyas, L.Nemec, P.Hrma, "Mathematical model of spinel settling in a real Waste glass melter", Proceeding "Waste Management 01", Tucson, AZ, 2001

[3] P.Schill, M.Trochta, "Advanced mathematical modeling of special glass furnaces", 2002 Glass Odyssey, 6th ESG CONFEENCE, Montpellier, France, June 2-6, 2002

[4] HLW Melter Thermal-Hydraulic Model, Report created by Glass Service, Ltd. for Duratek, Inc., November 2001.

[5] Modeling the behavior of noble metals during HLW vitrification, Report created by Glass Service, Inc. for VSL the CUA, Washington, D.C., October 2004

[6] On the issue of noble metals in the DWPF melter, WSRC-TR-2001-00337 report created by Westinghouse Savannah River Company, Aiken, SC and PNNL, Richland, WA, August, 2001

[7] Role of noble metals in electrically heated ceramic waste glass melters, Report created by Forschungszentrum Karlsruhe INE for CUA, August, 2003

Glass Service Inc.
Rokytnice 60
755 01 Vsetin
Czech Republic

# SIMULATION STUDY OF THE WTP MELTER

## Additional Cases

*Prepared by*

Petr Schill

Glass Service, Inc.
Rokytnice 60, Vsetin 75501
Czech Republic

*for*

Vitreous State Laboratory
The Catholic University of America
Washington, D.C.20064

June 17, 2005

## CONTENTS



## FIGURES

# INTRODUCTION

The purpose of this supplement was to model and report 4 additional cases according to the purchase order CUA 0000018061 dated 04/13/2005. This is a supplement to an earlier report by Glass Service, "SIMULATION STUDY OF THE WTP MELTER", 11/30/04.

The 4 cases that were modeled are as follows:

1. The first case (case A1) determined the total electrode current, voltage, flow field and temperature field for a condition where the noble metals (NM) build up reaches almost to the side power electrodes. The accumulated sludge shape was as specified in figure 1.
2. The second case (case A2) assessed the influence of increased bubbling rate on the temperature and flow fields for case B1. This case used 100 liters per minute per nozzle (3.5 ACFM), 10 nozzles, 170 bubbles per minute with a "hemispherical" bubble diameter of 130 mm. The previous modeling used a flow rate of 32.5 liters per minute per nozzle.
3. The third case (case A3) determined the temperature and flow fields for case B6 (with the assumption that two of the five assemblies were not operational) using a higher bubbling rate. This case also used 100 liters per minute per nozzle (3.5 ACFM), 6 nozzles, 170 bubbles per minute with a "hemispherical" bubble diameter of 130 mm. The previous modeling used a flow rate of 32.5 liters per minute per nozzle.
4. The fourth case (case A4) determined the bulk glass temperature during idling using a higher bubbling rate and higher average bulk temperature. The bulk glass temperature was set at 1075 C with a bubbling rate of 100 liters per minute per nozzle (3.5 ACFM), 10 nozzles, 170 bubbles per minute with a "hemispherical" bubble diameter of 130 mm.

For each of these modeling cases, the following information was provided:

- total electrode current and voltage
- data fields on disk for reviewing all the calculated data

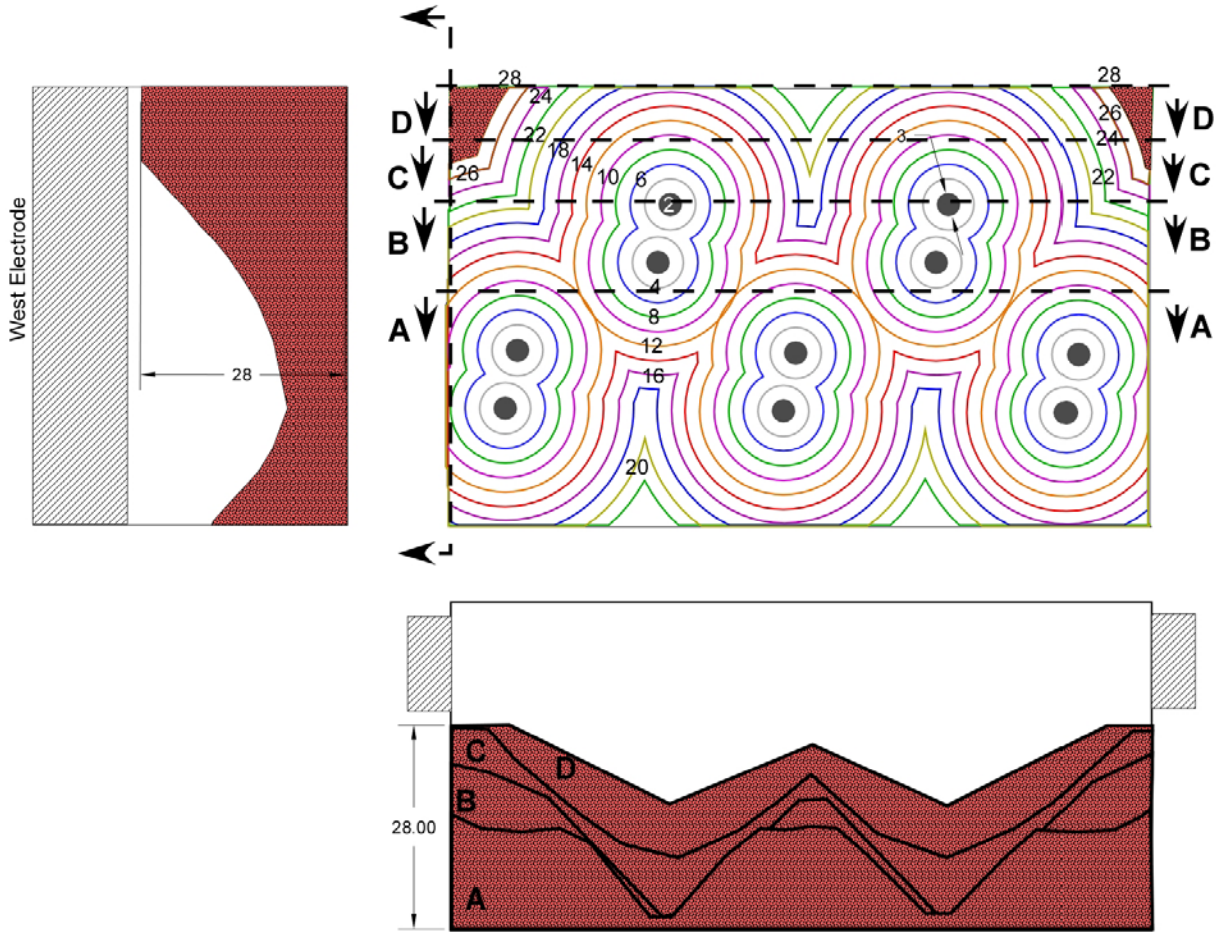


Figure 1 Form of the noble metal sludge to be modeled

# MODELING RESULTS

## NM Sludge properties and model shape

The NM sludge was approximated by a solid object of the required shape. The properties of this material were as follows:

Thermal conductivity (same as glass)

$\lambda = 2.73746 - 0.00242144.T + 1.86384.10^{-6}.T^2$ ; [W/(K.m.)] , [K]

valid for temperature range from 650 K to 1600 K

Electrical conductivity (corresponds to the maximal value for NM concentration 0.06 $m^3/m^3$ )

$\sigma = \sigma_{glass}(T) * 50.0 = \exp\{9.669373 - 1335.04 / (T - 771.441)\}$ ; [1/(Ω.m)] , [K]

valid for temperature range from 800 K to 1600 K

Reference density (at $T_{AS}$ = 915 C= 642 K, AS=Average Sludge)

$\rho_R = \rho_{glass}(T_{AS}) + 0.06.[\rho_{NM} + \rho_{glass}(T_{AS})] = 2590.0 + 0.06.(6970 + 2590.0) = 3163.6$ ; [$kg/m^3$]

Specific heat (same as glass)

$c_p$ = 1350 J/(kg.K)

The NM sludge was approximated according to figure 1 by one special model object, which is displayed in figure 2. This object can be extended up to desired position as needed to approach the side electrodes.

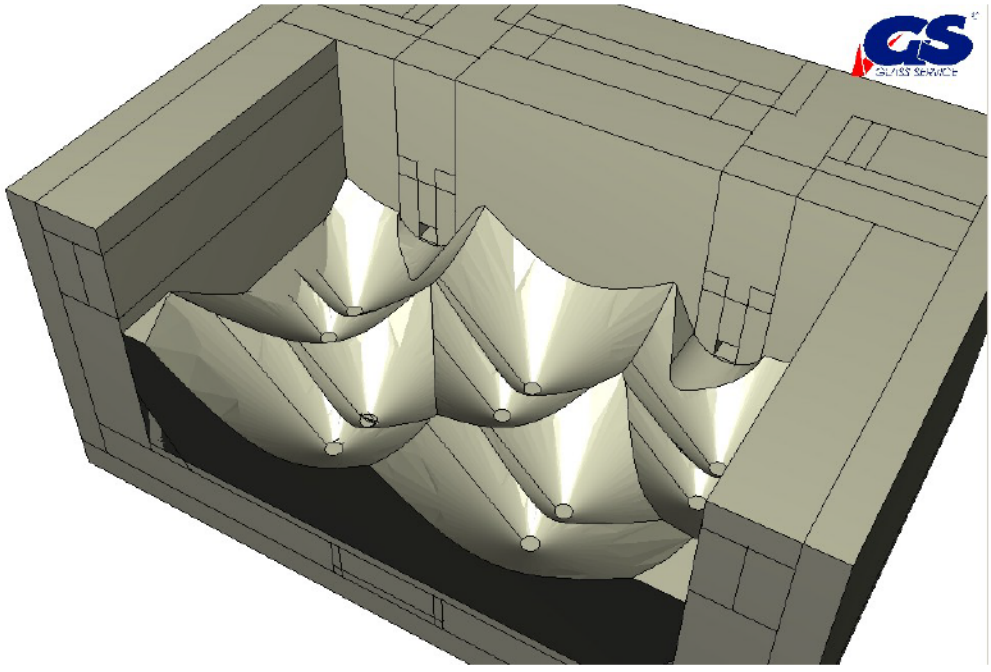

**Figure 2. Model approximation of the NM sludge**

## CALCULATED CASES

Using the GFM code, cases simulating WTP conditions A1, A2, A3 and idling A4 were calculated.

The electric heating was controlled by the model's PD controller of the electrode potentials with constants : P=1.5, D=20 within 5 iteration period. The average value of 6 temperature points located at the position of WTP thermocouples were used to adjust power input to maintain the setpoint temperature. The set-point control temperature was 1150 °C for cases A1, A2, A3 and 1075 °C for case A4.

### *Case A1*

In total, 5 conditions were calculated within this case. The condition A1-0 identifies the situation without any noble metals in the melter and it serves as a comparison with the NM filled cavity cases that follow. Cases A1-a, A1-b, A1-c identify the different maximum heights of NM fill, from 708 to 759 mm above the bottom. Case A1-d is the case where the NM contacts and overlaps the side electrode in the northwest and northeast corners by 29 mm. The resulting voltages, currents and the power for all five conditions are listed in table 1. Based on the WTP melter power supply limitations, A1-d indicates the melter would be unable to maintain the bulk glass temperature at the desired set point while remaining within the capabilities of the power supply. This case would indicate melter failure.

**Table 1 List of calculated electrical quantities for cases A1-0 to A1-d**

| Case | Maximum sludge height | Minimum distance: sludge to electrode | Electrode voltage | Electrode current | Total power |
|---|---|---|---|---|---|
| | (mm) | (mm) | [V] | [A] | [kW] |
| A1-0 | 0 | NA | 156 | 3,439 | 536 |
| A1-a | 708 | 76 | 134 | 4,316 | 578 |
| A1-b | 734 | 50 | 134 | 4,464 | 597 |
| A1-c | 759 | 25 | 134 | 4,730 | 635 |
| A1-d | 813 | -29 | 144 | 12,258 | 1,770 |

The following figures display the calculated flow, temperature and electrical fields in cases A1-0, A1-a, A1-b, A1-c, and A1-d.

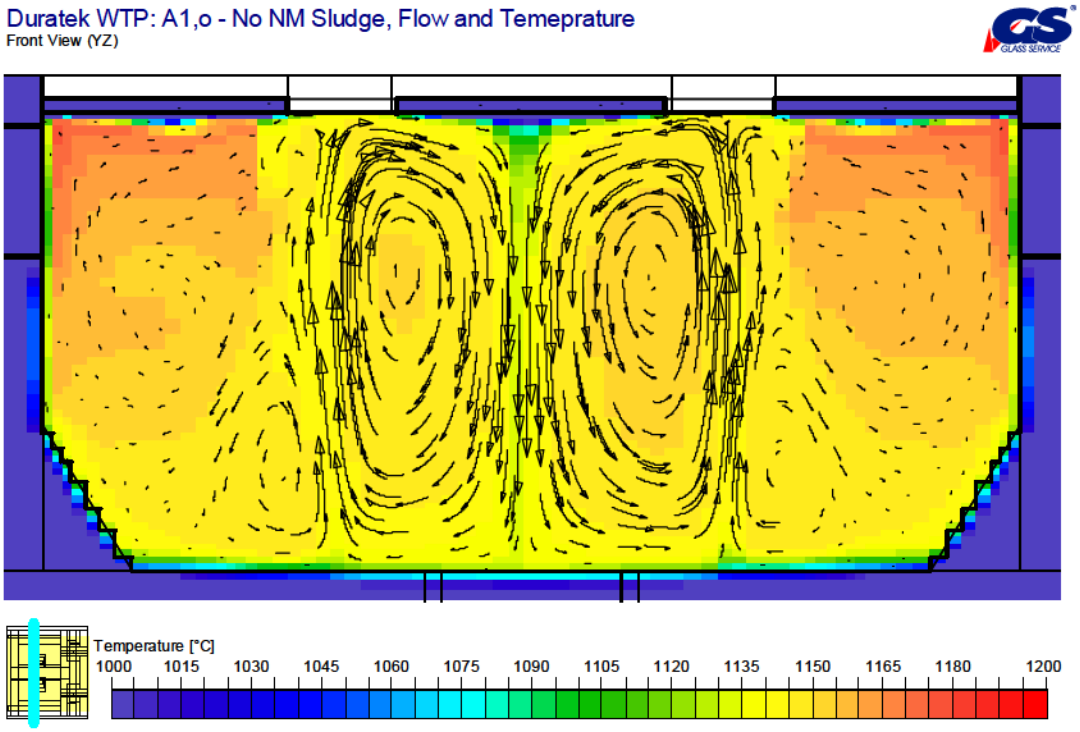


**Figure 3 Case A1-0: Flow and temperature distribution in YZ cut at x=1000mm (I=22)**

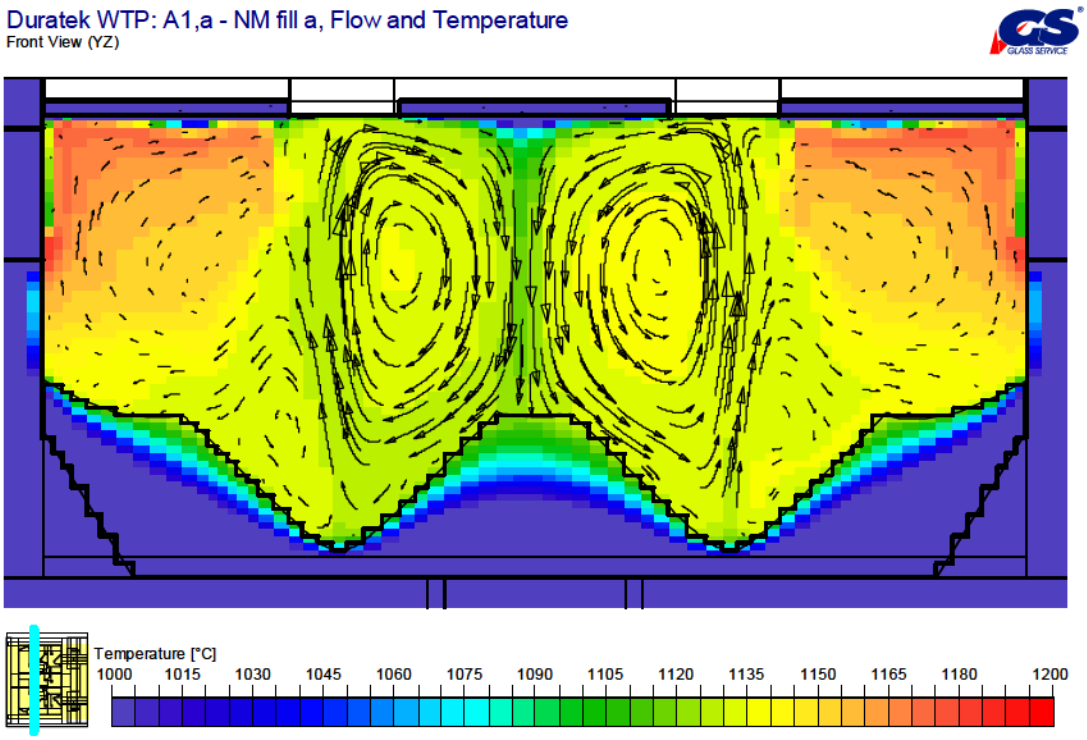


**Figure 4 Case A1-a: Flow and temperature distribution in YZ cut at x=1000mm (I=22)**

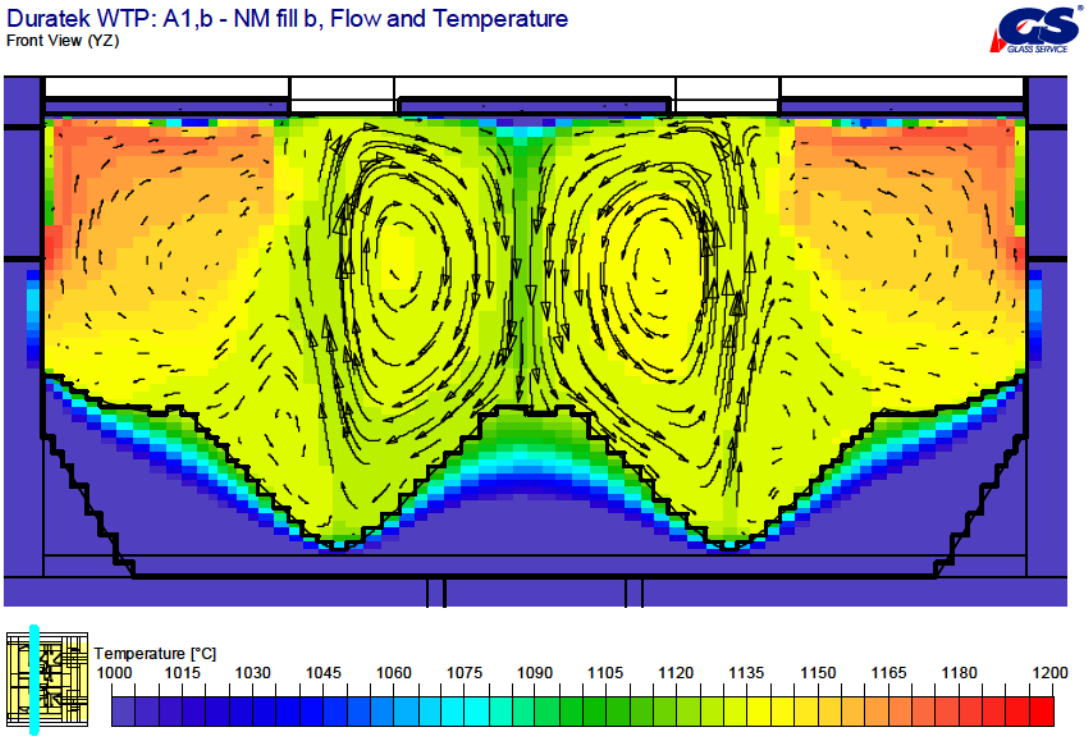


**Figure 5 Case A1-b: Flow and temperature distribution in YZ cut at x=1000mm (I=22)**

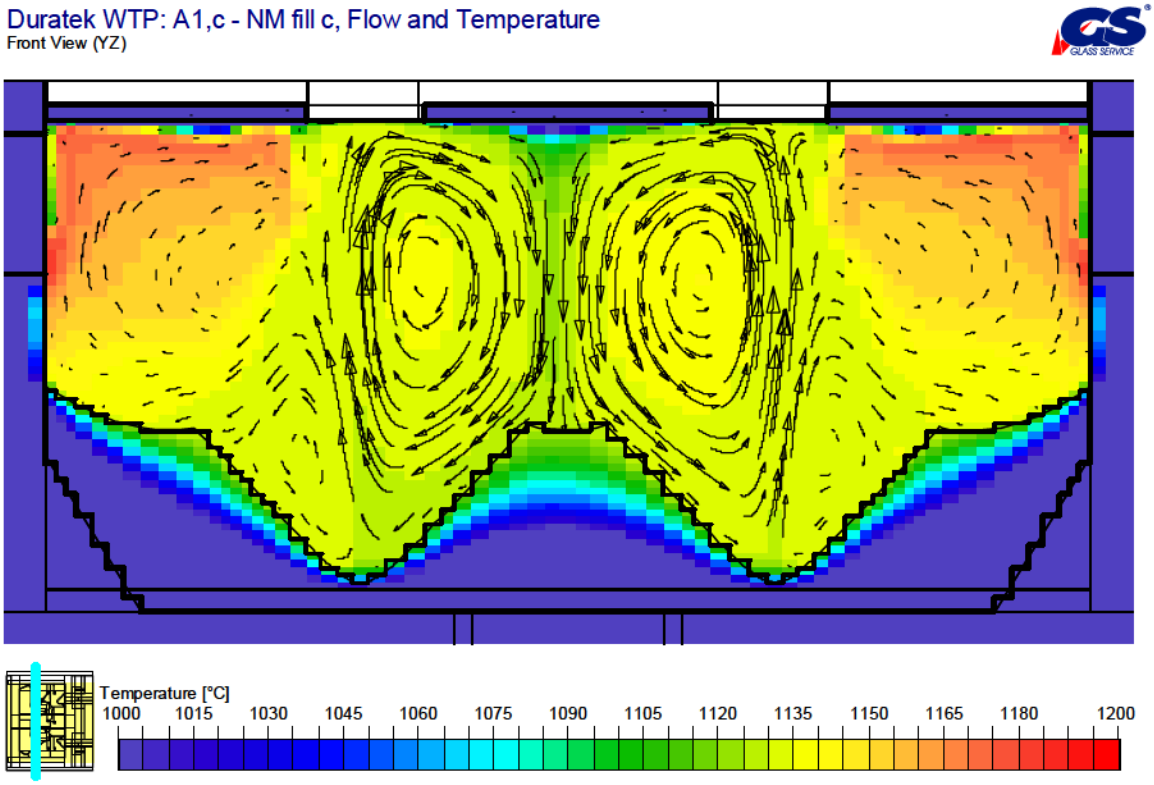


**Figure 6 Case A1-c: Flow and temperature distribution in YZ cut at x=1000mm (I=22)**

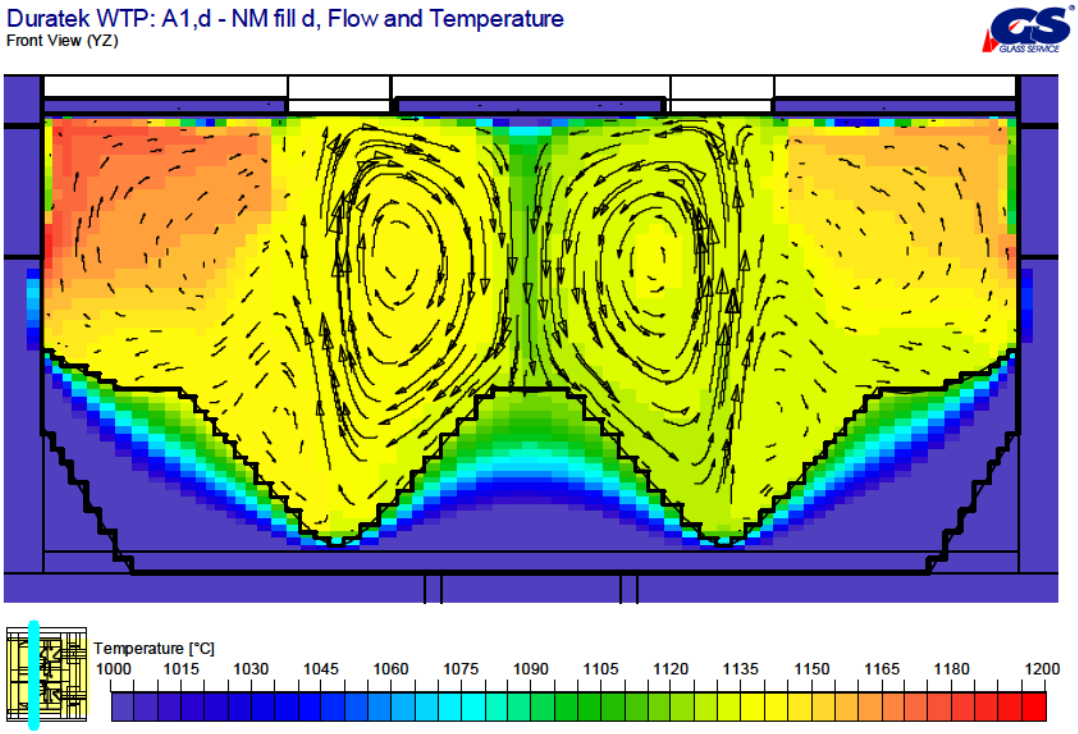


**Figure 7 Case A1-d: Flow and temperature distribution in YZ cut at x=1000mm (I=22)**

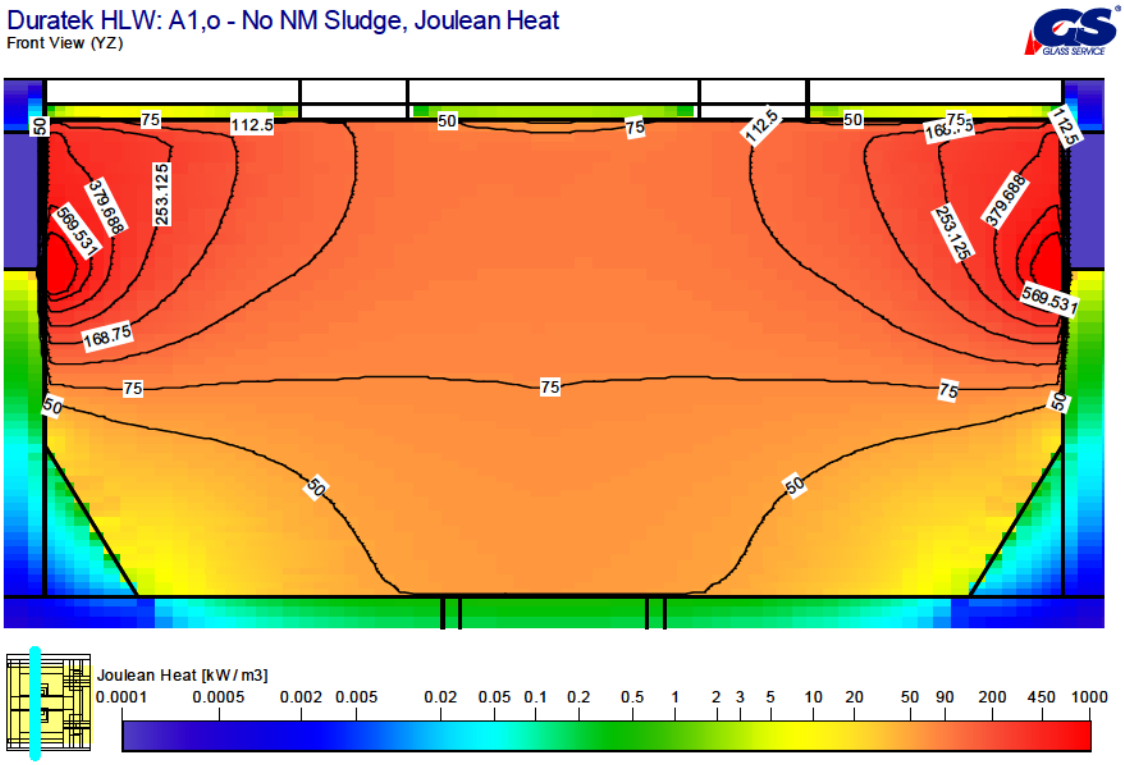


**Figure 8 Case A1-0: Joulean heat distribution (color fill) in YZ cut at x=1000mm (I=22)**

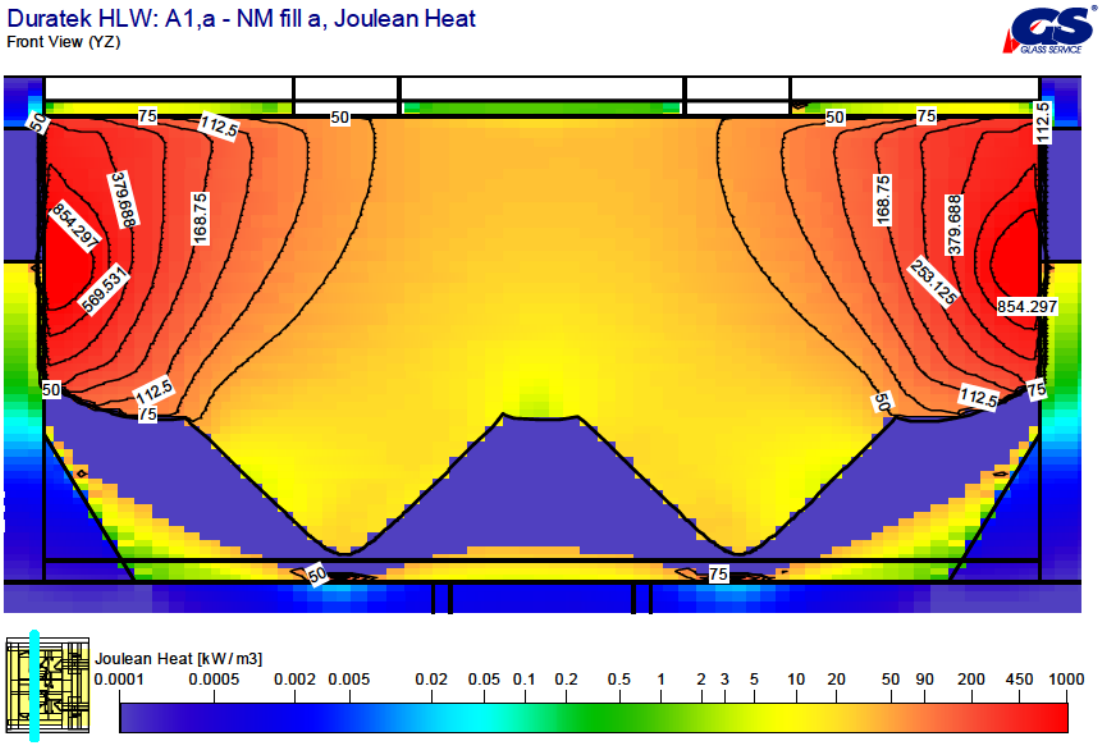


**Figure 9 Case A1-a: Joulean heat distribution (color fill) in YZ cut at x=1000mm (I=22)**

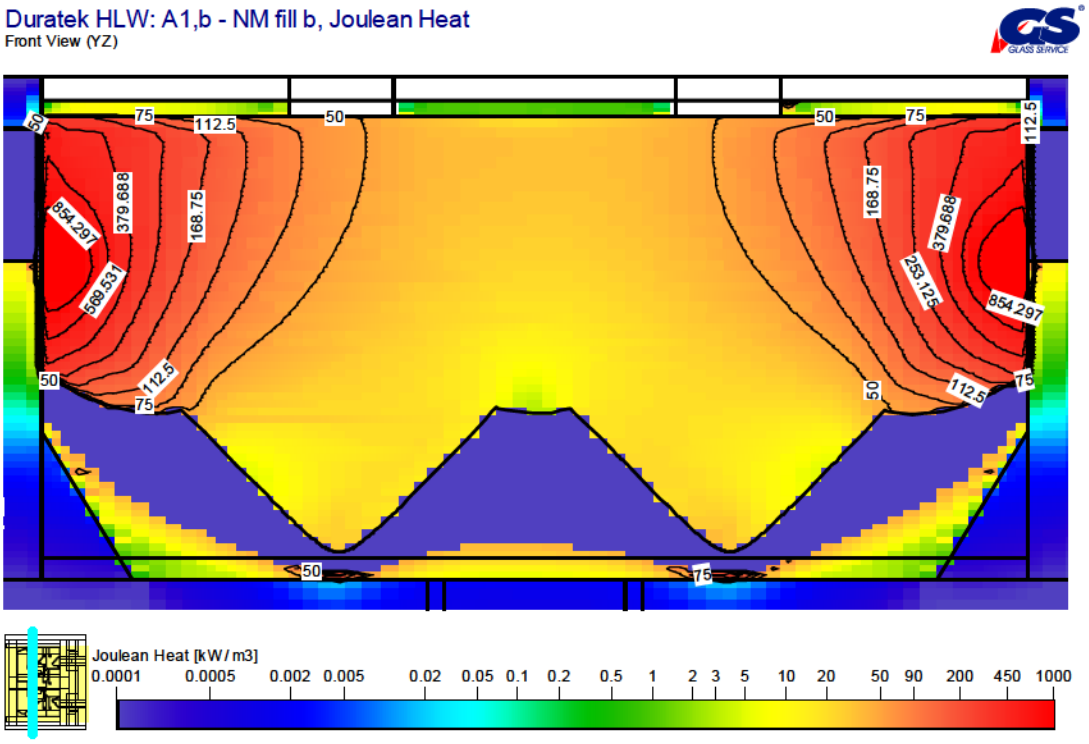


**Figure 10 Case A1-b: Joulean heat distribution (color fill) in YZ cut at x=1000mm (I=22)**

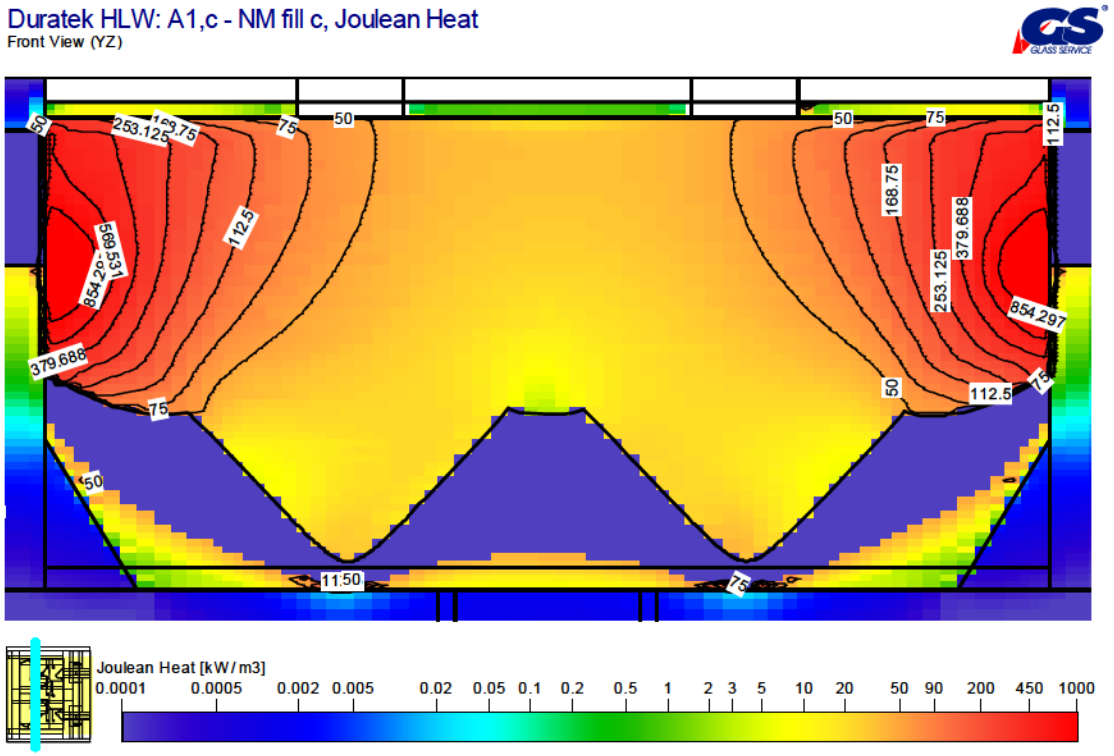


**Figure 11 Case A1-c: Joulean heat distribution (color fill) in YZ cut at x=1000mm (I=22)**

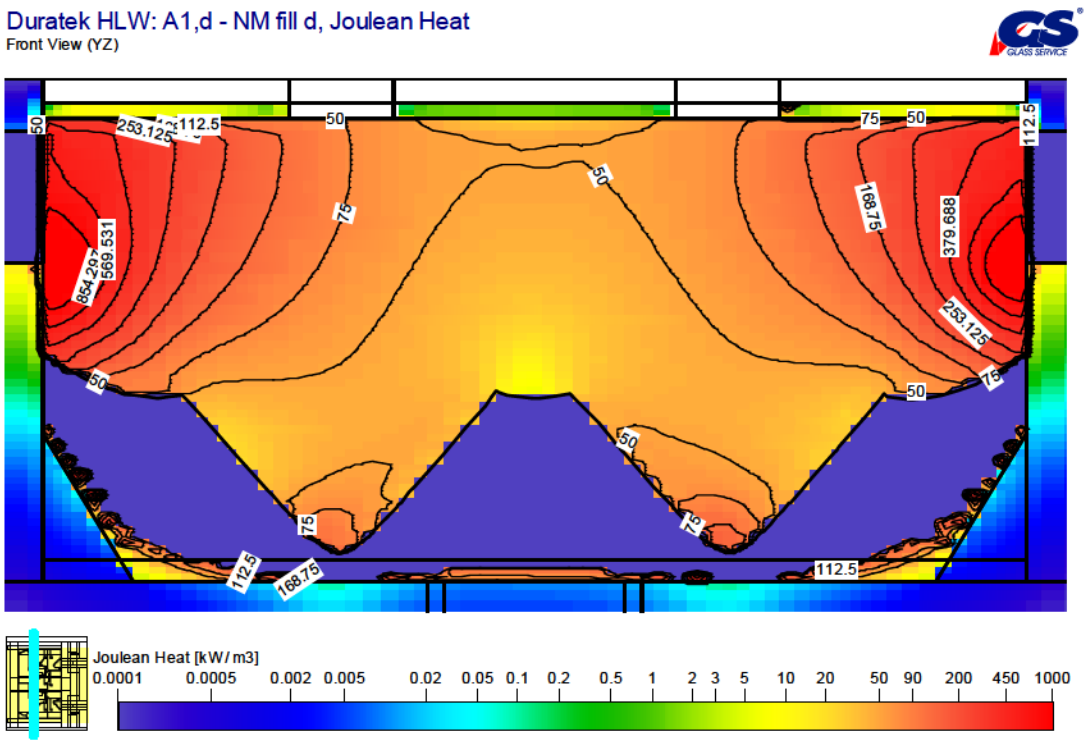


**Figure 12 Case A1-d: Joulean heat distribution (color fill) in YZ cut at x=1000mm (I=22)**

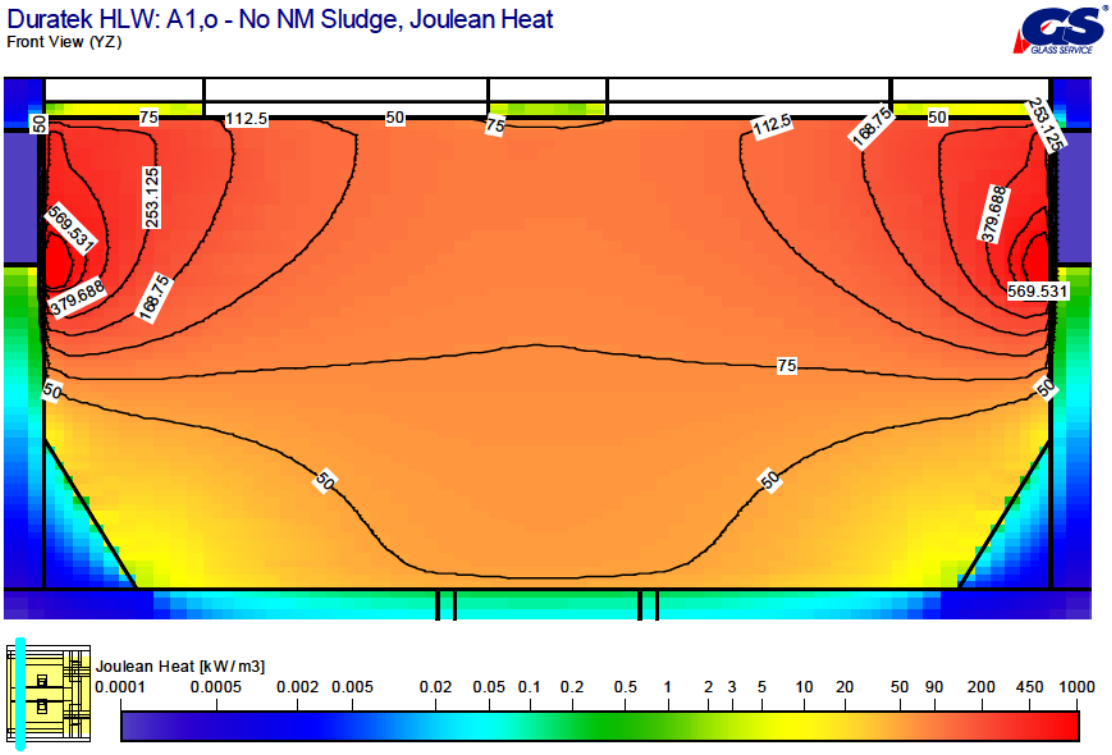


**Figure 13 Case A1-0: Joulean heat distribution (color fill) in YZ cut at x=469mm (I=10), at the highest position of NM fill**

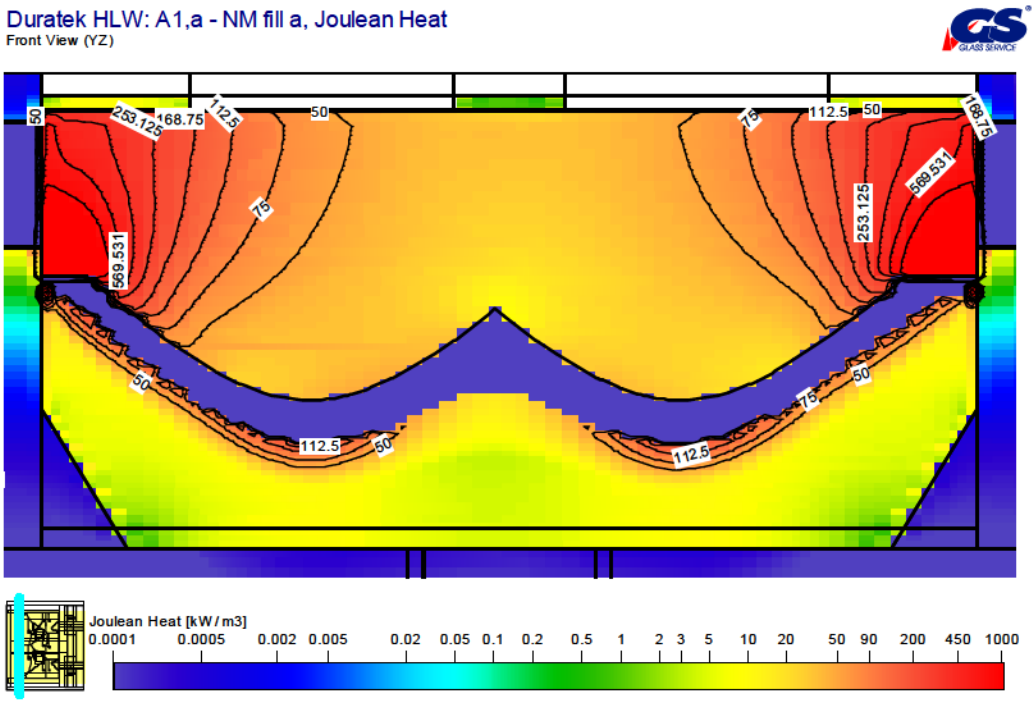


**Figure 14 Case A1-a: Joulean heat distribution (color fill) in YZ cut at x=469mm (I=10), at the highest position of NM fill**

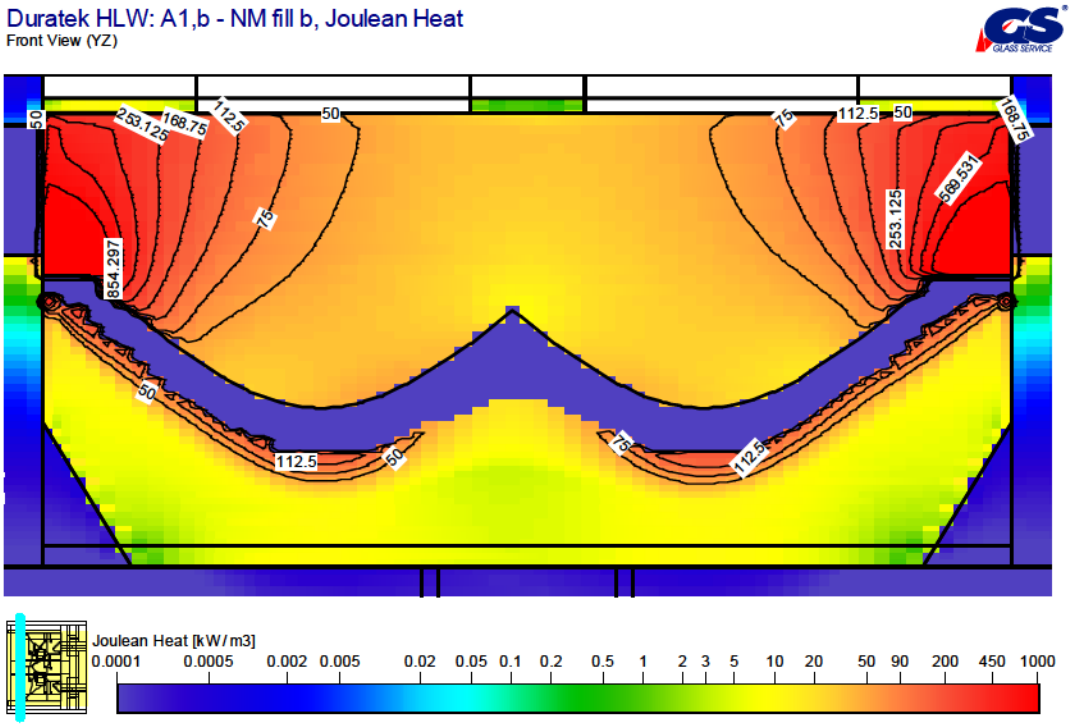


**Figure 15 Case A1-b: Joulean heat distribution (color fill) in YZ cut at x=469mm (I=10), at the highest position of NM fill**

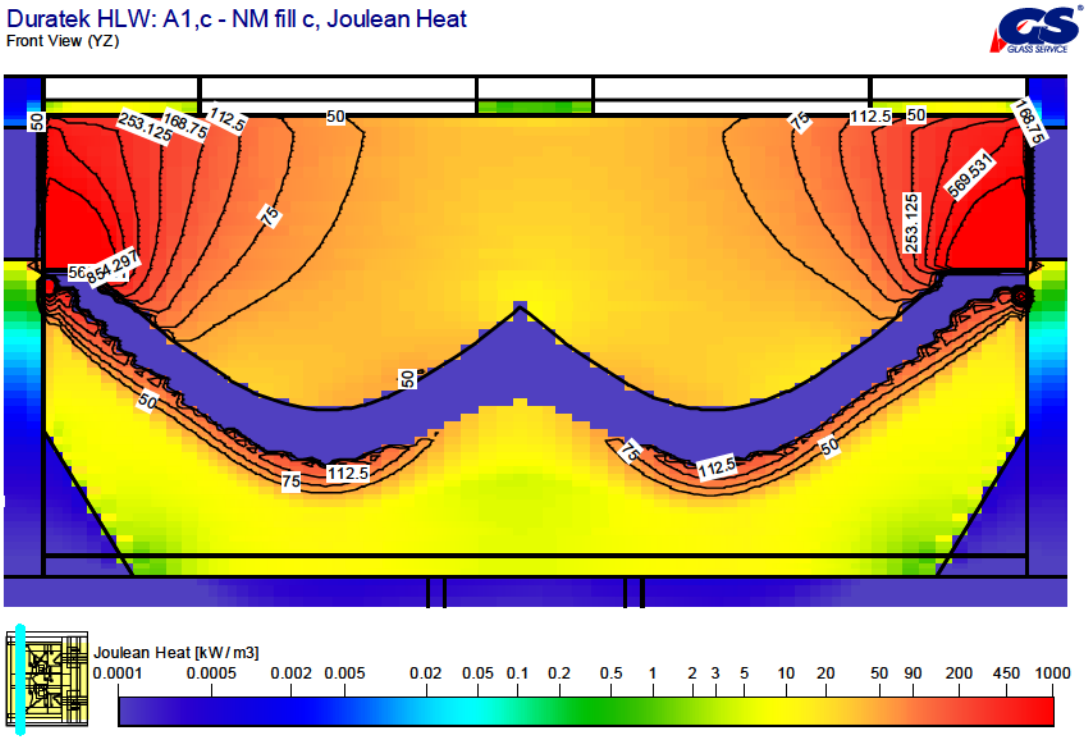


**Figure 16 Case A1-c: Joulean heat distribution (color fill) in YZ cut at x=469mm (I=10), at the highest position of NM fill**

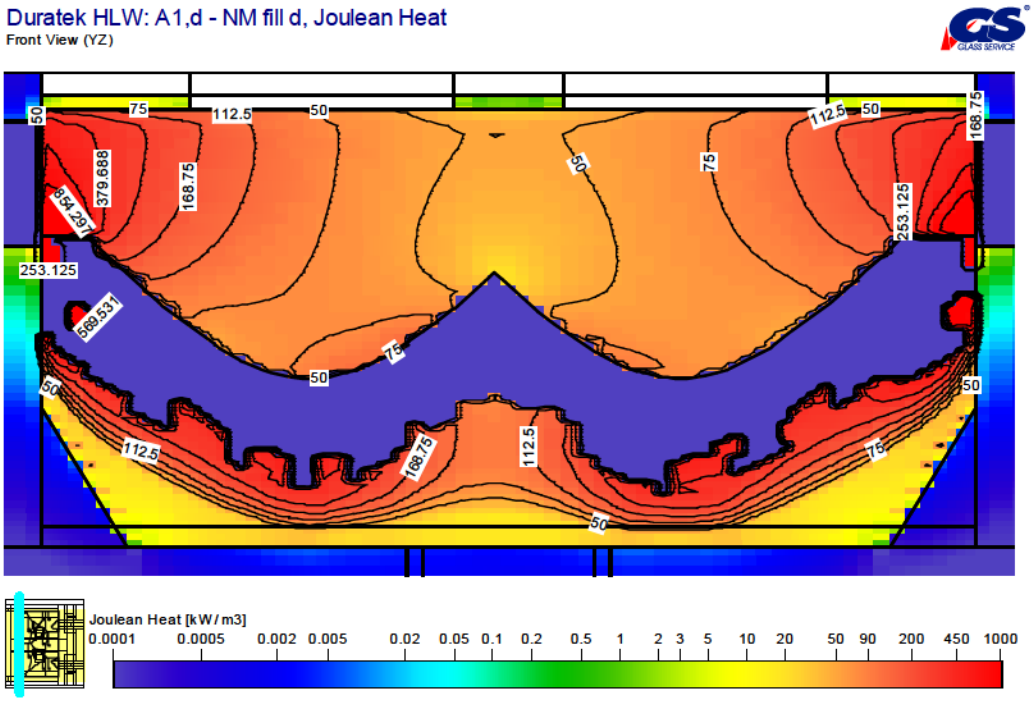


**Figure 17 Case A1-d: Joulean heat distribution (color fill) in YZ cut at x=469mm (I=10), at the highest position of NM fill**

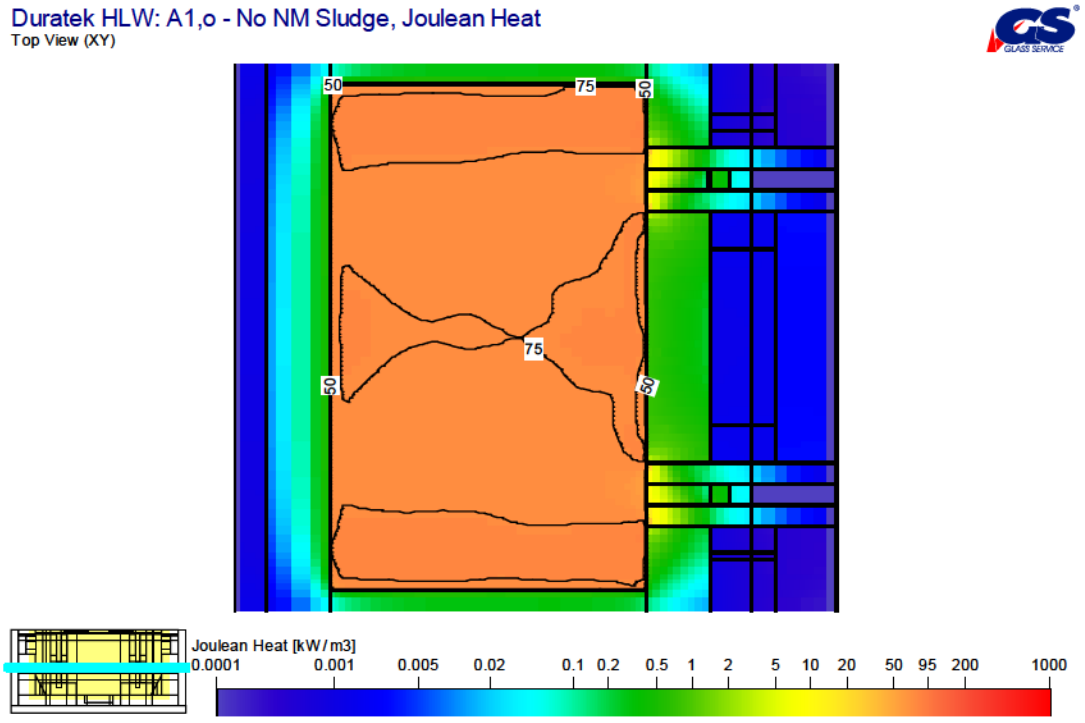


**Figure 18 Case A1-0: Joulean heat distribution (color fill) in horizontal XY cut at 507 mm above the bottom (K=38)**

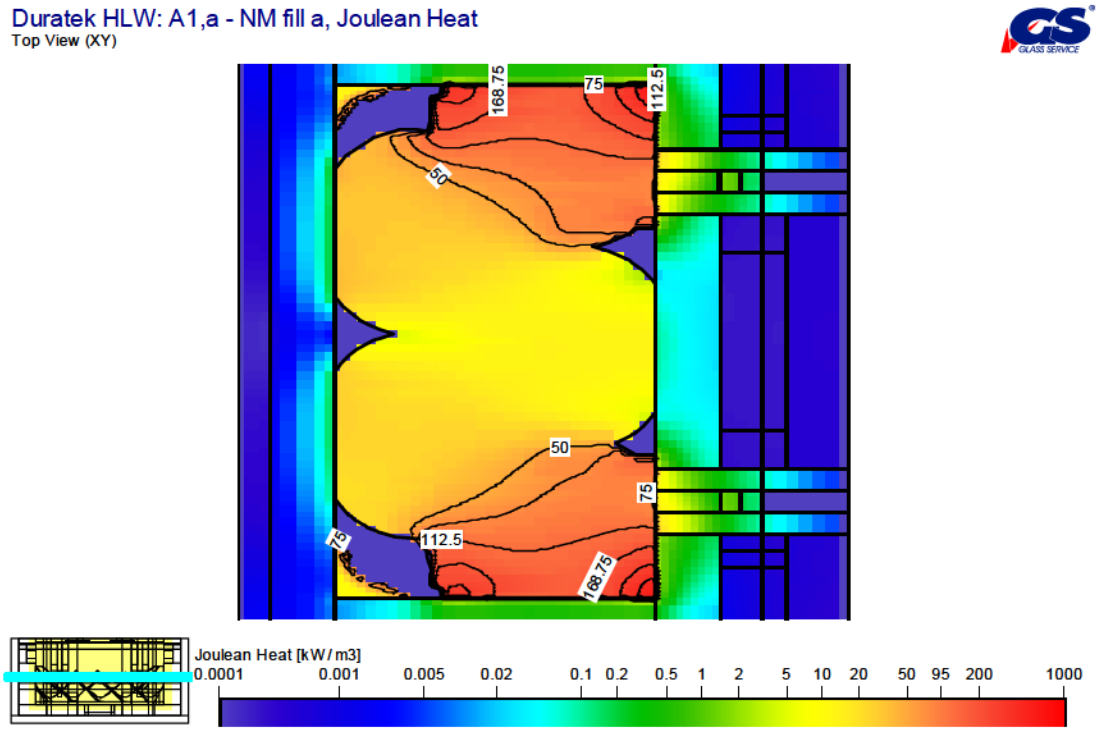


**Figure 19 Case A1-a: Joulean heat distribution (color fill) in horizontal XY cut at 507 mm above the bottom (K=38)**

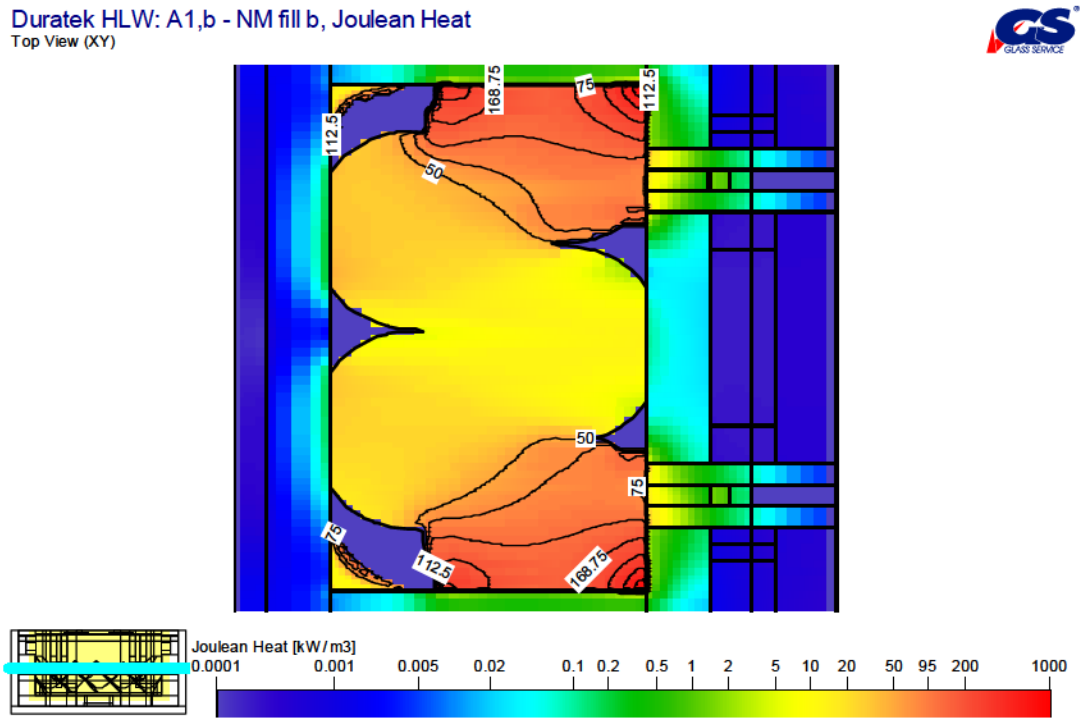


**Figure 20 Case A1-b: Joulean heat distribution (color fill) in horizontal XY cut at 507 mm above the bottom (K=38)**

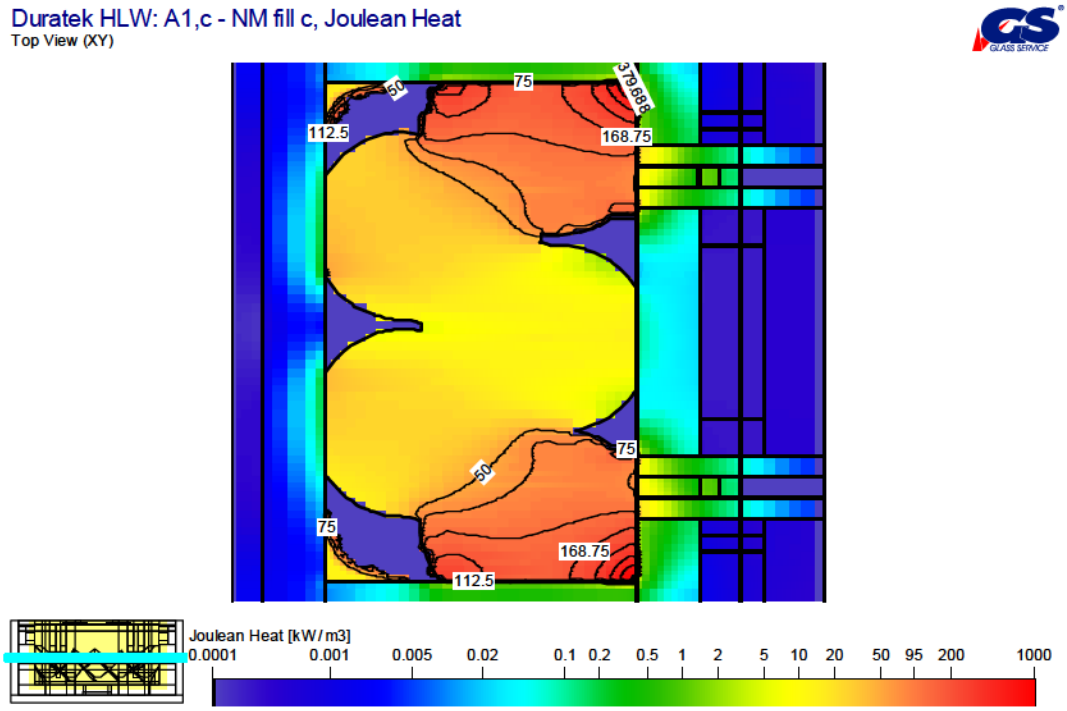


**Figure 21 Case A1-c: Joulean heat distribution (color fill) in horizontal XY cut at 507 mm above the bottom (K=38)**

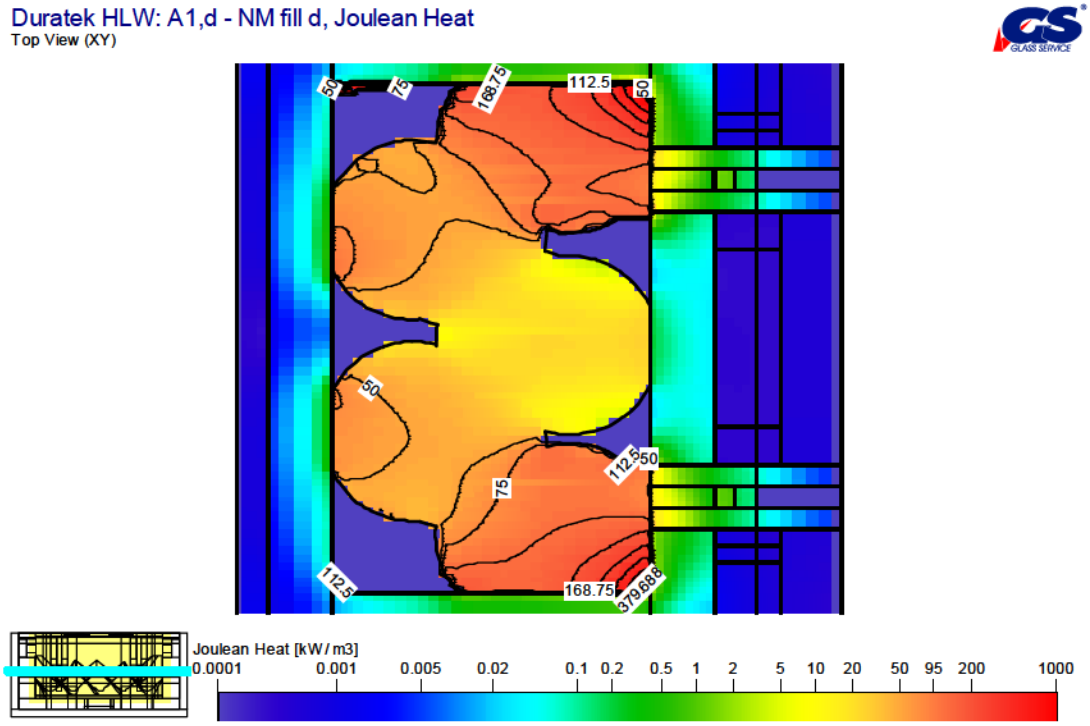


**Figure 22 Case A1-d: Joulean heat distribution (color fill) in horizontal XY cut at 507 mm above the bottom (K=38)**

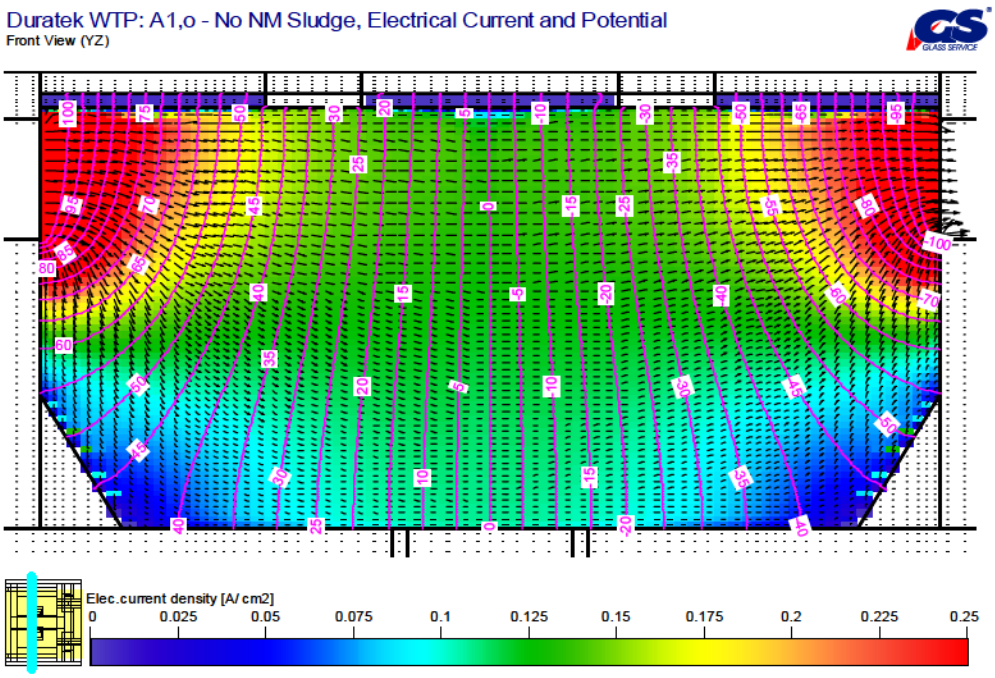


**Figure 23 Case A1-0: Electric current density [A/cm$^2$] (color fill), vector of electrical current, and electrical potential isolines in the YZ cut at x=1000mm (I=22)**

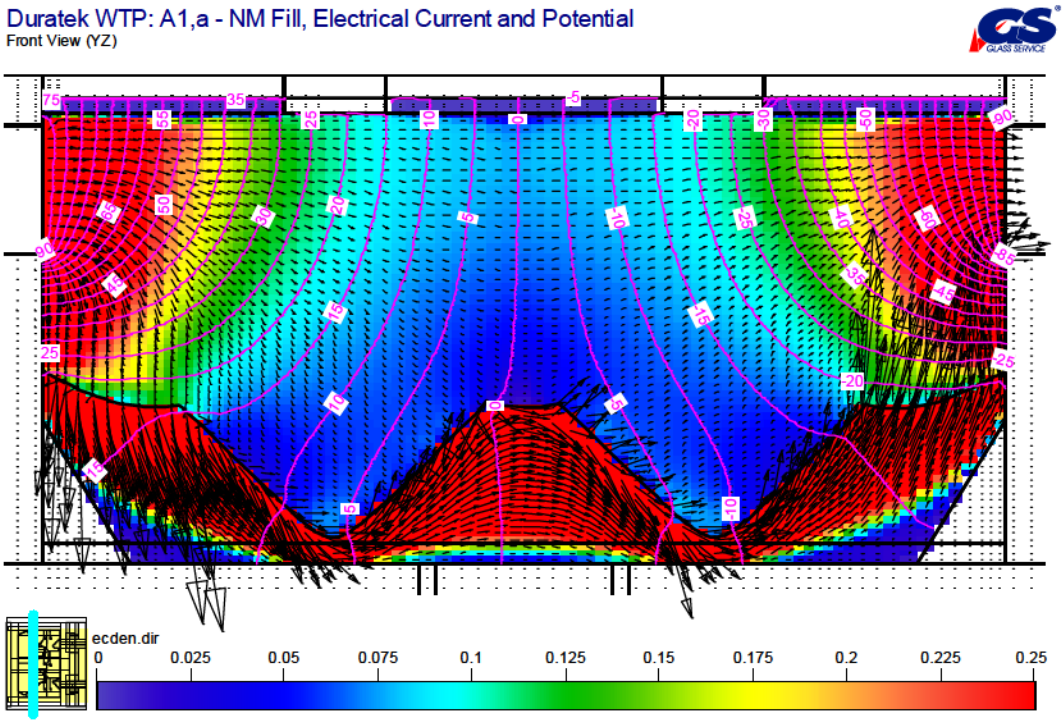


**Figure 24 Case A1-a: Electric current density [A/cm$^2$] (color fill), vector of electrical current, and electrical potential isolines in the YZ cut at x=1000mm (I=22)**

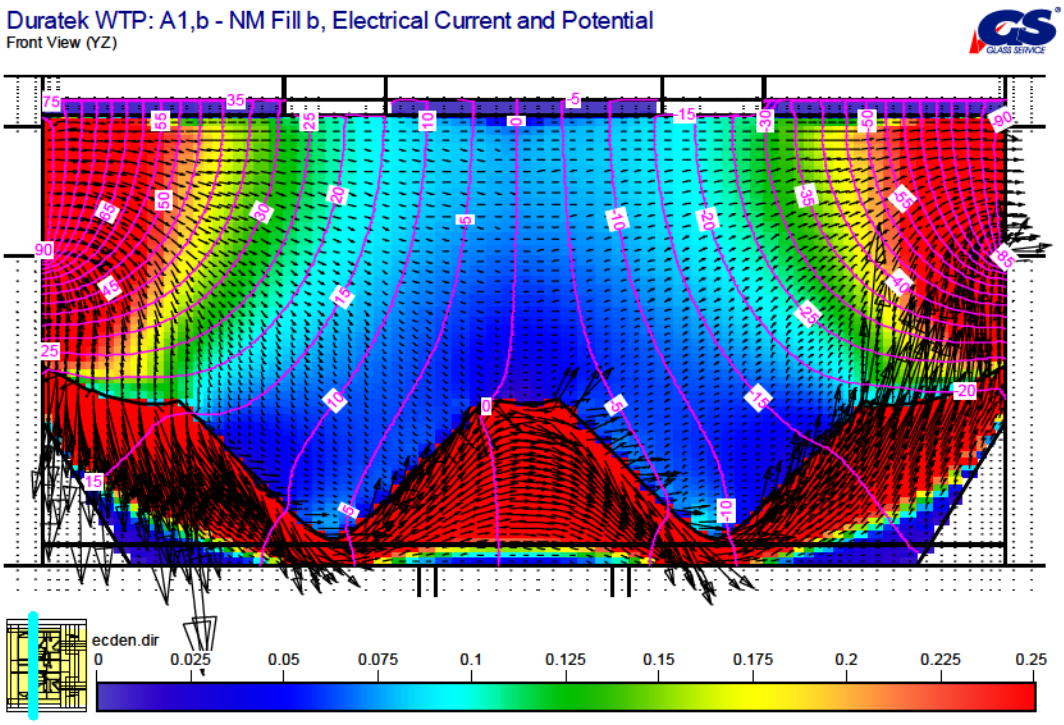


**Figure 25 Case A1-b: Electric current density [A/cm$^2$] (color fill), vector of electrical current, and electrical potential isolines in the YZ cut at x=1000mm (I=22)**

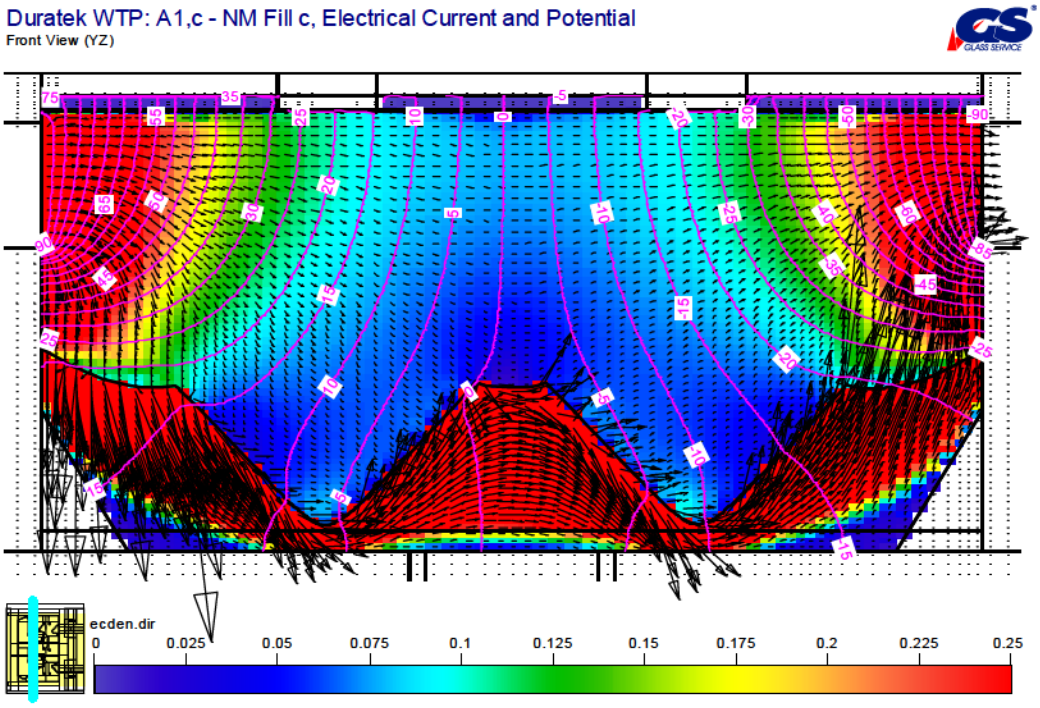


**Figure 26 Case A1-c: Electric current density [A/cm$^2$] (color fill), vector of electrical current, and electrical potential isolines in the YZ cut at x=1000mm (I=22)**

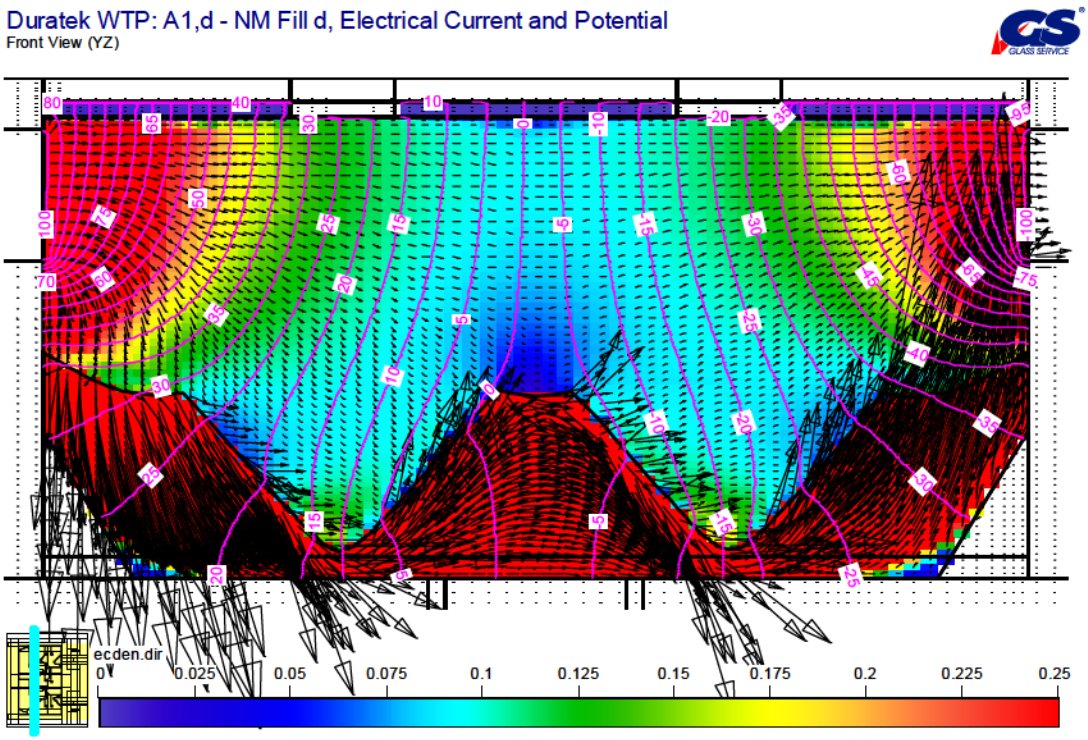


**Figure 27 Case A1-d: Electric current density [A/cm$^2$] (color fill), vector of electrical current, and electrical potential isolines in the YZ cut at x=1000mm (I=22)**

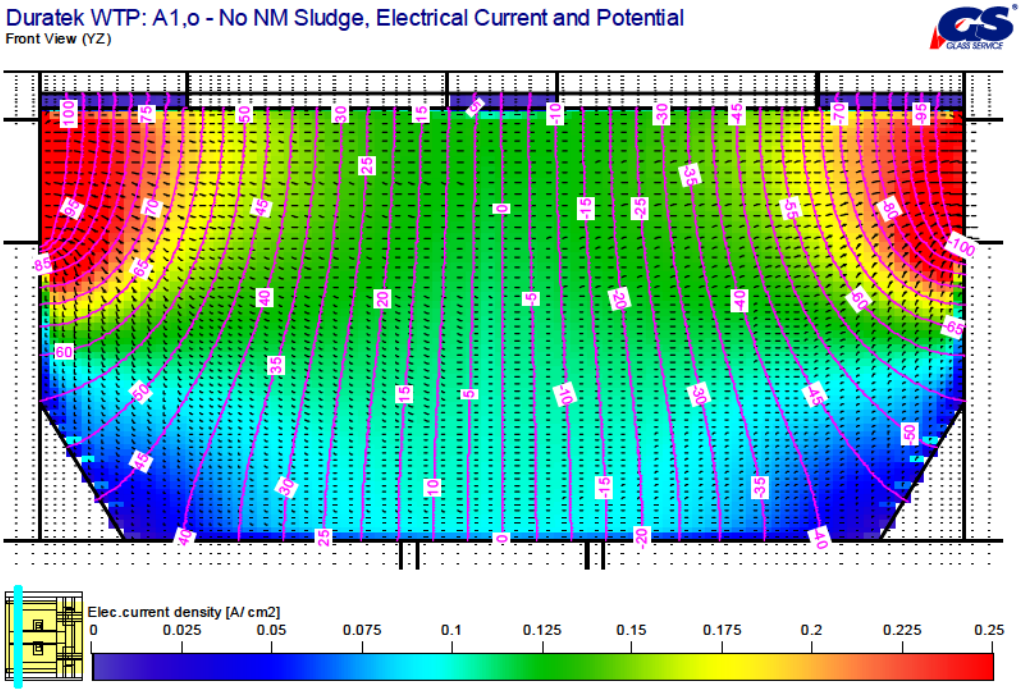


**Figure 28 Case A1-0: Electric current density [A/cm$^2$] (color fill), vector of electrical current, and electrical potential isolines in the YZ cut at x=469mm (I=10), at the highest position of NM fill**

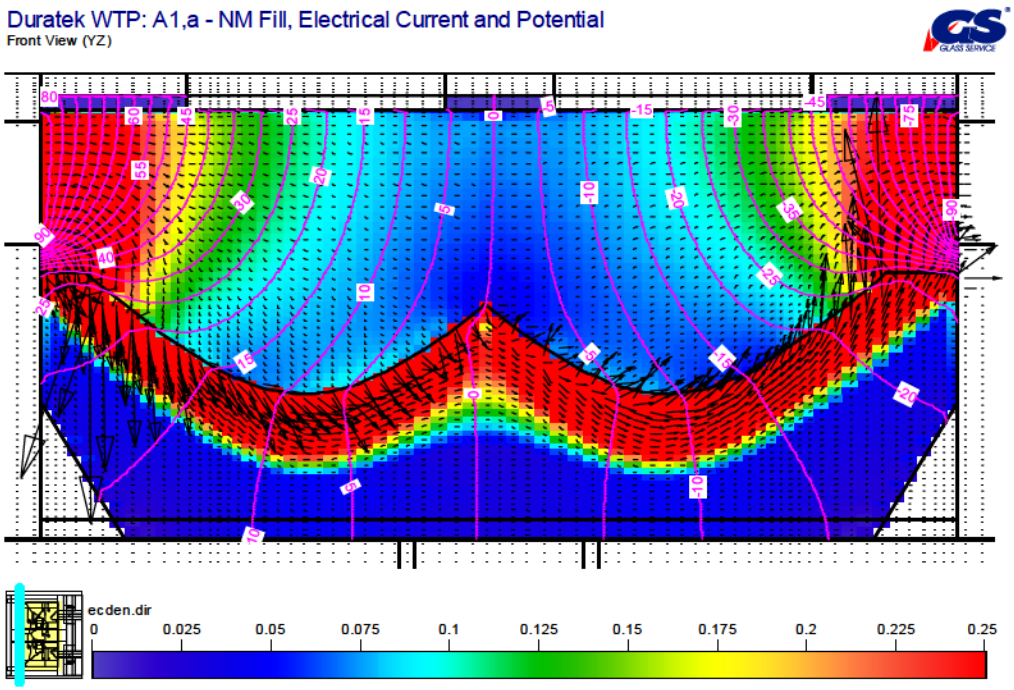


**Figure 29 Case A1-a: Electric current density [A/cm$^2$] (color fill), vector of electrical current, and electrical potential isolines in the YZ cut at x=469mm (I=10), at the highest position of NM fill**

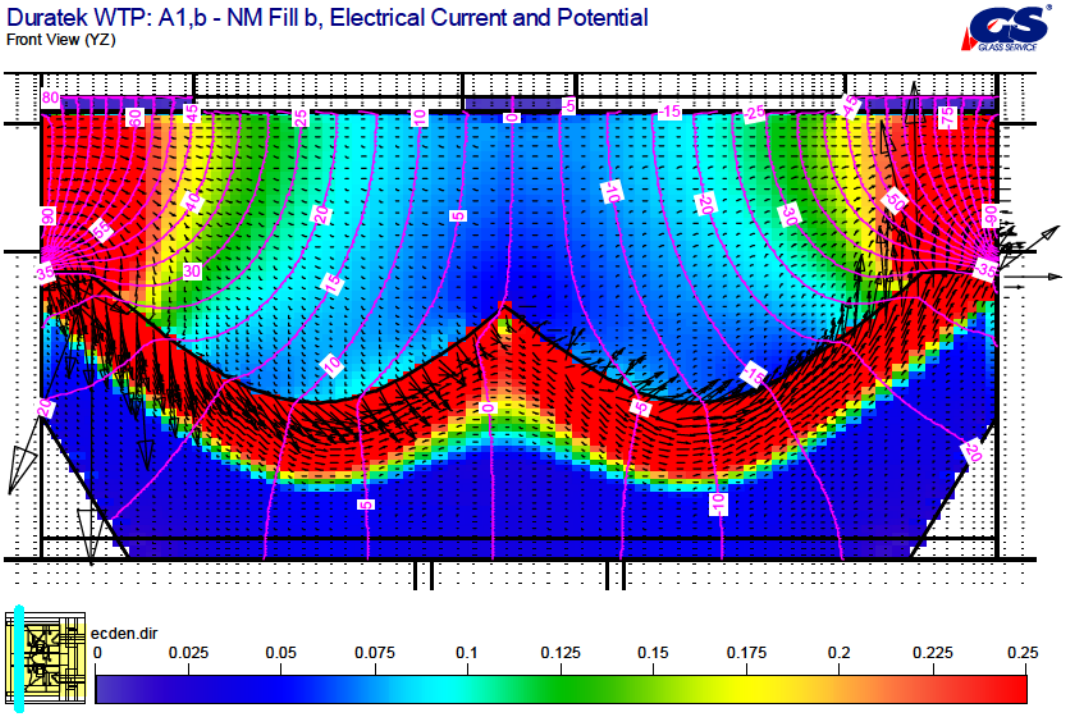


**Figure 30 Case A1-b: Electric current density [A/cm$^2$] (color fill), vector of electrical current, and electrical potential isolines in the YZ cut at x=469mm (I=10), at the highest position of NM fill**

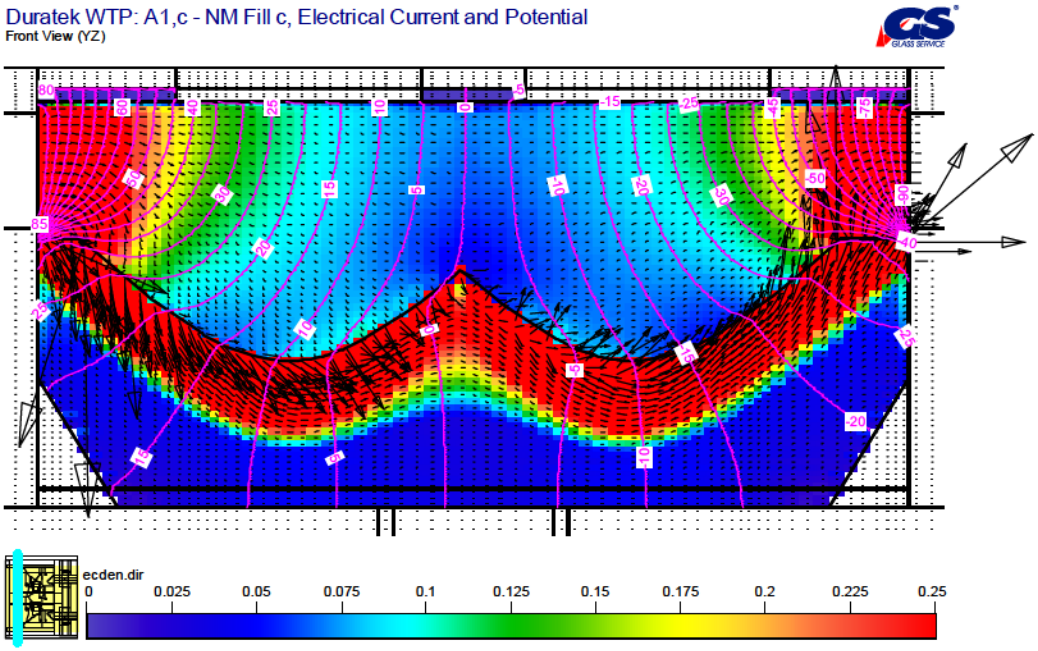


**Figure 31 Case A1-c: Electric current density [A/cm$^2$] (color fill), vector of electrical current, and electrical potential isolines in the YZ cut at x=469mm (I=10), at the highest position of NM fill**

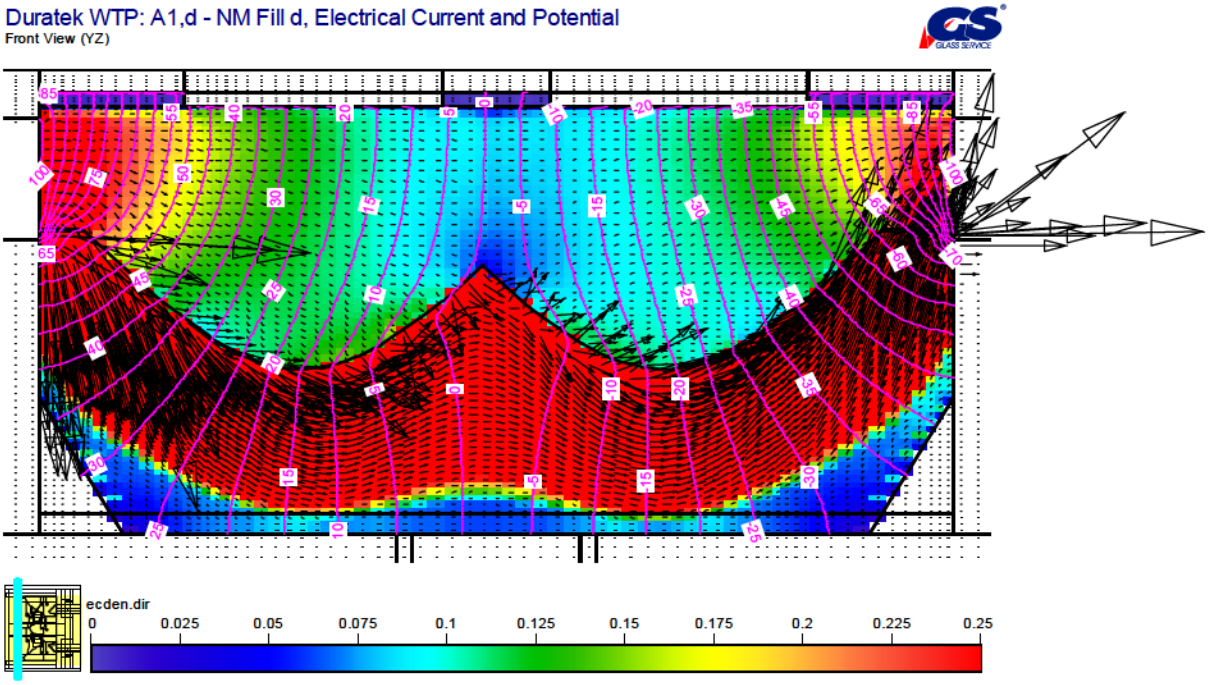


**Figure 32 Case A1-d: Electric current density [A/cm$^2$] (color fill), vector of electrical current, and electrical potential isolines in the YZ cut at x=469mm (I=10), at the highest position of NM fill**

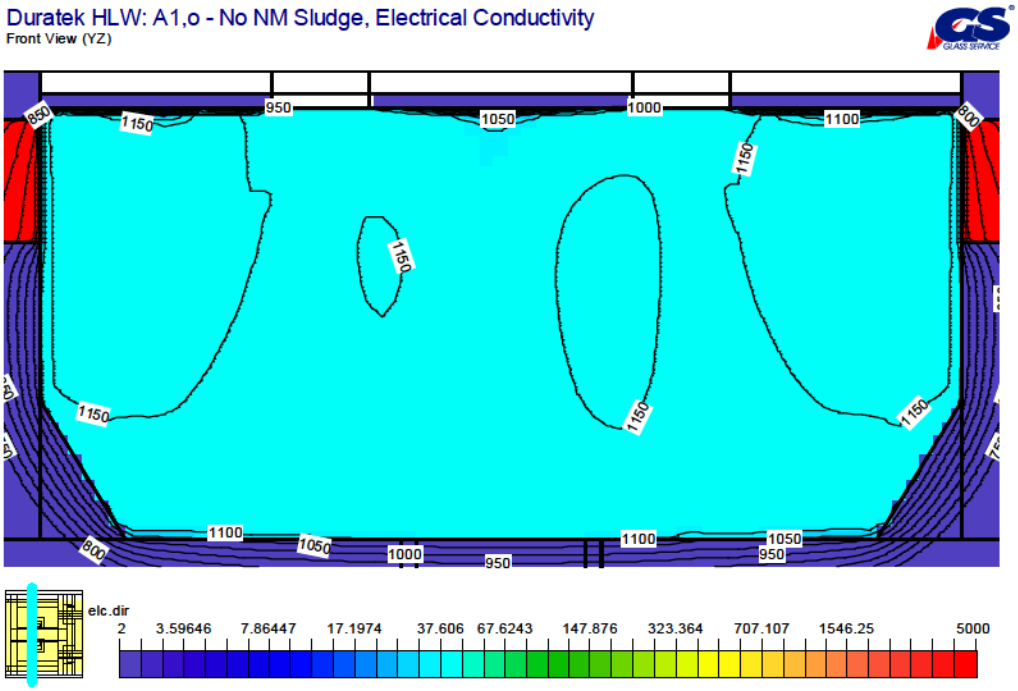


**Figure 33 Case A1-0: Electrical conductivity [1/Ohm.m] (color fill), and temperature [C] (isolines) in the YZ cut at x=1000mm (I=22)**

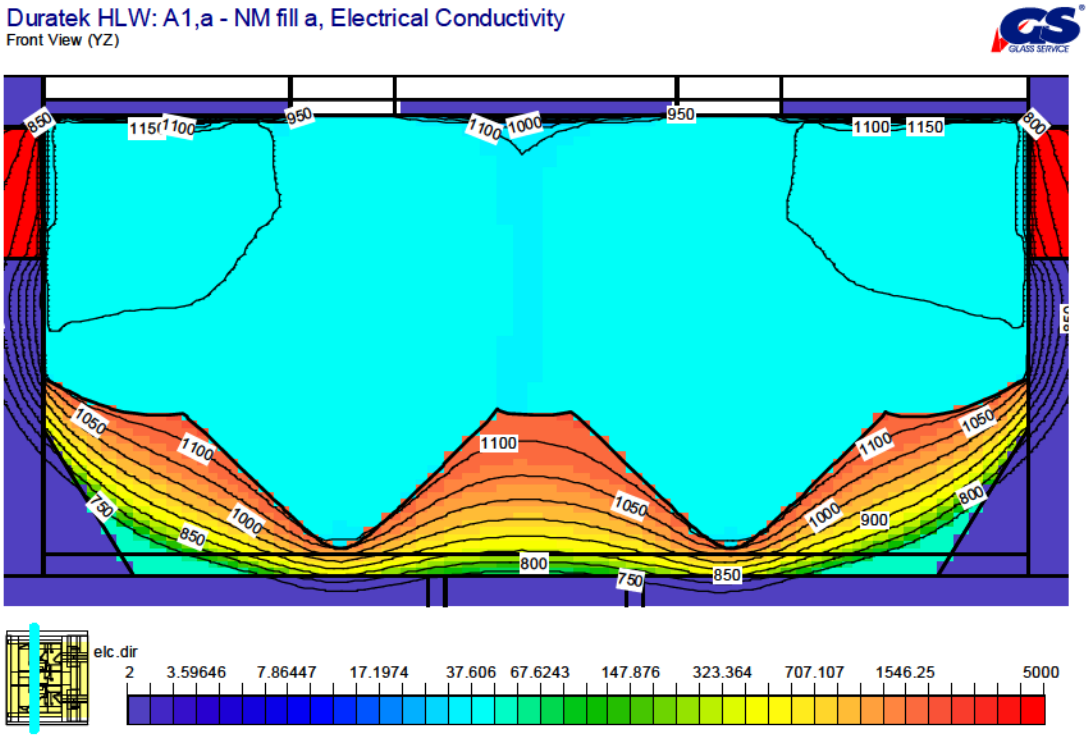


**Figure 34 Case A1-a: Electrical conductivity [1/Ohm.m] (color fill), and temperature [C] (isolines) in the YZ cut at x=1000mm (I=22)**

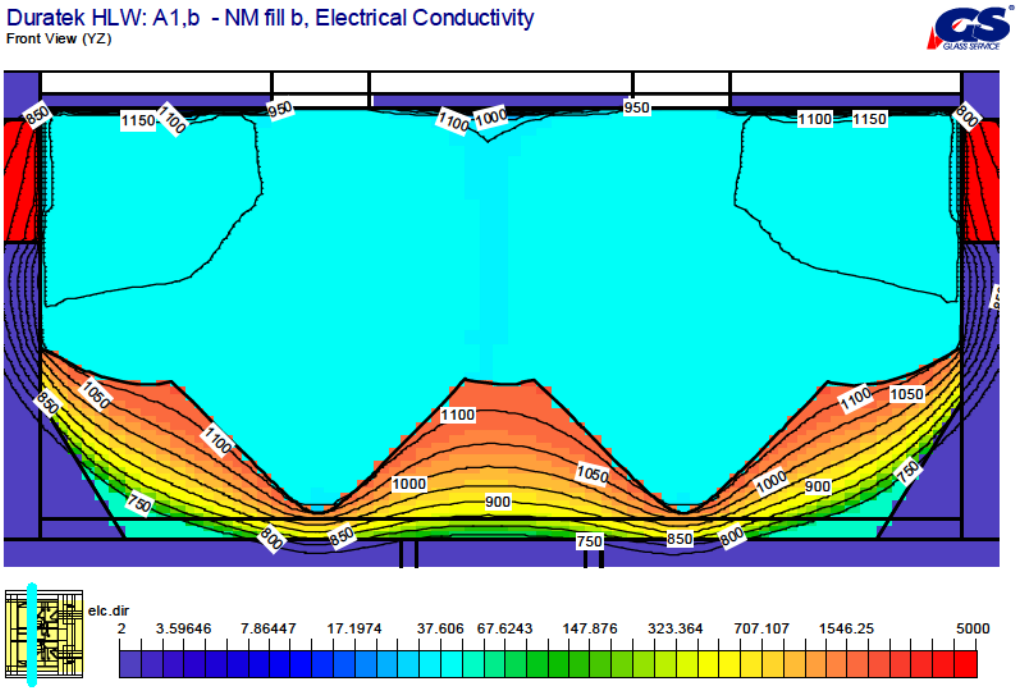


**Figure 35 Case A1-b: Electrical conductivity [1/Ohm.m] (color fill), and temperature [C] (isolines) in the YZ cut at x=1000mm (I=22)**

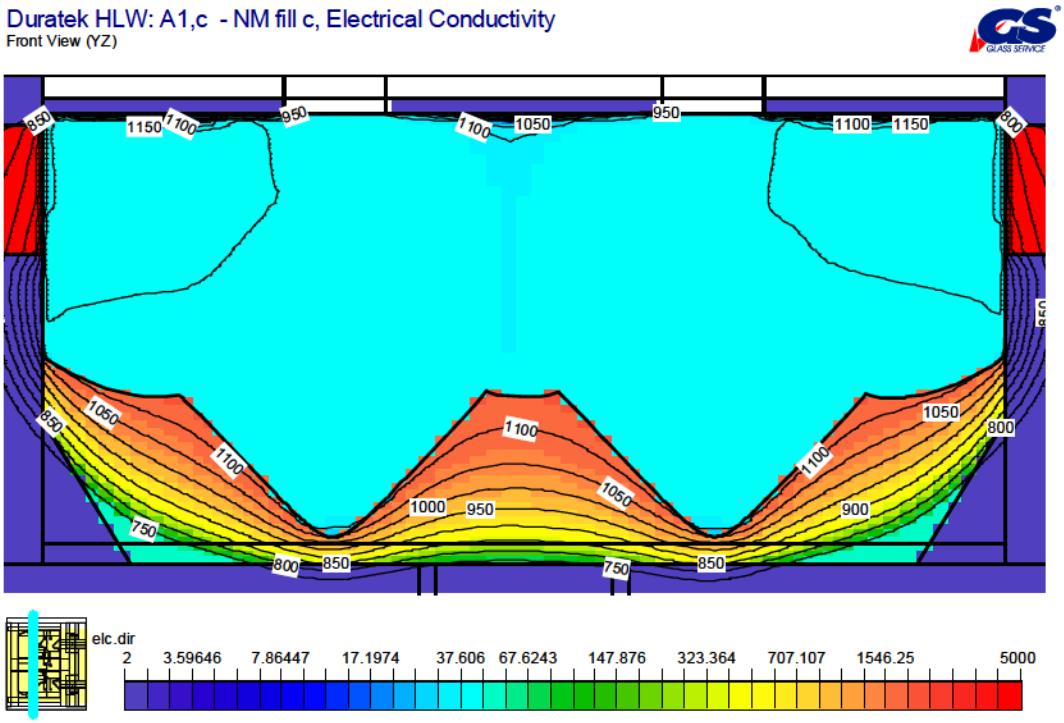


**Figure 36 Case A1-c: Electrical conductivity [1/Ohm.m] (color fill), and temperature [C] (isolines) in the YZ cut at x=1000mm (I=22)**

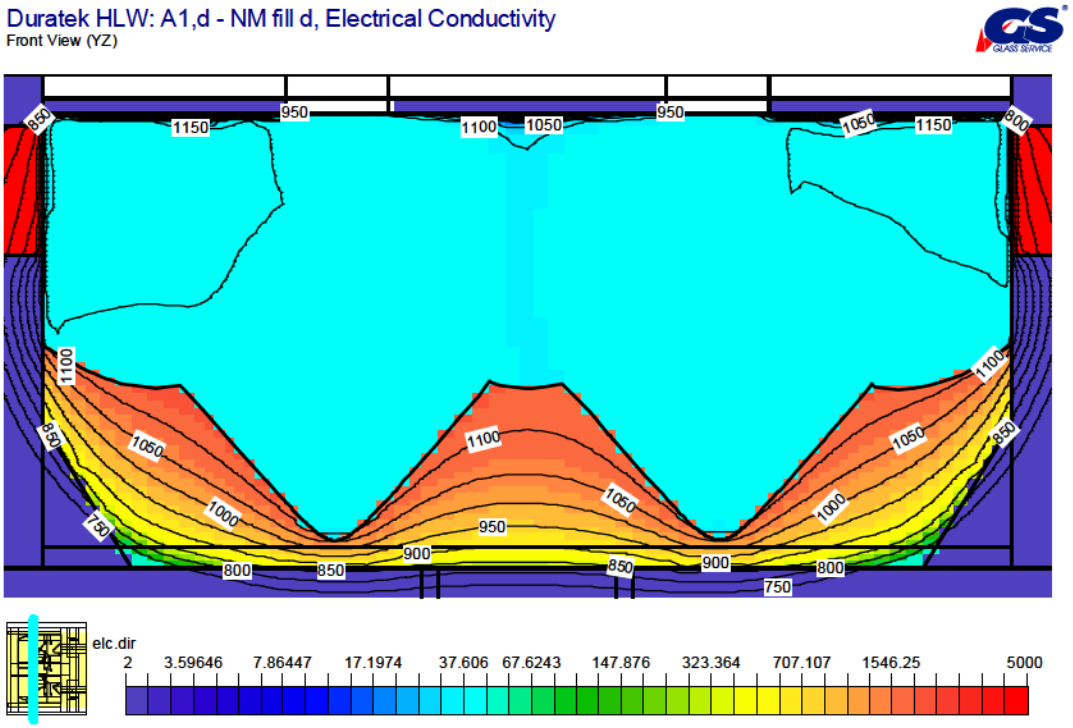


**Figure 37 Case A1-d: Electrical conductivity [1/Ohm.m] (color fill), and temperature [C] (isolines) in the YZ cut at x=1000mm (I=22)**

### *Case A2, derived from case B1 with high bubbling*

Case A2 assesses the influence and contrasts the temperature and flow fields for case B1 but using a higher bubbling rate than before. In case A2 the bubbling rate was set at 100 liters per minute per nozzle (10 nozzles), 170 bubbles per minute with a "hemispherical" bubble diameter of 130 mm.

The resulting electrical, flow, and temperature values are listed in table 2 for cases A2, A3, and A4).

WTP melter -- high bubbling cases

Table 2. List of calculated electrical quantities and temperatures for cases A2, A3, A4

| case | maximal vertical velocity | minimal vertical velocity | voltage | current | total power | glass temperature maximal | glass temperature average |
|---|---|---|---|---|---|---|---|
| | mm/s | mm/s | [V] | [A] | [kW] | C | C |
| **A2** (B1) | -263.8 | 74.8 | 160 | 3,172 | 505.9 | 1,182 | 1,142 |
| **A3** (B6) | -244.3 | 72.1 | 155 | 3,068 | 475.3 | 1,179 | 1,139 |
| **A4** (B7) | -221.1 | 44.4 | 124 | 1,910 | 237.5 | 1,089 | 1,069 |

The following figures display the calculated flow, temperature and electrical fields for case A2.

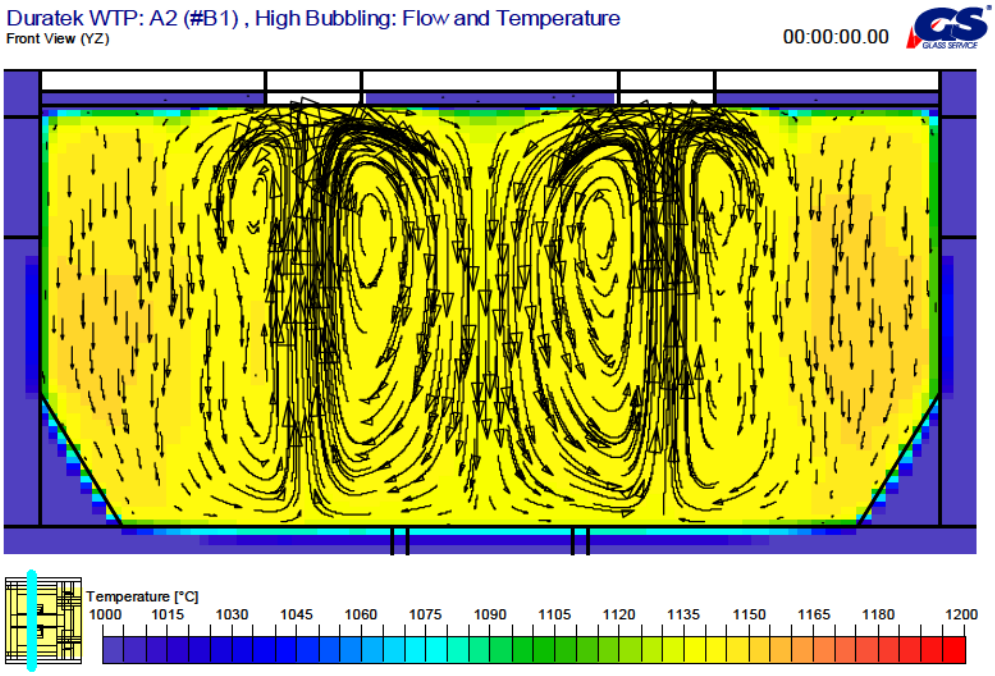


**Figure 38 Case A2: Flow and temperature distribution in YZ cut at x=1000mm (I=22)**

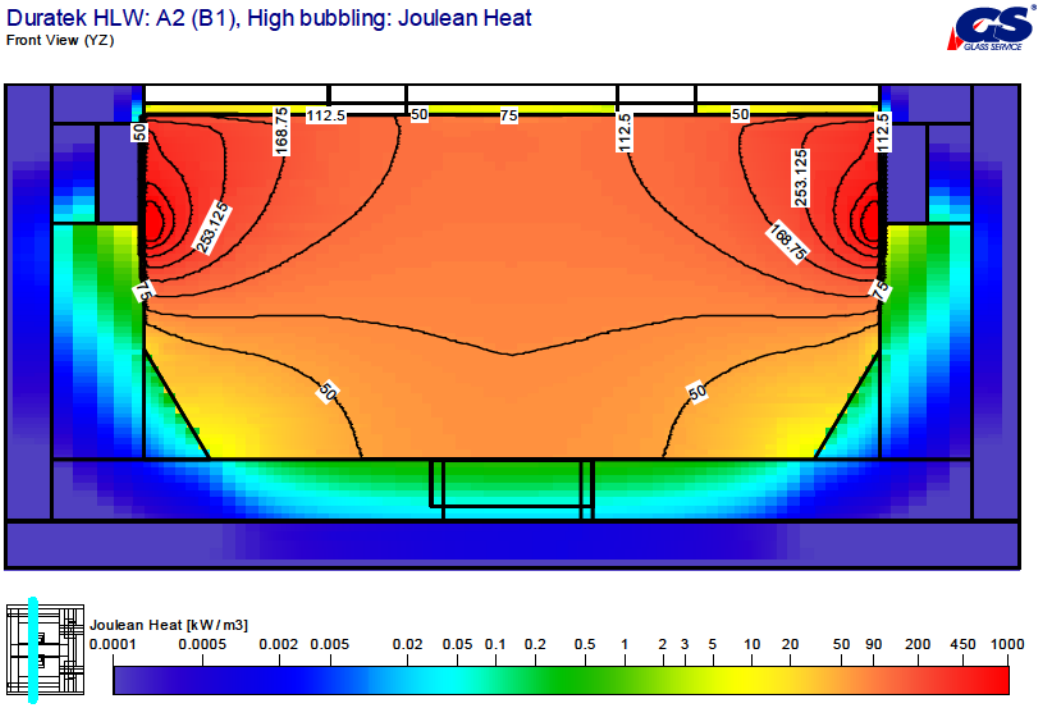


**Figure 39 Case A2: Joulean heat distribution (color fill) in YZ cut at x=1000mm (I=22)**

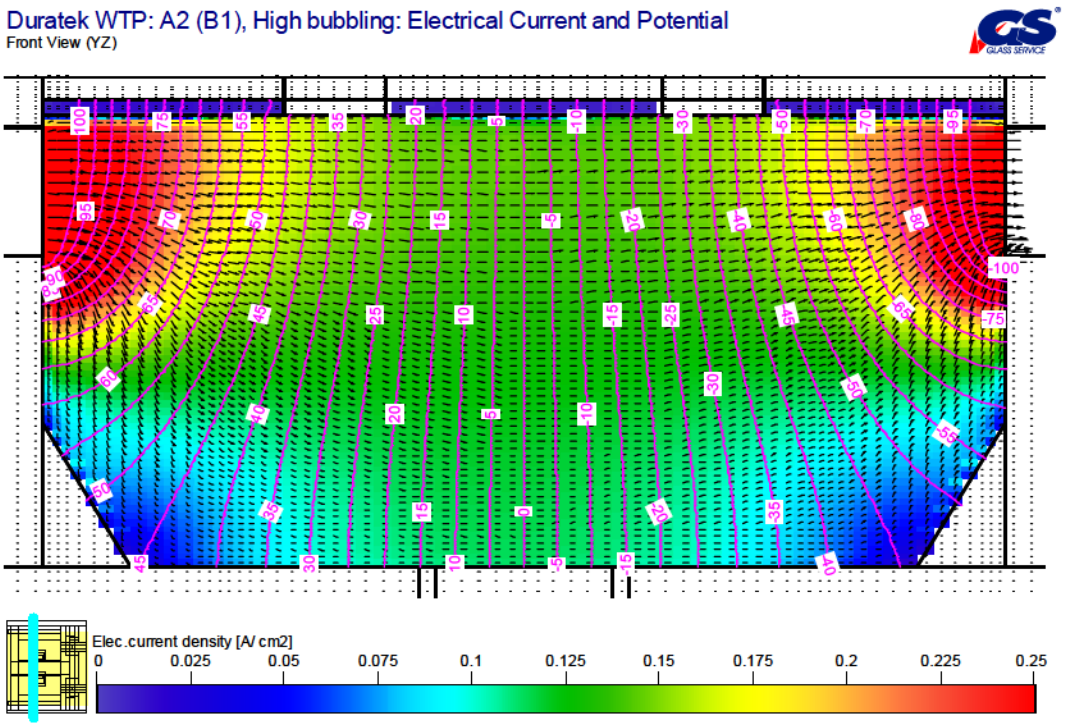


**Figure 40 Case A2: Electric current density [A/cm$^2$] (color fill), vector of electrical current, and electrical potential isolines in the YZ cut at x=1000mm (I=22)**

### *Case A3, derived from case B6 with high bubbling*

Case A3 assesses the influence and contrasts the temperature and flow fields for case B6 but using a higher bubbling rate than before. In case A3, the bubbling rate was set at 100 liters per minute per nozzle (3.5 ACFM), 6 nozzles, 170 bubbles per minute with a "hemispherical" bubble diameter of 130 mm.

The following figures display the calculated flow, temperature and electrical fields for case A3.

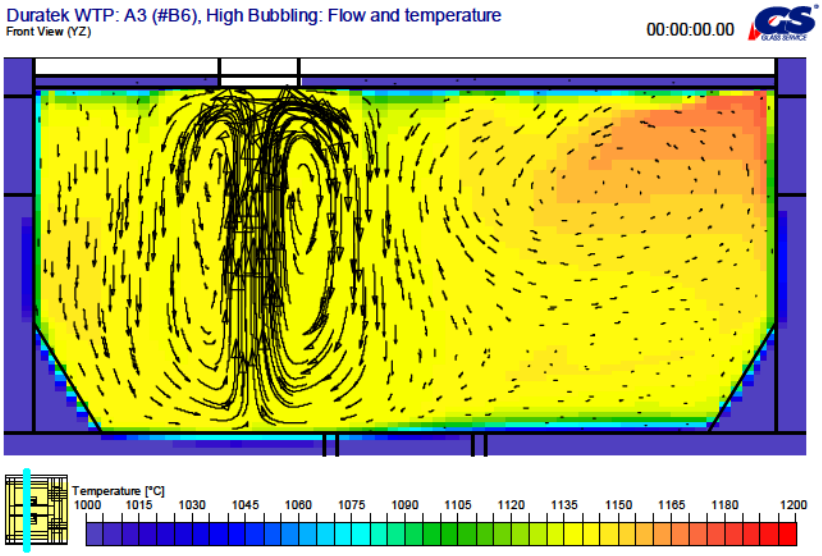


**Figure 41 Case A3: Flow and temperature distribution in YZ cut at x=1000mm (I=22)**

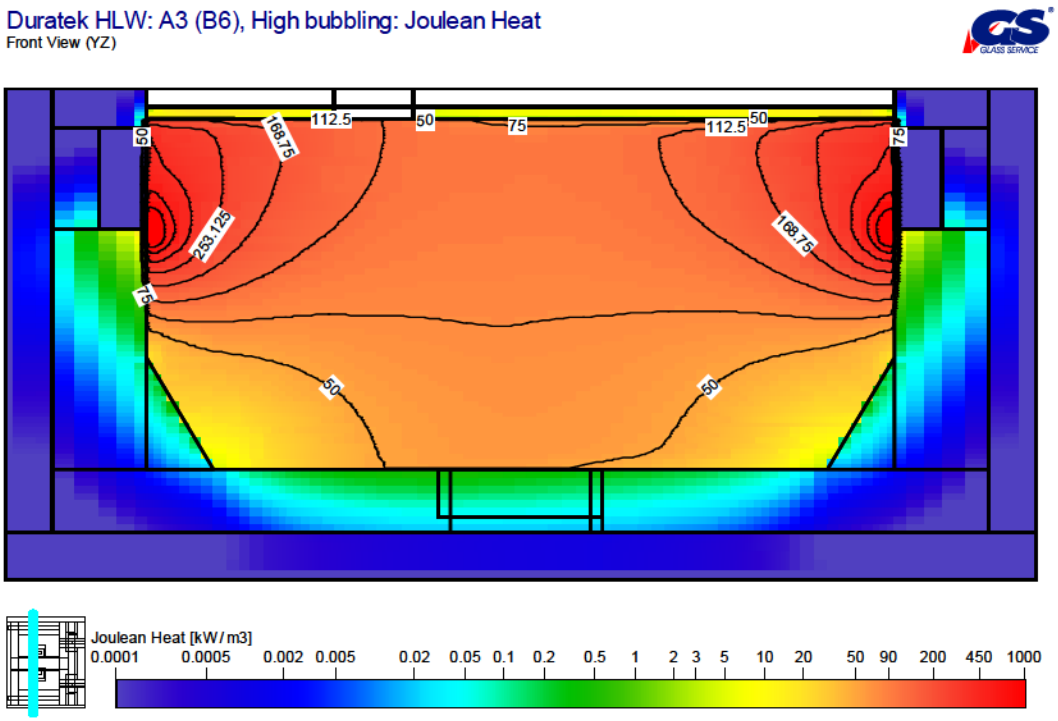


**Figure 42 Case A3: Joulean heat distribution (color fill) in YZ cut at x=1000mm (I=22)**

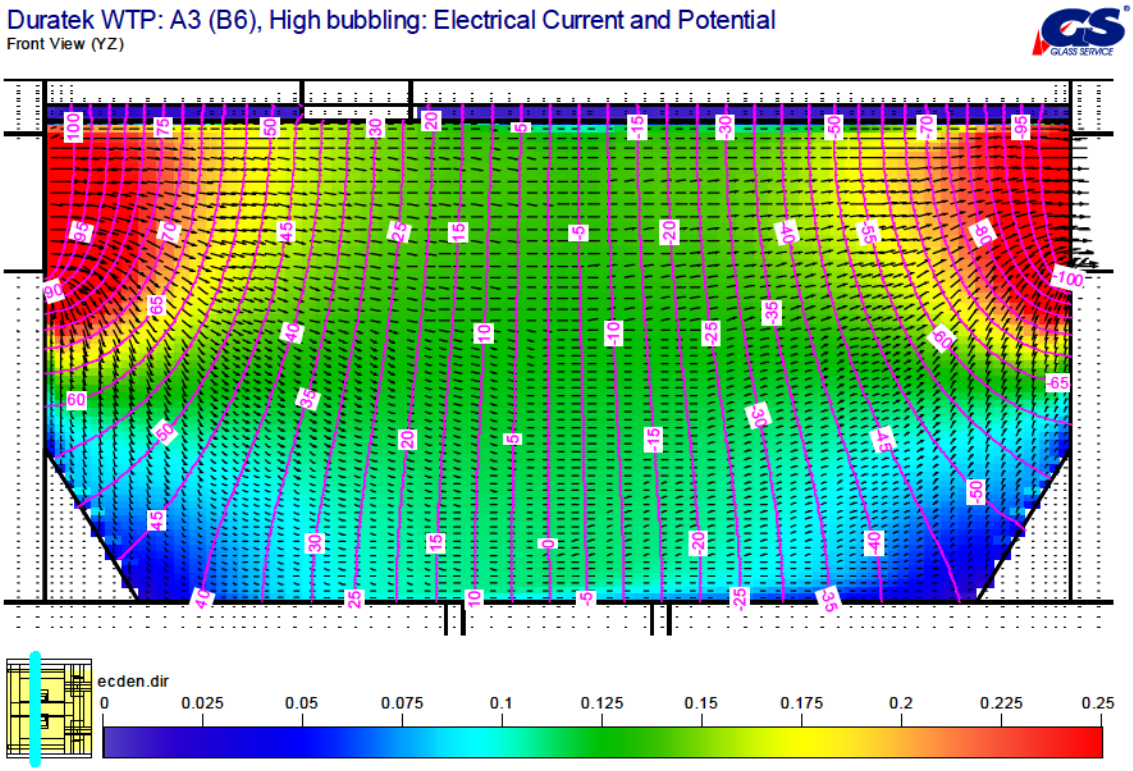


**Figure 43 Case A3: Electric current density [A/cm$^2$] (color fill), vector of electrical current, and electrical potential isolines in the YZ cut at x=1000mm (I=22)**

### *Case A4, derived from case B7 with high bubbling*

Case A4 determined the bulk glass temperature during idling using a higher bubbling rate and higher average bulk temperature than in case B7. This case used a bulk glass temperature of 1075 C and a bubbling rate of 100 liters per minute per nozzle (3.5 ACFM), 10 nozzles, 170 bubbles per minute with a "hemispherical" bubble diameter of 130 mm. In the prior case B7, the average flow rate per nozzle was 32.5 liters per minute (1.15 ACFM).

The following figures display the calculated flow, temperature and electrical fields in case A4.

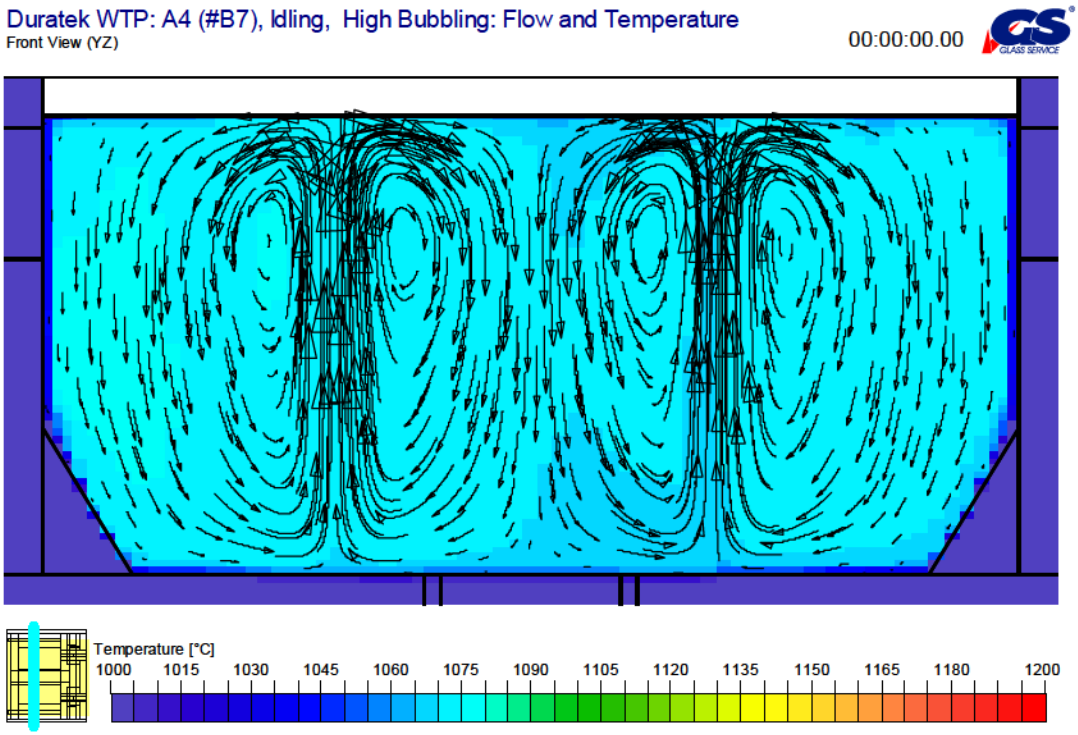


**Figure 44 Case A4: Flow and temperature distribution in YZ cut at x=1000mm (I=22)**

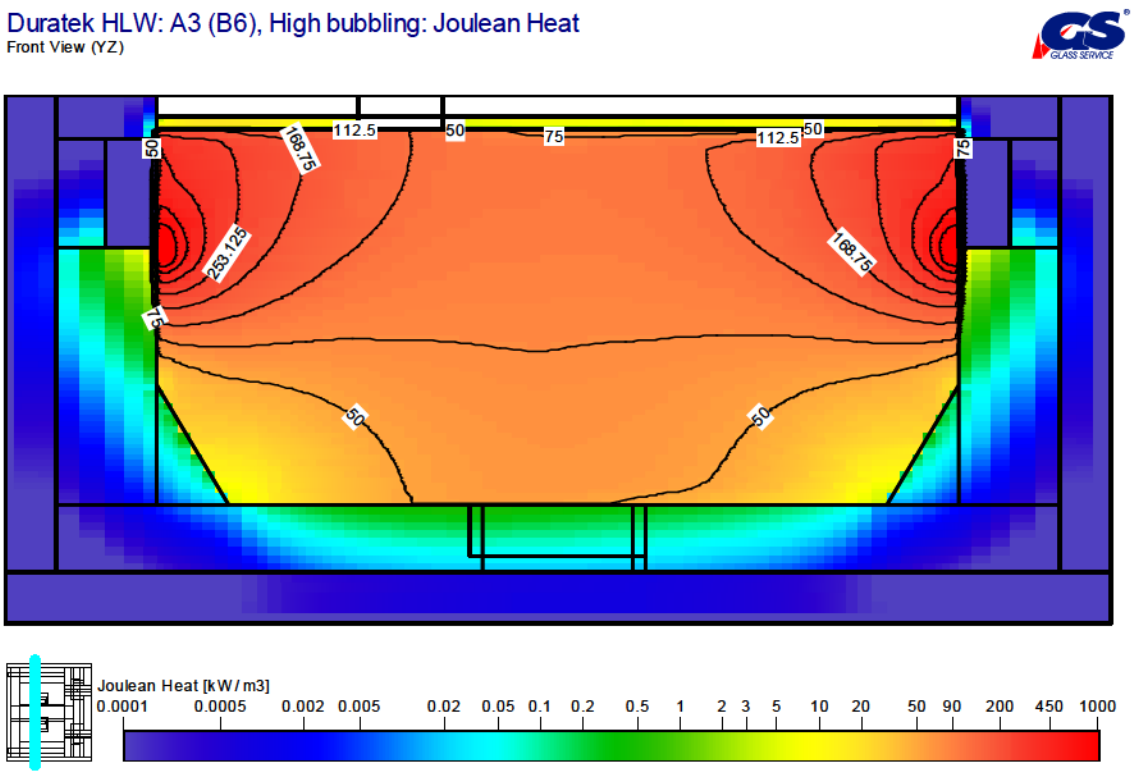


**Figure 45 Case A4: Joulean heat distribution (color fill) in YZ cut at x=1000mm (I=22)**

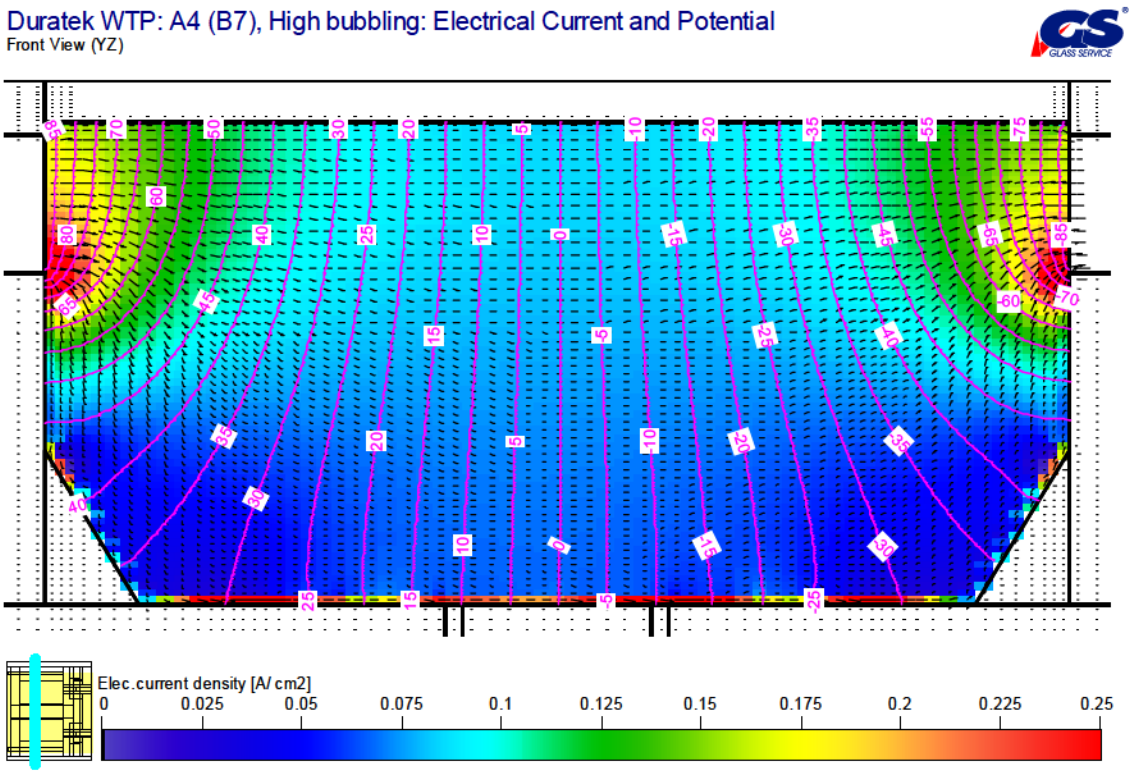


**Figure 46 Case A4: Electric current density [A/cm$^2$] (color fill), vector of electrical current, and electrical potential isolines in the YZ cut at x=1000mm (I=22)**

## SUMMARY AND CONCLUSIONS

This report presents the results from modeling the specified additional cases for the WTP melter. The results show that the electrical quantities (Joulean heat-, electrical density, and electrical current (vector)-distribution) in the NM sludge fill in the melter are modified in accordance with the modified electrical conductivity distribution. Since the bottom part of the sludge fill is at lower temperature, the electrical conductivity is also lower in that region (see Fig. 6B). The electrical density- and Joulean heat-distribution follow the electrical conductivity distribution. As the NM level was increased, the effect on the total melter current, voltage, and power was relatively small until contact with the electrodes was made.

The higher bubbling rate in cases A2, A3, A4 had a significant effect on the resulting flow field and, consequently, the temperature field is also modified in such a way that temperature gradients are decreased.